CERN, 14.11.2003

RD50 Status Report 2002/2003

Radiation hard semiconductor devices for very high luminosity colliders

Centro Nacional de Microelectrónica (IMB-CNM, CSIC)
Francesca Campabadal, Celeste Fleta, Martyn Key, Manuel Lozano, Giulio Pellegrini, Joan Marc Rafí, Miguel Ullán

Dipartimento Interateneo di Fisica & INFN - Bari, Italy
Donato Creanza, Mauro De Palma, Valeria Radicci, Luigi Schiavulli

Berlin IKZ
Hinz, Klaus Irmscher, Rossberg, Günter Wagner

Brookhaven National Laboratory, Upton, NY, USA
Jim Kierstead, Zheng Li

Department of Physics, University of Bologna, Bologna, Italy
Anna Cavallini

National Institute for Materials Physics, Bucharest - Magurele, Romania
Sorina Lazanu, Lucian Pintilie, Ioana Pintilie, George Sarau

University of Bucharest, Faculty of Physics
Ionel Lazanu

CERN, Geneva, Switzerland
Veronique Boisvert, Paula Collins, Karl Aaron Gill, Maurice Glaser, Christian Joram, Michael Moll[♣]

[♣] Deputy Spokesperson

NCSR DEMOKRITOS, Institute of Materials Science, Aghia Paraskevi Attikis, Greece
Apostolos Kontogeorgakos, George Kordas, Christos Trapalis

Universitaet Dortmund, Lehrstuhl Experimentelle Physik IV, Dortmund, Germany
Claus Goessling, Jonas Klaiber-Lodewigs, Reiner Klingenberg, Olaf Krasel, Renate Wunstorf

CiS Institut für Mikrosensorik gGmbH, Erfurt, Germany
Ralf Roeder, Dieter Stolze, Hartmut Uebersee

University of Exeter, Department of Physics, Exeter, EX4 4QL, United Kingdom
James Adey, A. Blumenau, J. Coutinho, T. Eberlein, C. Fall, J. Goss, B. Hourahine, Robert Jones, N. Pinho

Fermilab, USA
Rita Coluccia, Simon Kwan, Greg Sellberg

INFN - University of Florence, Italy
Emilio Borchi, Mara Bruzzi[♦]*, Ettore Focardi, Stefano Lagomarsino, Anna Macchiolo, David Menichelli, Stefania Miglio, Monica Scaringella, Silvio Sciortino*

Dept. of Physics & Astronomy, Glasgow University, Glasgow, UK
Adwan Al-Ajili, Richard Bates, Andrew Blue, Liam Cunningham, Alison Gouldwell, Lina Haddad, Meg Horn, Keith Mathieson, J. Melone, Val OShea, Chris Parkes, Mahfuzur Rahman, Patrick Roy, Victoria Wright

University of Halle; Dept. of Physics, Halle, Germany
V. Bondarenko, R. Krause-Rehberg

Institute for Experimental Physics, University of Hamburg, Germany
Peter Buhmann, Devis Contarato, Eckhart Fretwurst, Frank Hönniger, Gunnar Lindström, Uwe Pein, Jörg Stahl

Helsinki Institute of Physics, Helsinki, Finland
Jaakko Härkönen, Katri Lassila-Perini, Panja Luukka, Saara Nummela, Jukka Nysten, Eija Tuominen, Esa Tuovinen

High Energy Division of the Department of Physical Science, University of Helsinki, Helsinki, Finland
R. Lauhakangas, R. Orava, K Osterberg, J. Sanna, T. Schulman

♦ RD50 Spokesperson

Ioffe Phisico-Technical Institute of Russian Academy of Sciences, St. Petersburg, Russia
Vladimir Eremin, Igor Ilyashenko, Alexandr Ivanov, Nikita Strokan, Elena Verbitskaya

Institute of Electronic Materials Technology, Warszawa, Poland
Adam Barcz, Andrzej Brzozowski, Lech Dobrzanski, Andrzej Hruban, Pawel Kaminski, Andrzej Kowalik, Roman Kozlowski, Zygmunt Luczynski, Elzbieta Nossarzewska-Orlowska, Bronislaw Piatkowski, Wlodzimierz Strupinski, Barbara Surma, Piotr Zabierowski

University of Karlsruhe, Institut fuer Experimentelle Kernphysik, Karlsruhe, Germany
Wim de Boer, Alexander Dierlamm, Florian Hauler, Levin Jungermann, Valery Zhukov

Institute for Nuclear Research of the Academy of Sciences of Ukraine, Radiation PhysicDepartments
L. Barabash, A. Dolgolenko, A. Groza, A. Karpenko, V. Khivrich, V. Lastovetsky, A.P. Litovchenko, P. Litovchenko, L. Polivtsev

Department of Physics, Lancaster University, Lancaster, United Kingdom
Timothy John Brodbeck, Duncan Campbell, Alexandre Chilingarov, Gareth Hughes, Brian Keith Jones, Terence Sloan

Lappeenranta University of Technology, Finland
Tuure Tuuva

Department of Physics, University of Liverpool, United Kingdom
P.P Allport, Stephen Biagi, Themis Bowcock, Gianluigi Casse, Igor Stavitski

Jozef Stefan Institute and Department of Physics, University of Ljubljana, Ljubljana, Slovenia
Vladimir Cindro, Gregor Kramberger, Igor Mandic, Marko Mikuz, Marko Zavrtanik

Physics Department, Kings College London, United Kingdom
Gordon Davies, Ruth Harding, Shusaku Hayama, Tan Jin, Alison Mainwood

Université catholique de Louvain, Institut de Physique Nucléaire, Louvain-la-Neuve, Belgium
S. Assouak, Eric Forton, G. Grégoire

Department of Solid State Physics, University of Lund, Sweden
Mats Kleverman, Lennart Lindstrom, Leonid Murin

INFN and University of Milano, Department of Physics, Milano, Italy
Attilio Andreazza, Mauro Citterio, Tommaso Lari, Chiara Meroni, Francesco Ragusa, Clara Troncon

Dipartimento di Fisica-Università di Modena e Reggio Emilia, Italy
Alberto Basile, Claudio Canali, Andrea Mazzanti, Filippo Nava, Paolo Vanni, Giovanni Verzellesi

Groupe de la Physique des Particules, Université de Montreal, Canada
F. Gamaz, Marie-Helene Genest, Alain Houdayer, Celine Lebel, Claude Leroy

State Scientific Center of Russian Federation, Institute for Theoretical and Experimental Physics, Moscow, Russia
Gleb Bondarenko, Victor Golovine, Eugene Grigoriev, Aleksey Karpov, Michail Kozodaev, Pavel Polozov, Alexander Suvorov, Alexander Zaluzhnyi

Russian Research Center "Kurchatov Institute", Moscow, Russia
P. Alexandrov, E. Baranova, N. Belova, A. Brukhanov, V. Cvetkov, S. Franchenko, S. Latushkin, V. Litvinov, Alexander Ryazanov

University of New Mexico
Igor Gorelov, Martin Hoeferkamp, Giuseppe Latino, Dmitri Naoumov, Sally Seidel

SINTEF Electronics and Cybernetics Microsystems P.O.Box 124 Blindern N-0314 Oslo, Norway
Berit Sundby Avset

University of Oslo, Physics Department/Physical Electronics, Oslo, Norway
Giovanni Alfieri, Andrej Kuznetsov, Edouard Monakhov, Bengt G. Svensson

Dipartimento di Fisica and INFN, Sezione di Padova, Italy
Dario Bisello, Andrea Candelori, Alexei Litovchenko, Riccardo Rando

I.N.F.N. and Università di Perugia - Italy
Gian Mario Bilei, Francesco Moscatelli, Daniele Passeri, Giorgio Umberto Pignatel, Andrea Scorzoni

Universita` di Pisa and INFN sez. di Pisa, Italy
Laura Borrello, Alberto Messineo, Daniel Sentenac, Andrey Starodumov

Institute of Physics, Academy of Sciences of the Czech Republic, Praha, Czech Republic
Jiri Popule, Petr Sicho, Michal Tomasek, Vaclav Vrba

Czech Technical University in Prague&Charles University Prague, Czech Republic
Jan Broz, Dominik Chren, Zdenek Dolezal, Tomas Horazdovsky, Peter Kodys, Zdenek Kohout, Vladimir Linhart, Stanislav Pospisil, Michael Solar, Bruno Sopko, Alexej Tsvetkov, Josef Uher, Ivan Wilhelm

Paul Scherrer Institut, Laboratory for Particle Physics, Villigen, Switzerland
Roland Horisberger, Tilman Rohe

Purdue University, USA
Gino Bolla, Daniela Bortoletto, Kim Giolo, Jun Miyamoto, Carsten Rott, Amitava Roy, Ian Shipsey, SeungHee Son

Rutgers University, Piscataway, New Jersey, USA
L. Perera, S. Schnetzer, R. Stone, Steven Worm

Dept of Physics and Astronomy, University of Sheffield, Sheffield, U.K.
Craig Buttar, Ian Dawson, Paul Dervan, Chris Grigson

Department of Physics, University of Surrey, Guildford, United Kingdom
Paul Sellin

Experimental Particle Physics Group, Syracuse University, Syracuse, USA
Marina Artuso

Tel Aviv University, Israel
J. Guskov, Sergey Marunko, Arie Ruzin, Tamir Tylchin

University of Torino
Floriana Fasolo, Franco Fizzotti, Alessandro Lo Giudice, Claudio Manfredotti, Paolo Olivero, Chiara Paolini

ITC-IRST, Microsystems Division, Povo, Trento, Italy
Maurizio Boscardin, Gian - Franco Dalla Betta, Paolo Gregori, Claudio Piemonte, Georg Pucker, Sabina Ronchin, Mario Zen, Nicola Zorzi

Universita di Trieste & I.N.F.N.-Sezione di Trieste, Italy
Luciano Bosisio, Selenia Dittongo

IFIC Valencia, Apartado 22085, 46071 Valencia, Spain
Carmen Garcia, Jose Enrique Garcia-Navarro, Sergio González Sevilla, Salvador Marti i Garcia

Institute of Materials Science and Applied Research, Vilnius University, Vilnius, Lithuania
Eugenijus Gaubas, Kestutis Jarasiunas, Vida Kazlauskiene, Vaidotas Kazukauskas, Stanislavas Sakalauskas, Jurgis Storasta, Markas Sudzius, Juozas Vidmantis Vaitkus

Table of contents

1 Introduction

The objective of the CERN RD50 Collaboration is the development of radiation hard semiconductor detectors for very high luminosity colliders, particularly to face the requirements of a possible upgrade scenario of the LHC to a luminosity of $10^{35}cm^{-2}s^{-1}$,corresponding to expected total fluences of fast hadrons above $10^{16}cm^{-2}$ and a reduced bunch-crossing interval of ~10 ns [1].

The CERN RD50 collaboration has been recommended for approval in May 2002 by the LHCC and approved in June by the CERN Research Board. This document reports status of research and main results obtained after the first year of activity of the collaboration.

Presently, RD50 counts a total of 280 members with 55 participating institutes, from 47 different countries in West and East Europe, 7 from North America (USA, Canada) and one from middle east (Israel). During the first year of activity three workshops and collaboration board meetings have been held at CERN to discuss the recent results and co-ordinate the research activities of RD50: Oct. 2-4, 2002, May 18-20 and Nov. 3-5, 2003 . Each workshop has registered a quite high rate of participation, counting an average of 80 participants with about 34 talks. More details can be found at the collaboration web-site: http://www.cern.ch/rd50/.

During the first year, the research activity of RD50 has been presented in form of invited oral contributions at several international conferences [2]:

- The PIXEL2002 International Workshop, Carmel, CA, USA, Sept. 9-12, 2002 [3].
- 11th International Workshop on Vertex Detectors, VERTEX 2002, Hawaii, November 3-8, 2002. Invited Talk, paper published in Nucl.Instr.and Meth.A [4].
- Frontier Detectors for Frontier Physics, Elba, May 2003, in press on Nucl. Instr. and Meth. A [5].
- 6th International Conference on Large Scale Applications and Radiation Hardness of Semiconductor Detectors, September 29-October 1, 2003, Firenze, Italy. Invited Talk, Paper submitted on Nucl. Instrum. Meth. A.[6].
- Innovative Detectors for Supercolliders, Erice, Italy, September 2003 [7].
- IEEE NSS-MIC , October 2003, Portland, Oregon, USA: Overview Talk, paper under submission to IEEE Trans. Nucl. Sci. [8]

The research activity of RD50 has been organised in two major lines, Material Engineering and Device Engineering, each of the two lines has been subdivided into three projects as shown in Table 1. The management of the projects has been assigned to members of RD50 of proven relevant experience (conveners). In the framework of the research activity of each project, working groups have been created with specific tasks. Each working group is composed by few institutes, which are directly involved in the research program and co-ordinated by an RD50 member. Besides working groups, common activities have been started on subjects of common interest. Some of these activities are partially supported with the RD50 common fund. Table 1 lists working groups and common activities within each project, with the corresponding co-ordinator.

In the next section our scientific work is reviewed in an executive summary. This section is followed by six sections describing the status of the research activities of each individual research line. Finally a work plan, milestones and an overview about the needed resources for 2004 is given.

	Line	Project Convener	Main Research Activity	Working groups and common acitivities
Spokesperson / Deputy Mara Bruzzi (INFN and Uni. of Florence) / Michael Moll (CERN)	Material Engineering	**Defect/Material Characterisation** Bengt G. Svensson Univ. Oslo, Norway	Characterisation of the microscopic properties of standard-, defect engineered and new materials, pre- and post-irradiation.	(1) DLTS Calibration (B.G. Svensson)
		Defect Engineering Eckhart Fretwurst Univ. of Hamburg, Germany	Development and testing of defect engineered silicon: Oxygen enriched FZ (DOFZ), High res. Cz, Epitaxial, Si enriched with Oxygen dimers	(1) Oxygen Dimer (M. Moll)
		New Materials Juozas Vaitkus Univ. of Vilnius, Lithuania	Development of new materials with promising radiation hard properties: bulk and epitaxial SiC, GaN	(1) SiC (I. Pintilie) (2) GaN (J. Vaitkus) (3) Other Materials
	Device Engineering	**Pad Detector Characterisation** Jaakko Harkonen Helsinki Inst. Physics, Finland	Characterisation of macroscopic properties of heavily irradiated single pad detectors in different operational conditions.	(1) Standardisation of macroscopic measurements (A. Chilingarov) (2) Common Irradiation
		New Structures Mahfuzur Rahman Univ. of Glasgow, UK	Development of 3D, semi-3D and thin detectors and study of their pre- and post-irradiation performance.	(1) 3D (M. Rahman) (2) semi-3D (Z. Li) (3) Thinned detectors (M. Boscardin)
		Full Detector Systems Gianluigi Casse Univ. of Liverpool, UK	- Systematic characterisation of segmented (microstrips, pixels) LHC-like detectors. - Links with LHC epxeriments	(1) Comparison between detectors made by different manufacturers

Table 1.: Organisation structure of the research activity in RD50

2 Executive Summary

Defect and Material Characterization (DMC)

During 2002/2003 the activities in the DMC-line have been focused on the following tasks/research areas;

1. *Cross calibration of Deep Level Transient Spectroscopy (DLTS) equipments* (involving 10 partners)
2. *Characterization of processed and irradiated detector structures fabricated using high resistivity silicon wafers of different types, e.g.,* Standard Float Zone (STFZ), Diffusion oxygenated Float Zone (DOFZ) and Czochralski-grown (CZ). For the first time it is shown that both the change of the effective doping concentration (depletion voltage) and the free charge carrier generation (reverse current) can be completely understood by the formation of defects detected by spectroscopic techniques. This is regarded to be a major breakthrough for the understanding of radiation damage and will hopefully also pave the road for an optimization of radiation tolerant detectors including hadron induced damage.
3. *Characterization of irradiation-induced defect clusters in silicon*. Using photoluminescence two frequent defects are observed; the so-called W and the X optical centers. Recent results discussed in this report suggest that the W-center is more likely interstitial-related than vacancy-related.
4. *Characterization of processed and irradiated detector structures fabricated using high purity and lightly doped epitaxial layers of n-type Silicon Carbide (SiC).* At least 6 different electrically active defects have been revealed after irradiation by MeV protons and electrons but the introduction rate of these defects is relatively modest. A most pronounced effect is a high carrier removal rate but until now no evidence has been found for type inversion.

Main results and achievements in these four areas are summarized in Section 3.

Defect Engineering (DE)

In the frame of the Defect Engineering (DE) research line the activities during 2002/2003 were focused on the following projects:

1. *Oxygen enriched FZ silicon (DOFZ):* A break through in the understanding of gamma induced changes of the macroscopic detector properties on the basis of microscopic defects was achieved by recent studies on standard and differently oxygen enriched high resistivity float zone silicon. Numerous studies on charged hadron damage (protons of different energy, pions, neutrons, Lithium-ions) as well as electron damage (15 MeV, 900 MeV) had been performed on standard and oxygen enriched FZ silicon processed by different institutions on different FZ material from different manufacturer. The improved radiation tolerance of devices processed on oxygen enriched FZ-silicon was substantiated.
2. *High resistivity Cz silicon:* The radiation hardness of MCz silicon grown by Okmetic and Cz silicon produced by Sumitomo-Sitix has been investigated by several irradiation campaigns. Due to the high oxygen concentration of this material the radiation induced change of the effective space charge concentration or the depletion voltage is considerably smaller compared to DOFZ material. Microscopic studies have proven that in this material the formation of shallow oxygen related donors (early thermal donors) by irradiation play a major role in the macroscopic behavior of the Cz-devices.

3. *Epitaxial silicon:* A different approach for increasing the radiation tolerance of silicon detectors is the use of thin epitaxial silicon layers. A first production of detectors was performed by CiS on 50 μm thick low resistivity (50 Ωcm) epitaxial silicon layers grown on Cz substrates by ITME. The superior radiation tolerance of these devices with respect to the radiation induced change of the depletion voltage has been demonstrated for irradiation with 20 GeV protons, 58 MeV Li ions and reactor neutrons up to fluences of $\Phi_{eq} \approx 10^{16}$ cm^{-2}. For charged hadron damage no type inversion is observed which can be explained by a generation of shallow donors which overcompensates the creation of deep acceptor like defects at high fluences. The creation of shallow donors by proton irradiation was proven by TSC measurements.
4. *Oxygen dimers in silicon:* In a first experiment a dimerization process of silicon had been performed by irradiation of 3 mm thick Cz samples of different oxygen and carbon concentration, a 3mm thick FZ sample and different 300 μm thick diodes (FZ, DOFZ and Cz) with 6 MeV electrons at 350°C up to a fluence of about 10^{18} cm^{-2}. IR absorption measurements on the 3mm thick samples were done at Lund. The final analysis is in progress. First electrical characterizations and TSC measurements on the different diodes have shown, that the devices are heavily damaged and cannot be operated at fully depletion. Further studies are in progress.
5. *Defect engineering by pre-irradiation treatments:* Various pre-radiation processes with fast reactor neutrons followed by subsequent annealing of float zone (FZ) silicon were tested by IR optical transmission and Hall-effect measurements. It has been demonstrated that e.g. the carrier removal rates of pre-irradiated samples after gamma as well as neutron irradiation are considerably smaller compared to not pre-irradiated ones. Processing of detectors on pre-irradiated FZ- and Cz- material is planed for the beginning of 2004.

A detailed report on these activities is given in Section 4.

Pad Detector Characterisation (PDC)

In the frame of the Pad Detector Characterisation (PDC) research project a wide campaign of irradiations has been performed on single pad detector structures made with standard FZ, DOFZ and CZ Si with different particles, energies and fluences of up to $\Phi_{eq} \approx 10^{16}$ cm^{-2}. Measurements of macroscopic parameters (leakage current, full depletion voltage, charge collection efficiency and annealing parameters) have been carried out. The study has been carried out in collaboration with the DE project, as it has been performed mostly with defect engineered Si. Main results achieved during 2002-2003 are:

1. Establishment of the radiation tolerance of epitaxial Si detectors having a 50μm thick epitaxially grown active layer.
2. High resistivity Czochralski grown Si detectors (crystal growth by standard and magnetic field assisted Czochralski methods) have been found to be less prone to radiation induced changes of the full depletion voltage than standard Fz-Si or diffusion oxygenated Fz-Si (DOFZ).
3. Leakage current in gamma and low energy proton irradiated oxygenated Si: The leakage current increase in oxygen rich (Cz-Si and DOFZ) detectors seems to be smaller than in standard devices if the bulk is damaged by low energy protons or gammas. This is believed to be due to the non-clustered point defects induced by this kind of radiation.
4. Design and processing of common RD50 test structures. A common test structure for irradiation tests has been designed. The production of common devices is in progress.

A detailed report on these activities is given in Section 5.

New Materials (NM)

1. *Epitaxial SiC Growth and detector processing.* Six high quality (by means of minority carrier lifetime and thickness mapping) 2" n-type 4H-SiC epilayers (maximum thickness 50μm and different doping) were grown by IKZ-Berlin. A mask for processing Schottky contacts was designed and fabricated, the first batch of common test structures has been produced.
2. *Characterization of epitaxial SiC detector.* Different detector structures with epitaxial SiC were fabricated and tested. The detectors were characterized, before and after irradiation, by I-V, C-V and charge collection efficiency (CCE). A 100% CCE, has been observed with α and β-particles (^{90}Sr) in unirradiated detectors with a thickness of 40μm. The signal is stable and reproducible: no priming or polarization effects are observed. No increase in the leakage current was observed after irradiation up to the highest fluence/dose in epitaxial 4H-SiC detectors irradiated with electrons (8.2 MeV) and γ-rays (^{60}Co source) at fluences and doses ranging from 0 to 9.48×10^{14} e/cm^2 and 40 Mrad, respectively. In 6H-SiC triode structures a gain effect of about 20 was achieved. The processed diode detector structures based on 4H-SiC p-type epitaxial layers can be operated. No significant degradation of detector characteristics was revealed. After irradiation with 8MeV protons up to a fluence of 10^{14} cm^{-2} the CCE (measured with α-particles) after irradiation was about 80%.
3. *Semi-Insulating SiC detectors.* The charge collection efficiency of semi-insulating bulk 4H-SiC (CREE, USA) detectors (550μm thick thinned to 100μm) has been studied. A vanadium compensation process is used by CREE to give very high material resistivities, $\rho>10^{11}\Omega$cm. The CCE of vanadium compensated material is 60% prior irradiation and 50% after 10^{13} pions/cm^2. The study suggests that vanadium compensated materials should be avoided in the production of SiC detectors. A new supplier of Semi Insulating SiC is now involved (Okmetic, Finland) providing samples without vanadium compensation.
4. *Semi-Insulating GaN Detectors.* The electrical properties of thin SI-GaN structures (grown in Tokushima University) were investigated before and after irradiation with reactor neutrons ($5x10^{14}$cm^{-2}) and X-rays (600 Mrad). The CCE investigation was performed by α particles from ^{241}Am source and from 2 MeV accelerator. The CCE decreased from ~92% to 77% after neutron irradiation. SI-GaN irradiation up to 10^{16}cm^{-2} with reactor neutrons and intermediate dose (~10^{15}cm^{-2}) with protons (24 GeV/c in CERN) are in progress. The growth of high resistivity structure on lattice matched substrate from ITME was not successfully achieved due to the large content of oxygen, which avoid the production of semi-insulating GaN. A new supplier of high resistivity GaN is now involved (Lumilog, Ltd) and preliminary tests on new samples are in progress.

A detailed report on these activities is given in Section 7.

New Structures (NS)

During 2002/2003 the activities in this project have been focused on the following tasks:

1. *3D detectors.* One primary thrust of this year has been to design 3D detector structures and readout electronics suitable for LHCb/Velo trials. The design and masks for Velo have been completed and the electronic readout of the 3D device to a different chip gave operation. 3D devices were made and irradiated with pions to fluences of 10^{14}cm^{-2}. There was a slight degradation in the charge collection efficiency from 60% down to 45%, but the results show promise.

2. *Semi 3D detectors*. Semi-3D structures have been intensively simulated, the design has been implemented and the processing of the first batch of test structures is nearly complete.
3. *Thin Detectors*. Thin single pad detectors have been designed and manufactured with thickness down to 57μm. Electrical characterisation of non-irradiated devices has been performed, showing good performances.

A detailed report on these activities is given in Section 6.

Full Detector Systems (FDS)

During 2002/2003 the activities in this project have been focused on the following tasks:

1. *Design and process of common test structures.* Design of an RD50-FDS mask set for microstrip detectors using input from experiments and simulations. Manufacturing is under process.
2. *Characterisation of segmented detectors with defect engineered Si*. First miniature microstrip detectors have been manufactured with oxygen enriched FZ, CZ, epitaxial and p-type substrate silicon. Some of these detectors have been irradiated up to 10^{16} 24GeV/c p/cm^2, tests are in progress.
3. *Quantification of the characteristic trapping times for electrons and holes*. The existing pixel and microstrip miniature and full size detectors produced with standard and oxygen enriched substrates were used for systematic studies of the charge trapping parameters.
4. *Simulation of detector performances at very high fluences*. Simulations have been carried out to determine the survival scenario of pixel devices with different thickness and geometries in the fluence range up to 10^{16} cm^{-2}. Performed a first simulation of the electric field profile in microstrip detectors at fluences up $5 \cdot 10^{14}$cm^{-2}
5. *Links with other experiments* A number of research activities have started in collaboration with experiments at LHC, as listed here: a test beam with 120GeV muons and pions on Cz Si microstrip detector has been carried out in collaboration with LHCb VeLo; it has been decided the manufacturing of pixels with Cz Si in collaboration with the CMS pixel group; the simulation of the efficiency of pixels with ATLAS geometry has been carried out up to 10^{16}cm^{-2}; devices with different distances of the active volume from the cut edge for possible applications in TOTEM have been designed and will be processed soon.

A detailed report on these activities is given in Section 8.

3 Defect and Material Characterization

3.1 Cross calibration study of DLTS systems

In order to compare and cross calibrate the various Deep Level Transient Spectroscopy (DLTS) apparatuses available to RD50 the following study was performed:
A set of silicon p^+n-diodes (detectors) originating from the same wafer was used. The samples of type "W311"[9] were processed by ST Microelectronics (Catania, Italy) from silicon of ~1 kΩcm resistivity and <100> orientation. The diodes have an active area of 5x5 mm^2 and underwent an oxygenation process (1200 °C, 30 h) prior to device processing. The average effective doping concentration of the processed diodes was $N_d=(4.5\pm0.5)x10^{12}$ cm^{-3}. A part of the samples was irradiated at room temperature with 15 MeV e^- at the KTH Stockholm to a fluence of $3x10^{12}$ cm^{-2}. Each of the 10 participating institutes received 1 unirradiated and 1 irradiated diode. The measurement conditions were specified as follows: Reverse bias: 10 V, Pulse voltage: 10 V, Pulse width: 10 ms, Guard ring: Floating. The measurement results should be obtained for the DLTS signals of the three major peaks in the spectrum: "VO(-/0)", "V_2(=/-)" and "V_2(-/0)" and the two questions posed to all participating institutes were:

a) *Determine the peak positions of the peaks!*

b) Determine 2(ΔC/C)N_d (=N_T), without λ-correction, for the three peaks!

The result of the study are given in Table 2 . The determined peak positions agree very well while the determined concentrations show a rather big variation for the VO center. Therefore, further tests and calibrations are under way to understand the deviations found by some of the participating institutes.

Defect level	Averaged level position	Averaged concentration
VO(-/0)	0.17±0.01 eV	$(4.5\pm1)\ 10^{11}cm^{-3}$
V_2(=/-)	0.235±0.015 eV	$(1.3\pm0.25)\ 10^{11}cm^{-3}$
V_2(-/0)	0.415±0.015 eV	$(1.45\pm0.2)\ 10^{11}cm^{-3}$

Table 2.: Averaged values of determined defect levels and defect concentrations.

3.2 Characterization of point defects in high resistivity Si detectors

3.2.1 Characterization prior to irradiation

A search for process-induced defects has been performed before irradiation [10]. The p+nn+ diodes investigated in this work are manufactured from high resistivity (3-4 kΩcm) n-type FZ silicon grown in the <111> and <100> direction from Wacker. The processing and oxygen enrichment has been performed by the company CiS. The oxygen doping was achieved by diffusion for 24h, 48h and 72h at 1150°C in nitrogen and the oxygen and carbon concentration depth profiles have been measured by IR absorption and SIMS. Besides the FZ material, also CZ from Sumitomo with a resistivity of 1.2 kΩcm and epitaxial material from ITME-Warsaw was included in the investigation. The epi layers with a thickness of 50 µm were grown on a 300 µm (0.05 Ωcm) Cz-substrate. The phosphorus doping of the epitaxial layer was $7x10^{13}cm^{-3}$.

Five different defect levels have been discovered in the float zone material. As an example Figure 1 shows DLTS spectra for electron and hole injection. The electrical properties of these defects are listed in Table 3.: and their concentrations are given in Table 4.

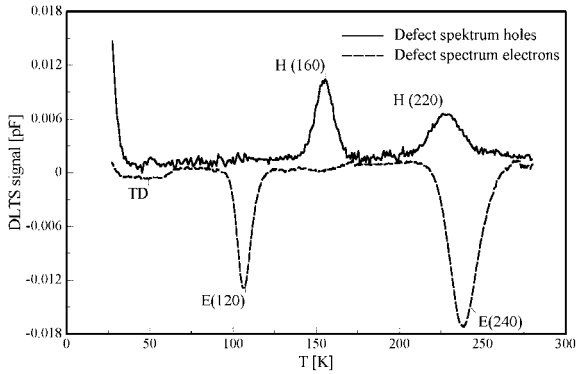

Figure 1.: DLTS-measurement of electron and hole traps in a 24h oxygenated <100> sample.

Name	sign	E_a[eV]	$\sigma_{n,p}$[cm^2]
TDD	E	-0.137	$1.58\cdot10^{-13}$
E(120)	E	-0.236	$1.00\cdot10^{-14}$
E(240)	E	-0.545	$5.41\cdot10^{-15}$
H(160)	H	+0.370	$2.88\cdot10^{-13}$
H(220)	H	+0.494	$1.65\cdot10^{-14}$

Table 3.: Electrical properties of the material defects

Name	CA	CB	CC	CD	CE	CF	CG	CH	CZ	EPI
Orient.	<111>	<111>	<111>	<111>	<100>	<100>	<100>	<100>	<100>	<100>
O-diff [h]	0	24	48	72	0	24	48	72	0	0
O [cm^{-3}]	$<5\cdot10^{16}$	$6.2\cdot10^{16}$	$1.0\cdot10^{17}$	$1.2\cdot10^{17}$	$<5\cdot10^{16}$	$2\cdot10^{17}$	$3.2\cdot10^{17}$	$3.1\cdot10^{17}$	$8\cdot10^{17}$	$6\cdot10^{16}$
C [cm^{-3}]	$<5\cdot10^{16}$	$2.8\cdot10^{15}$	$5.8\cdot10^{15}$	$3.9\cdot10^{15}$	$<5\cdot10^{16}$	$3.3\cdot10^{15}$	$3.9\cdot10^{15}$	$3.9\cdot10^{15}$	$<5\cdot10^{15}$	$<5\cdot10^{15}$
TD [cm^{-3}]	$<10^{9}$	$6.0\cdot10^{9}$	$1.6\cdot10^{10}$	$2.4\cdot10^{10}$	$<10^{9}$	$6.9\cdot10^{9}$	$7.2\cdot10^{9}$	$1.5\cdot10^{10}$	$3\cdot10^{11}$	x
E(120) [cm^{-3}]	x	X	X	x	x	$1.7\cdot10^{10}$	$5.0\cdot10^{9}$	$2.0\cdot10^{9}$	x	x
E (240) [cm^{-3}]	$0.8\cdot10^{9}$	X	X	x	x	$1.2\cdot10^{10}$	$7.9\cdot10^{9}$	$3.7\cdot10^{9}$	x	x
H (160) [cm^{-3}]	x	X	X	x	x	$9.7\cdot10^{9}$	x	x	x	x
H (220) [cm^{-3}]	$2.4\cdot10^{9}$	$4.0\cdot10^{9}$	$5.2\cdot10^{9}$	$2.7\cdot10^{9}$	$<10^{9}$	$6.3\cdot10^{9}$	$5.7\cdot10^{9}$	$1.0\cdot10^{10}$	x	x

Table 4: Concentration of material defects

One of these defects is the so-called thermal double donor TDD. As can be seen in Table 4 the amount of TDD's is correlated with the oxygen content of the differently oxygenated devices, but the concentrations in the material with <100> orientation (CF-CH) are smaller compared to the material with <111> orientation.

There is no measurable amount of TDD's observed in STFZ-material (Wafers CA and CE). The other four defects are so far unknown. The electron trap E(120) appears only in oxygenated <100> material. The E(120) has an activation energy and capture cross section which are close to those of the doubly negative charge state of the divacancy V_2(=/-) but no indication of the singly negative charge state of V_2(-/0) is revealed. The defect E(240) is a very deep level and from its properties this level is mainly responsible for the measured generation current. H(160) is a hole trap and it was just visible in the <100> wafer with 24h oxygenation by optical carrier injection. H(220) is also a hole trap. The concentration of this defect is independent of the oxygenation concentration and orientation of the wafer, but depends on the position of the diode on the wafer, i.e. the concentration increases with the distance from the center of the wafer to the edge. According to the material investigation the <111> material contains less defects than the <100> material. The only defect detected in CZ material is the TDD.

No defect could be detected in the epitaxial material, but the effective doping concentration of this material was about 50 times higher than the one of the float zone material, so defects in the concentration below 10^{10} cm^{-3} are below the limit of detection of the DLTS method.

3.2.2 Radiation-induced point defects of crucial importance for the radiation hardness of silicon detectors

Radiation induced *point defects* in silicon diodes were investigated after exposure to high doses of ^{60}Co gamma irradiation, using Deep Level Transient Fourier Spectroscopy (DLTFS) and Thermally Stimulated Current (TSC) methods. The main focus was on differences between standard and oxygen enriched material and the impact of the observed defect generation on the diode properties. It was shown that the beneficial oxygen effect consists not only in suppressing of deep acceptors (responsible for the type inversion effect in oxygen lean material) but in shallow donors creation as well. For the very first time it is shown that both the change of the effective doping concentration (depletion voltage) and the free charge carrier generation (reverse current) can be completely understood by the formation of defects detected by DLTFS and TSC methods. This is regarded to be a major breakthrough for the understanding of radiation damage and will hopefully also pave the road for an optimization of radiation tolerant detectors including hadron induced damage.
From the multitude of electrically active defects formed during irradiation three new ones have been found to be responsible for the macroscopic changes in float zone silicon diodes. Two of them (I and Γ) have close to midgap acceptor like levels and are generated in higher concentrations in STFZ silicon than in DOFZ (see Figure 2). The third one is a bi-stable donor (BD) generated in oxygen enriched silicon-DOFZ and epitaxial silicon (see Figure 2)[11-18].

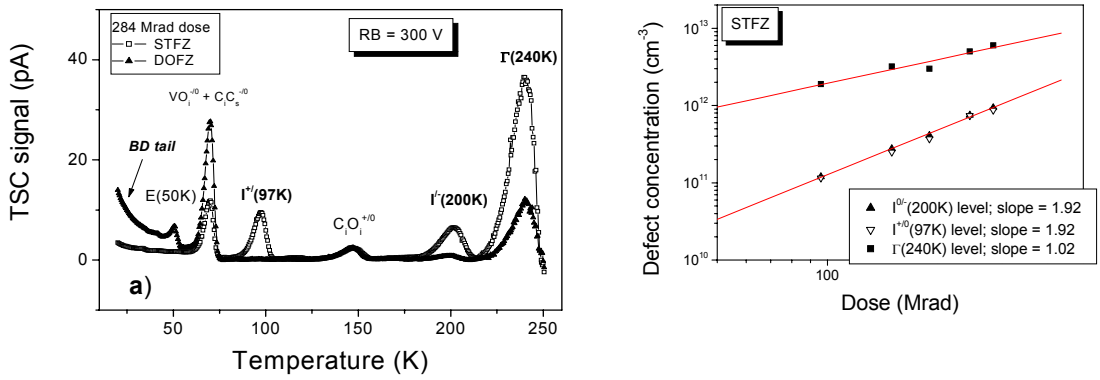

Figure 2.: a) TSC spectra for STFZ and DOFZ; b) dose dependence of I and Γ defects.

The formation of BD centers is largely enhanced in EPI/CZ diodes (epitaxial silicon grown on CZ substrate). The donor activity of the BD(98K) was proven via the Poole Frenkel effect when different reverse biases (RB) were applied during the TSC measurements (seeFigure 3).
The change in the activation enthalpy was evaluated from Arrhenius plots of the increasing part of the peak resulting in a zero field activation enthalpy of 0.225 eV. These properties of the BD center (donor activity, bi-stability, the zero field activation energy) together with the strong generation in oxygen enriched material suggest an identification with an oxygen-related donor center (cf TDD's which occur in CZ-Si).
The "Γ " defect has an acceptor level at E_v + 0.68 eV, linear dose dependence and can explain about 10% of the damage.

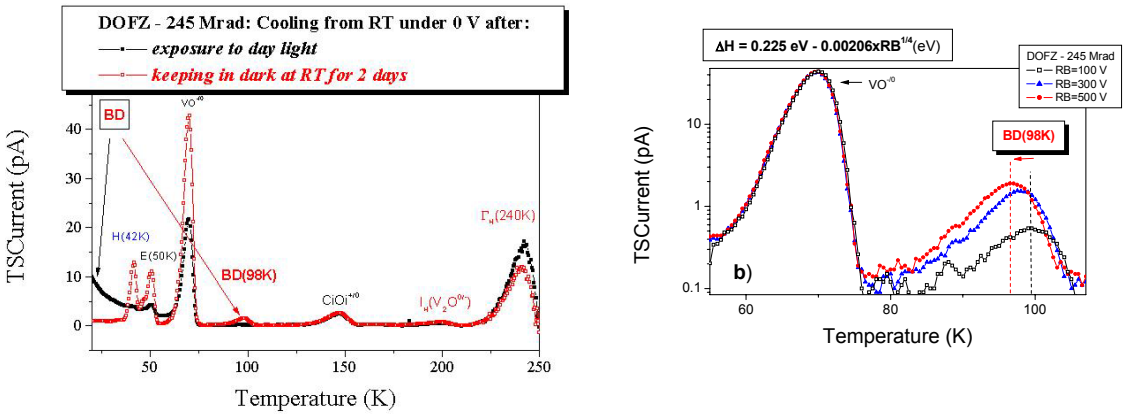

Figure 3.: The bistability (a) and the donor activity (b) of BD defects

The "I" defect is of amphoteric nature having both an acceptor state at E_c - 0.54 eV and a donor state at E_v + 0.23 eV, has a quadratic dose dependence, Fig.2b, and proved to be the main cause for the observed inversion of the space charge sign in the depletion region of STFZ diodes (alone it can account for more than 85% of the damage caused by gammas – shown in Figure 4).

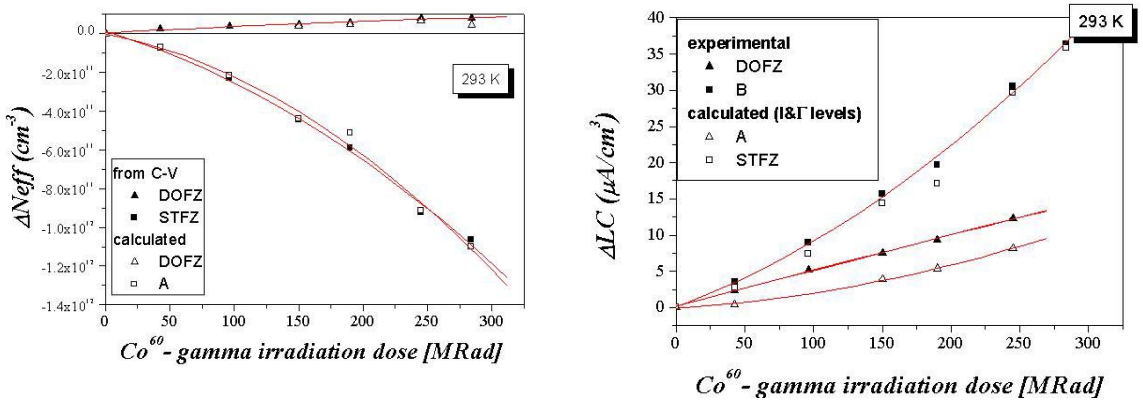

Figure 4.: The contribution of "I", "Γ" and "BD" centers to the change of the diodes properties with increasing dose.

The I-level is a good candidate to be associated with the divacancy-oxygen center (V_2O) based on various experimental data and kinetic modelling results [11-16]. According to these results the observed 2nd order generation of V_2O would suggest a formation via the reaction: VO+V= V_2O. This identification is, however, controversial since recent results for low-dose proton- and electron-irradiated DOFZ-samples and CZ-samples, with low carbon and hydrogen content, show the formation of a new defect, labelled the X-center, when the divacancy (V_2) anneals out [19-22].

Similar to V_2, the X-center is a double acceptor with level positions at E_c-0.46 eV (0/-transition) and E_c-0.20 eV (-/=), i.e., very close to those of V_2. As illustrated in Figure 5 by data obtained from high-resolution Laplace-DLTS, a close one-to-one correlation holds between the loss of V_2 and the growth of X. Further, the transformation process from V_2 to X exhibits first-order kinetics with a transformation rate that is proportional to the oxygen content, within the

experimental accuracy, in the Si-samples, Figure 6. Hence, there is strong evidence for assignment of the X-levels to the V_2O center. In addition, theory suggests that V_2O should be a double negative acceptor center with two levels in the upper part of the bandgap [23, 24]. On the other hand, theory also predicts a donor level in the lower part of the bandgap, as reported for the I-center but not for X-center. Further collaborative work is being pursued intensively by the different partners in order to resolve this issue and reach consensus about the identification of V_2O.

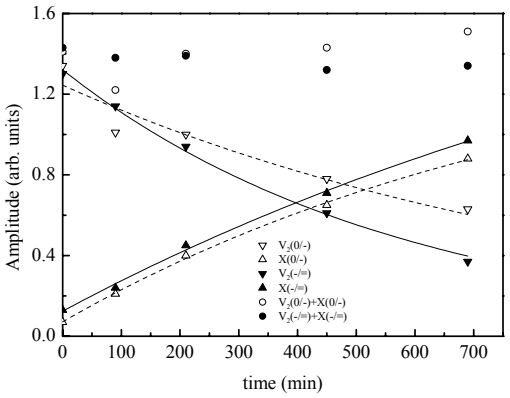

Figure 5: The amplitudes of the $V_2(0/-)$, X(0/-), $V_2(-/=)$ and X(-/=) peaks as a function of time during isothermal annealing at 250°C, obtained from high-energy resolution Laplace-DLTS measurements.

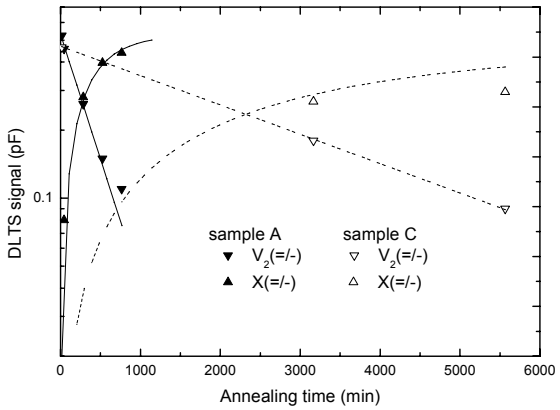

Figure 6.: Amplitude of the $V_2(=/-)$ and X(=/-) levels as function of annealing time at 250°C for sample A (oxygen content (2-3)x10^{17} cm^{-3}) and sample C (oxygen content (1-2)x10^{16} cm^{-3}). The solid and dashed curves represent the exponential loss/growth curves with rates of 4.2x10^{-5} s^{-1} and 5.2x10^{-6} s^{-1} for samples A and C, respectively.

From the above mentioned *point defects* which can influence the device properties only the I center and the BD defects could be detected after proton irradiation [16].

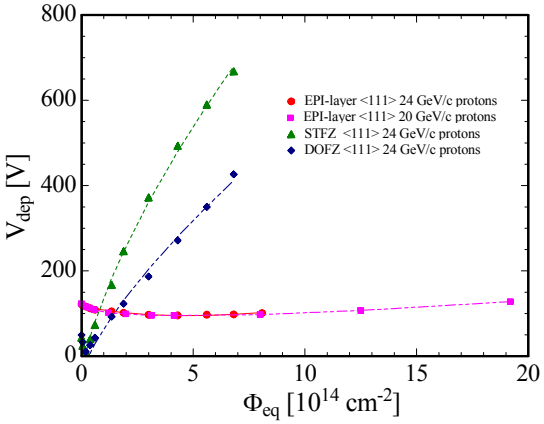

Figure 7.:
CERN-scenario experiment

Experiments have shown that the EPI/CZ devices are highly superior with respect to radiation tolerance to any standard or oxygenated float zone silicon devices and that contrary to those they do not exhibit any type inversion (see Figure 7) [17, 18]. The effect is attributed to damage induced generation of the bistable donor BD, tentatively associated as TDD. A distinct difference between TSC spectra, displayed in Fig.2.8a, for STFZ and EPI/CZ diodes is observed. The EPI/CZ sample shows in contrast to the FZ one a complete absence of the I-level and in the 80-

100K range the already mentioned BD (identification as shallow donor via the Poole-Frenkel effect – Fig.2.8b), whereas in L(90) seen for the STFZ sample much of the intensity for the donor state of the I center is contained.

A tentative explanation for the donor generation in EPI/CZ diodes is based on the fact that oxygen dimers present in the CZ-substrate will predominantly migrate into the EPI-bulk during the growth process, such that the ratio of dimers to interstitial Oxygen is much higher in epi than in standard or even oxygenated FZ silicon. Dimers are known to be precursors for irradiation induced thermal donor generation thus leading to an increase of the net positive space charge, more than balancing the negative space charge generation seen in FZ devices due to generation of deep acceptors.

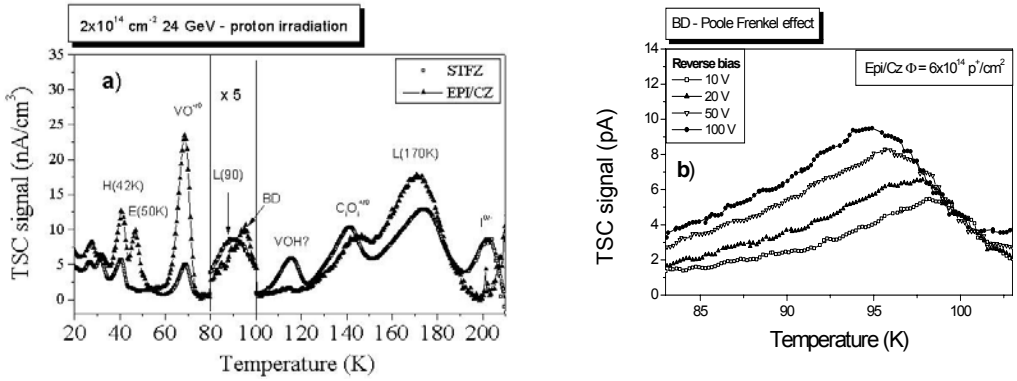

Figure 8.: a) TSC spectra measured after proton irradiation; b) Poole-Frenkel effect of the BD after proton irradiation

3.2.3 Shallow levels in gamma-irradiated STFZ and DOFZ Silicon

A detailed study of the role of shallow levels in determining the macroscopic properties of the detector is now in progress: this will be necessary for getting a complete overview of the phenomena of SCSI in FZ, DOFZ and CZ Si. To study shallow levels we used an experimental system which consists of a He liquid dewar where the sample holder is inserted: the temperature is determined by the height of the sample over the liquid He surface. The system provides an exceptionally good thermal exchange, allowing to probe with high sensitivity a very low temperature range, down to 4.2K. This temperature range was never studied before in TSC. Figure 9 shows preliminary results of TSC in the range (4.2 to 80K) with two samples, standard FZ Si and DOFZ Si γ-irradiated up to 300Mrad from ^{60}Co. Several peaks are observed: the identification of the related energy levels is still in progress.

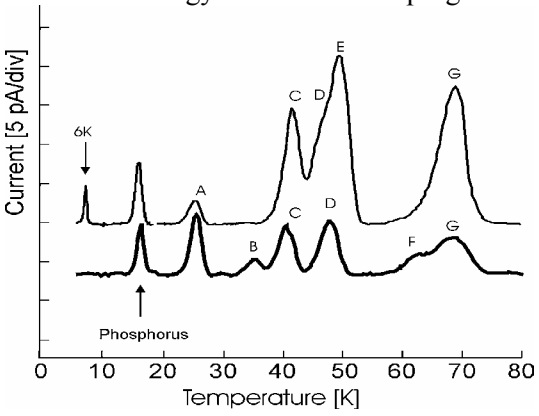

Figure 9.: TSC peaks observed in the range 4.2-80K in DOFZ and STFZ Si samples after irradiation with 300 MRad gammas. Solid line STFZ, light line DOFZ [25].

A peak at 6K that was never detected before in any Si material was found after irradiation of the DOFZ sample. Also peak E, at 50K, appears to be characteristic of the DOFZ Si. The TSC measurements performed in this range will allow us to detect the shallow levels related to traditional dopants as Phosphorus and Boron, as well as Thermal Donors (TDs), defects related to Oxygen aggregates often present in oxygen enriched Si. The measurements will be carried out also on CZ and epitaxial Si before and after irradiation to put into evidence the role of TDs in these materials.

3.3 Modeling of defect reaction kinetics in irradiated silicon

Applying the theory for diffusion-limited reactions, originally developed by Waite[26], a systematic simulation study of the roles of initial impurities and irradiation flux on the defect evolution during HEP-experiments has been initiated [27].

The starting material assumed is silicon with 10^{14} P/cm^3 (lower resistivity than detector grade silicon), with different concentrations of oxygen and carbon: ($2x10^{15}$ O/cm^3 and $3x10^{15}$ C/cm^3); ($2x10^{18}$ O/cm^3 and $3x10^{15}$ C/cm^3); ($2x10^{15}$ O/cm^3 and $3x10^{18}$ C/cm^3); and ($2x10^{18}$ O/cm^3 and $3x10^{18}$ C/cm^3), respectively. In the model calculations, one could observe a strong correlation between the effective concentration of donors and acceptors, the inversion phenomenon, the rates of generation of defects and the concentrations of impurities [28].

These results are now compared with experimental data in order to improve the modeling and to make the model reliable enough for predictive use.

3.4 Characterization of irradiation-induced defect clusters in silicon

One of the key problems identified in RD50 is understanding the reaction sequence that starts with 'violent' reactions in silicon. We are investigating this problem by subjecting silicon to bombardment by Si ions with MeV energies. Photoluminescence studies are being made of this material – we have shown that luminescence continues to be a useful monitor of the atomic-sized defects in the crystals at very large doses (after some annealing if necessary).

Two very frequently observed defects following 'violent' damage are the W and the X optical centers. The W centre has been variously identified with a penta-vacancy or a tri-interstitial complex. The stability ranges of these and other common defects are given below.

The W centre is believed to be an intrinsic centre, with no strong dependence on impurities, it has trigonal symmetry, it is 'hard' under compressive stress suggesting possibly an interstitial centre. There is said to be a quadratic increase in strength with the dose of electron irradiation.

Samples have been irradiated/implanted with 4-MeV Si ions to doses of $1x10^8$ to $1x10^{10}$ cm^{-2} using both p-type materials (samples 'A') and n-type materials (samples 'B') of similar boron and phosphorus concentrations, and similar carbon concentrations.

The radiation doses are sufficiently small that there is little quenching of the luminescence by heavy radiation damage. The p-type samples are shown in Figure 10. Following irradiation, the luminescence intensity of the W line is only slightly super-linear in the implant dose. With increasing annealing temperature, the strengths of the W luminescence in all the samples increases, as expected, and reaches a maximum that is again essentially linear in the dose; the temperature at which the maximum is reached moves to higher temperature with increasing dose, as is common with defects in irradiated silicon.

One key indicator of local environment is the width of a zero-phonon line, which measures the local strain near the optical centre. For example, the line width decreases with annealing, as the defects are annealed out. However, the extraordinary result is that for the relatively low doses used here, the width of the W line *decreases* with *increasing dose*, Figure 10. This result suggests that

the W centers have migrated from the heavily damaged regions formed by the 'violent' damage incident – suggesting the origin of the W centre is more likely to be interstitial-related than vacancy-related [29].

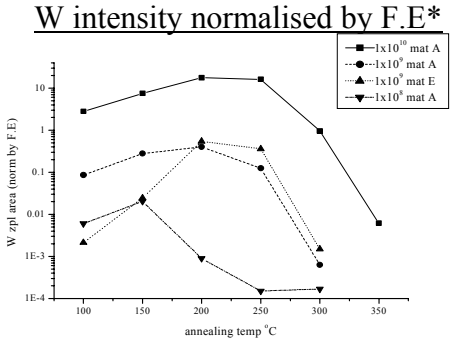

*Effect of using free exciton signal (F.E.) to normalise may *overestimate* dose dependence - at low dose W centre could saturate, so F.E normalisation decreases W too much; at high dose W centre may be less sensitive to competition than F.E so F.E. norm relatively increases W signal by too much

Figure 10.: Intensity of the W optical signal (normalized to the optical free exciton signal) in MeV self-ion irradiated/implanted p-type silicon.

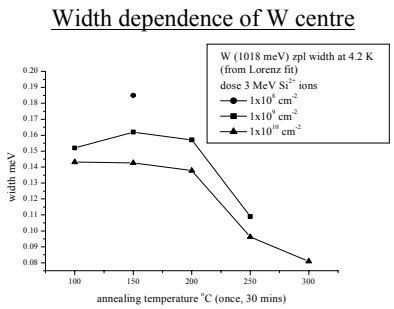

Figure 11.: Width of the W line at 4.2 K versus annealing temperature for silicon samples implanted with 3 MeV Si ions to doses between $1x10^8$ and $1x10^{10}$ cm^{-2}

3.5 High purity and lightly doped epitaxial layers of n-type Silicon Carbide (SiC).

Schottky barrier diodes have been fabricated onto epitaxial 4H-SiC with thickness in the range 7-40μm. Results on the performance of these detectors are discussed in section 7.2. Here we report on the main defects observed after irradiation up to ~$3x10^{13}$ cm^{-2} of 6.5 MeV protons [30] in 7μm-thick 4H-SiC n-type epilayers initially doped up to $4.43x10^{15}cm^{-3}$. DLTS measurements reveal at least 6 different irradiation-induced energy levels in the upper part of the bandgap ranging from ~0.2eV to ~1.6 eV below the conduction band edge (E_c)[30-32]. The most dominant level is associated with the so-called Z-center and located ~0.7 eV below E_c. The identity of the Z-center is not well established and different suggestions exist in the literature, e.g., a nitrogen-carbon related center or a carbon antisite-carbon vacancy (C_{Si}-V_C) complex [33-35]. The introduction rate of Z-centers is typically a few per cent per induced vacancy (or interstitial) for electrons and ions with energies in the MeV range.

A most prominent feature of irradiated n-type SiC-diodes is the high removal rate of charge carriers (electrons)[36]. This is exemplified in
Table 11 by results for diodes of the type discussed in 7.2.4. Removal rates as high as 400 cm^{-1} are observed for irradiation with 6.5 MeV protons. However, until now no indications of type inversion have been found for heavily irradiated SiC-diodes, which is a very promising result.

4 Defect Engineering

4.1 DOFZ silicon

It was demonstrated by the CERN RD48 (ROSE) collaboration that a considerable improvement in the change of the effective space charge concentration can be achieved in oxygen enriched silicon for charged hadron damage and gamma irradiation while after exposure to neutrons no or only little suppression was found [37,38]. The beneficial effect of oxygen had been discussed and modeled under the assumption that most probably the V_2O defect is responsible for a main part of the radiation induced negative space charge and that the formation of V_2O is suppressed in oxygen rich material [39, 40]. The model predictions support also the experimental observation that the oxygen effect is correlated with the radiation induced formation of point defects. This means that in neutron damage the oxygen effect is suppressed since the damage is dominated by the creation of defect clusters. On the other hand a maximal oxygen effect is expected when only point defects are created which is the case in ^{60}Co-gamma irradiation [38,41,42].

Numerous studies on hadron damage (protons of different energy, pions, neutrons, Lithium-ions) as well as electron damage (15 MeV, 900 MeV) had been performed on standard and oxygen enriched FZ silicon processed by different institutions on different FZ material from different manufacturer. The results of microscopic defect studies are presented in chapter “Defect and Material Characterization (DMC)” and those of macroscopic damage effects in chapter “Pad Detector Characterization (PDC)” of the status report.

Among these results a recent study of the Ioffe group had shown that by a special gettering treatment of n-type silicon a further reduction of β, i.e. the radiation induced increase of negative space charge per unit fluence, can be achieved in comparison to DOFZ material while for p-type material the effect is opposite [43] (see chapter PDC).

A break through in the understanding of gamma induced changes of the macroscopic detector properties on the basis of microscopic defects was achieved by recent studies on standard and differently oxygen enriched high resistivity float zone silicon irradiated up to a dose of 900 Mrad [11-14].

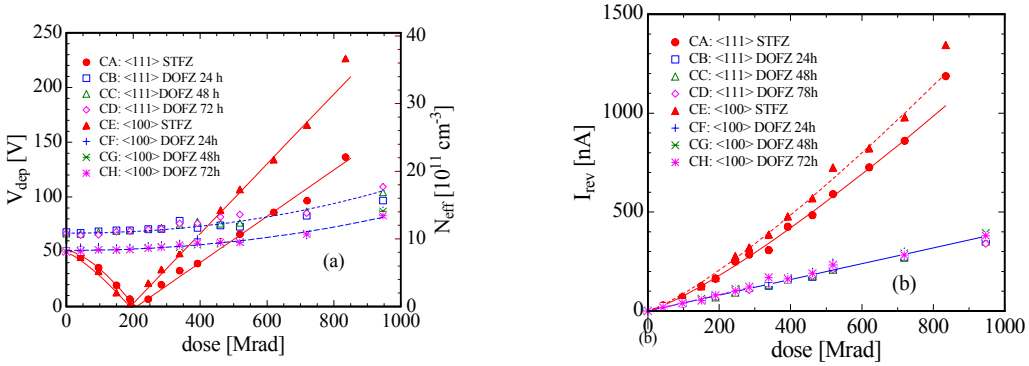

Figure 12: Dose dependence of the full depletion voltage (a) and the reverse current at full depletion (b) for standard (STFZ: <111>:full circle, <100> full triangle) and oxygenated (DOFZ: <111>:open symbols, <100>: crosses) devices.

Figure 12 demonstrates the development of the depletion voltage V_{dep} or effective space charge concentration N_{eff} and the reverse current at total depletion I_{rev} with the accumulated dose, for standard float-zone (STFZ) and three differently oxygenated float-zone (DOFZ) devices processed

by CiS (Germany) on <111> and <100> material. The main differences in the behavior of standard and oxygen enriched devices are:

- The detectors manufactured from standard material show the well known effect of space charge sign inversion (SCSI) at a specific dose of about 200 Mrad.
- For all oxygenated devices a small, monotonically and non-linear increase in the effective space charge density is observed. This implies that the effective space charge density becomes more positive caused by an introduction of donor like defects.
- The leakage current increase for standard material is found to be stronger than linear
- For all oxygenated detectors a linear dose dependence of the reverse current is observed.

In contrast to hadron damage the current increase of oxygen rich material is much smaller compared to that of the standard devices. But no differences in the reverse current increase could be observed between the differently oxygenated sensors themselves.

For the first time these observed changes of the macroscopic detector properties can be fully explained by radiation induced two deep acceptors and the creation of shallow donors being most probably early thermal double donors. These defects had been discovered and analyzed by detailed DLTS- and TSC-studies [11-13]. One of the deep acceptors can possibly be attributed to the V_2O complex, while the other one is so far an unknown defect (see chapter DMC). Further studies of these and other differently processed detectors were performed for irradiations up to ultra-high dose values between 0.9 and 1.76 Grad [44].

4.2 High resistivity Czochralski silicon

Silicon crystals grown by the Czochralski (Cz) method have a much higher oxygen concentration ([O] ≈ 4-20×10^{17} cm^{-3}) compared to any oxygen enriched DOFZ material ([O] ≈ 1-3×10^{17} cm^{-3}) due to the growth technology itself. But high resistivity Cz-silicon suited for detector application became available only in the last years after recent developments in the crystal growth technique (see e.g. [45]).

It is expected that such high concentration of oxygen will strongly influence the radiation induced creation of oxygen related defects and the defect kinetics resulting possibly in an improved radiation hardness beyond the level observed so far in DOFZ silicon. As shown by ^{60}Co gamma radiation damage studies of FZ silicon the formation of a deep acceptor (possibly V_2O) is strongly suppressed in oxygen enriched material and a creation of shallow donors (early TDD's) is observed (see chapter DMC). Both effects might be more pronounced in Cz material not only in case of radiation damage by gamma radiation but also by exposure to charged hadrons. In addition, it is known that in as grown Cz silicon oxygen is not only present as interstitial oxygen O_i but also in small concentration as oxygen dimers O_{2i} (see e.g. [46,47]) which also might have a strong impact on the defect formation (see section 4.4). Furthermore, it is well known that in Cz material different thermal donors can be formed or annihilated by specific heat treatments. This also may lead to a further possibility to influence the radiation tolerance of this material.

In the frame of this RD50 research project two different Cz materials have been investigated. Detectors were processed by two different groups. The group of the Helsinki Institute of Physics (HIP) initiated the manufacturing of detectors on high resistivity MCz (Magnetic Czochralski) silicon substrates at the Microelectronics Center of Helsinki University of Technology [48]. The MCz wafers were manufactured by Okmetic Ltd Finland. On the other hand devices were processed by the Hamburg-CiS collaboration (Germany) [49] on Cz-material grown by Sumitomo-Sitix (Japan). The material parameters are:

– MCz material: n-type, P doped, orientation <100>, resistivity ρ ≈ 900 Ωcm, thickness 380 µm, oxygen concentration [O] = 3.5×10^{17} cm^{-3}
– Cz material: n-type, P doped, orientation <100>, resistivity ρ ≈ 600 Ωcm, thickness 300 µm, oxygen concentration [O] = 8×10^{17} cm^{-3} , carbon concentration [C] = 5×10^{16} cm^{-3}.

The oxygen concentration of the MCz material had been measured by FTIR. For the Sumitomo-Sitix material the O- and C-concentration were measured by SIMS and IR by ITME [50]. In order to control the possible creation of thermal donors in this material radial resistivity profiles had been measured before processing, after standard oxidation and after a thermal treatment for annihilation of thermal donors (see Figure 13).

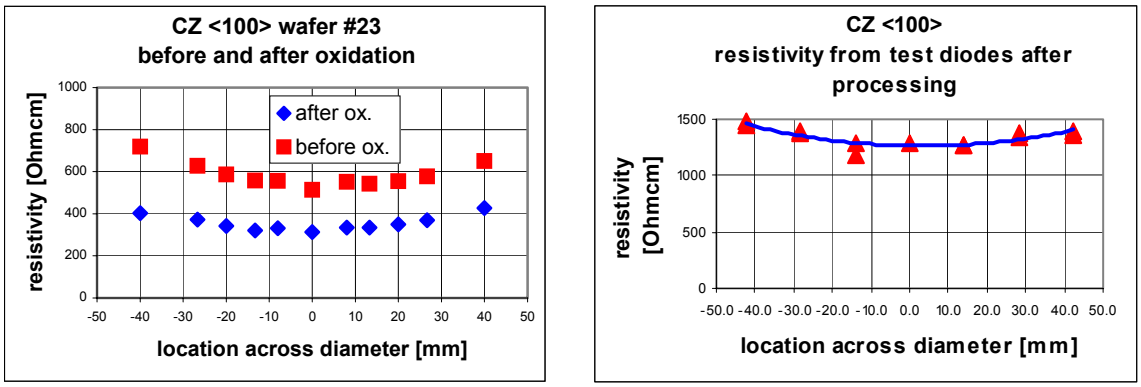

Figure 13.: Radial resistivity profile of Sumitomo-Sitix Cz silicon before and after thermal oxidation (left) and after annealing of thermal donors and final processing of test diodes (right).

Both materials had been characterized by DLTS after processing. For the MCz material two deep electron trap levels were detected and associated with thermally induced defects (see [51]). For the Cz- CiS devices no deep levels could be detected but a shallow level at E_C-0.12 eV, and a defect concentration of 3×10^{11} cm^{-3} was measured. This defect is associated with thermal double donors (TDD) which survived the so called thermal donor kill process or might be reactivated by the final process step. For a limited set of devices thermal donors were intentionally activated by thermal treatment at 400°C for 40 min. Due to this treatment the effective doping concentration changed from 3.3×10^{12} cm^{-3} to 7.1×10^{12} cm^{-3}.

The radiation hardness of both materials had been investigated by several irradiation campaigns at different facilities (see chapter PDC). The main results are:

MCz devices:

– For low energy protons (10 MeV, 20 MeV) space charge sign inversion (SCSI) is observed between 1×10^{14} cm^{-2} and 2×10^{14} cm^{-2} 1 MeV neutron equivalent fluence.
– The reverse current increase seems to be smaller compared to standard FZ- and DOFZ-devices.
– After neutron exposure the SCSI takes place between 3×10^{13} n/cm^2 and 8×10^{13} n/cm^2.
– After ^{60}Co gamma irradiation up to 1.2 Grad no SCSI can be detected and V_{dep} increases with dose due to a build-up of positive space charge.

Cz-devices:

- Irradiation experiments with 190 MeV pions at PSI and 20 GeV/c protons at CERN have shown that both the Thermal Donor (TD) killed as well as the TD generated material do not undergo SCSI in the full fluence range up to 1×10^{15} particles/cm^2 as measured by TCT (Transient Charge Technique). The overall change of the depletion voltage as function of fluence is considerably smaller compared to that of standard FZ- or DOFZ-silicon. The missing SCSI and the small change of V_{dep} can be explained by an introduction of shallow donors which at high fluences overcompensate the creation of deep acceptors. TSC measurements substantiated the introduction of shallow donors which are most probably early thermal double donors exhibiting a bistable behavior [16].
- No difference in the leakage current increase could be observed compared to standard FZ and DOFZ material.
- From TCT measurements trapping time constants were evaluated and the resulting damage parameter β_t is about the same as observed for STFZ and DOFZ detectors.
- Charge collection efficiency (CCE) measurements had been performed using a ^{244}Cm α-source. Up to fluences of about 6×10^{14} pions/cm^2 the degradation of CCE is about 15%.
- Beside the higher effective doping concentration of the TD generated material no substantial difference is observed in the fluence dependence of the effective doping concentration, the leakage current and the charge collection efficiency compared to the TD killed Cz material.

4.3 Thin epitaxial silicon layers

A different approach for increasing the radiation tolerance of silicon detectors is the use of thin epitaxial silicon layers. By the epitaxial growth technique a wide spread of silicon layers with different thicknesses and doping concentrations can be produced and also different types of substrate materials (Cz, FZ) with different doping can be used. This makes epitaxial silicon very attractive for the development of radiation hard thin pixel detectors. As a first step the growth of highly phosphorus doped epitaxial layers of 50 μm thickness was foreseen. The basic idea behind this approach is that a high doping concentration should lead to a considerable shift of the appearance of space charge sign inversion to much higher fluence values as observed for detectors processed on standard high resistivity FZ material. This assumption relies on experimental results on the so called donor removal presented in [52, 53]. It was shown that the donor removal constant decreases with increasing doping concentration. Due to the small thickness of the epi-layer also an out-diffusion of primary defects into the substrate and capture at gettering sites might play a role for the effective defect formation. A further benefit of using thin silicon layers is related to the requirement of low material budget in silicon vertex detectors for future hadron as well as lepton collider experiments. But this needs an efficient low cost thinning procedure of the substrate (see also section 6.2).

These considerations have led to the development and first production of detectors by CiS on thin low resistivity epitaxial silicon layers grown on Cz substrates by ITME. The material parameters are:

- EPI-layer: n-type P doped, orientation <111>, resistivity ρ = 50 Ωcm, thickness 50 μm
- Cz substrate: n-type, Sb doped, orientation <111>, resistivity ρ = 0.015 Ωcm, thickness 320 μm

The oxygen and carbon depth profiles as measured by SIMS are shown in Figure 14, and the resistivity profile is presented in Figure 15. Both the SIMS and resistivity measurements have been performed by ITME [54].

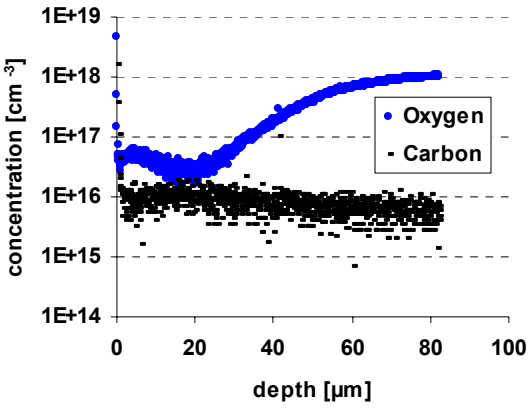

Figure 14: Depth profile of oxygen and carbon concentration measured by SIMS.

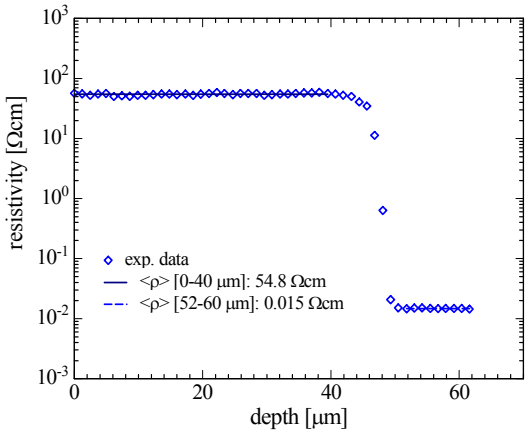

Figure 15: Resistivity depth profile of a 50 µm thick EPI-layer.

Due to the high oxygen content in the Cz-Si substrate and the high temperature during the epitaxial growth process an out-diffusion of oxygen into the epi-layer is present. A minimal concentration of about 3×10^{16} cm^{-3} is measured in the range between 15 µm and 20 µm, while the average concentration across the total layer thickness is 9×10^{16} cm^{-3}. On the other hand the carbon concentration is in average below 10^{16} cm^{-3} (detection limit). From the measurements of the resistivity profile (Figure 15) an average value of 54.8 Ωcm is deduced for the range between 0 and 40 µm. After device processing the resistivity was evaluated from C-V measurements resulting in slightly higher values of about 63 Ωcm corresponding to an effective doping concentration of 6.6×10^{13} cm^{-3}.
DLTS measurements on as processed devices had proven that the epitaxial process as well as the device process do not introduce electrically active defects with concentrations larger than approx. 10^{10} cm^{-3} , i.e. the detection limit, which is about 10^{-4} of the shallow doping concentration.

Several irradiation experiments with protons of different energy, reactor neutrons, Li-ions, high energy electrons and ^{60}Co gamma rays had been performed. The results derived from these experiments are partly published [16, 18, 55, 56] and presented in chapter PDC and DMC. Only the most significant results will be summarized here:

- For high energy protons up to about 10^{16} p/cm^2 the EPI-devices show no type inversion. The depletion voltage V_{dep} as function of fluence decreases slightly by about 25 % in the range 0-1×10^{15} p/cm^2 , traversing a shallow minimum and followed by an increase in the range up to 10^{16} p/cm^2. This is the most important feature of EPI silicon, even exceeding the expectation resulting from the higher initial doping concentration and the smaller amount of donor removal mentioned above. Therefore, the evolution of V_{dep} or N_{eff} with fluence can only be explained by an introduction of shallow donors overcompensating the generation of deep acceptors at high fluences. This hypothesis had been confirmed by TSC (Thermally Stimulated Current) studies concerning the detection of a “bistable” donor in proton irradiated EPI-diodes [16] (see also chapter DMC).
- In contrast to proton damage the neutron irradiated diodes undergo type inversion at about 2×10^{15} n/cm^2 This difference might be explained by the different defect generation mechanisms

involved in high energy proton and reactor neutron damage, where neutron damage leads predominantly to an introduction of clusters while proton damage results in a larger introduction rate for the formation of point defects compared to clusters.

– Studies on the charge collection efficiency after neutron damage show that at 8×10^{15} n/cm^2 the efficiency decreases to about 60 % for an average electric field strength of 26 kV/cm across the 50 μm thick epitaxial layer. Such loss in efficiency should be tolerable for the detection of minimum ionizing particles (mip) in thin pixel detectors by using state of the art readout electronics

Further steps of the R&D program will be the production and investigation of epitaxial layers with different thicknesses (25 μm, 75 μm), doping concentrations, oxygen enrichment of the epi-layer by oxygen diffusion from the SiO_2 surface layer and growth of epi-layers on highly doped FZ substrates.

4.4 Oxygen dimers in silicon

4.4.1 Introduction

One of the defect engineering approaches described in the RD50 proposal is the use of oxygen dimer enriched silicon. The main idea is to produce a silicon material that contains oxygen dimers (O_{2i}) instead of mono atomic oxygen (O_i). Such a defect engineered material has completely different defect kinetics during irradiation. For example, in standard silicon material subject to irradiation there is a production of VO (A center) defects and V_2O defects from the capture of moving vacancies in the silicon lattice by mono atomic oxygen. While the VO center will only be charged at cryogenic temperatures (<80 K) the V_2O defect is known to be charged up to 90% already at room temperature and therefore has detrimental effects on the macroscopic detector parameters. On the other hand, the capture of vacancies by oxygen dimers O_{2i} leads to the production of the VO_2 defect, known to be neutral and possibly less damageable to detectors. Furthermore, O_{2i} can act as a sink for migrating interstials I by forming the IO_{2i} defect [13, 57], and finally it is already accepted that O_{2i} are precursors for the formation of earlier stage thermal donors [58].

The goal of the dimer experiment is to produce dimers in different kind of silicon material and then test for the radiation hardness using 24GeV/c protons at the CERN PS. We have designed the experiment so that we could get confirmation that the material contained oxygen dimer after the dimerization process (Fourier Transform Infra Red characterization on bulk material) and also to allow both macroscopic and microscopic characterization of the silicon diodes after proton irradiation.

4.4.2 Samples description

To have the best resolution for the FTIR measurements we need bulk silicon a few mm thick. We got samples from ITME that included 3 wafers of Cz material with different oxygen and carbon concentration, resistivity and thickness, and one wafer of float zone material with a thickness of 3mm.

In order to study the performance of the silicon diodes we also have 0.25 cm^2 p^+nn^+ 300μm thick diodes from the Hamburg group. We had three types of diodes: standard float zone (initial depletion voltage around 60V), oxygenated float zone (initial depletion voltage around 50V) and Cz material (initial depletion voltage around 200V). We dimerized three diodes of each type.

4.4.3 Dimerization process

The way to produce the appearance of oxygen dimers in the silicon material is by carefully playing with the existing oxygen impurities and other defects present in the original material. This can be

performed by irradiating the samples with a point defect inducing radiation, like low energy electrons for example, and is a temperature dependent process. The reactions that are thought to lead to the formation of oxygen dimers are the capture of the mobile (hence the high temperature) *VO* defect by mono atomic oxygen ($VO_i + O_i \rightarrow VO_{2i}$) and then the capture of interstitials *I* in the silicon lattice by the formed VO_2 defect ($I + VO_{2i} \rightarrow O_{2i}$). J.L. Lindstroem demonstrated in 1997 [59] that it is possible to convert O_i into O_{2i} in silicon by irradiating the material with electrons of 2.5MeV at 350 °C up to a fluence of $1x10^{18}$ e/cm^2, using the Lund electron beam. This source not being available anymore, we used a source of 6 MeV electrons at the KTH (Stockholm) facility. The dimerization process happened in June 2003, the samples irradiated were 11 pieces total of the bulk material of different types and 9 diodes as described in the previous section.

4.4.4 CERN-scenario proton irradiation: preliminary results and interpretation

Once we received the dimerized diodes, we characterized them using the new probe station of B28 at CERN. We observed that the dimerized diodes could not be fully depleted. We then conducted a proton irradiation following a so-called CERN-scenario of one dimerized diode of each type and of 2 control diodes of each type for a total of 9 diodes. We reached a total fluence of $1.05x10^{14}$ p/cm^2 . As a function of fluence the control samples show the expected curves of depletion voltage and leakage current. As for the dimerized samples, since the depletion voltage couldn't be reached, we inferred it using the following relations:

$$C = A\sqrt{\frac{\varepsilon\varepsilon_0 q_0 N_{eff}}{2V}} \qquad N_{eff} = \frac{2\varepsilon\varepsilon_0 V_{fd}}{q_0 d^2}$$

That is, we took the slope of $1/C^2$ vs V to get N_{eff} and then computed V_{fd}. Those relations are valid for unirradiated material and at low voltages. To assess the reliability of this method we compared the inferred V_{fd} with the measured value for the control samples. Looking at the curve of the inferred V_{fd} as a function of fluence we see a very different behavior depending on the oxygen content of the material: for the standard float zone diode the inferred V_{fd} is of the order of 550V (corresponding to an effective concentration of defects of the order of a few 10^{12} /cm^3) and significantly decreases with fluence while for the oxygenated float zone and the Cz diodes, the inferred V_{fd} is of the order of 100,000V (and a corresponding N_{eff} around 10^{15}/cm^3) and is constant as a function of fluence. We show the curve of the standard float zone dimerized diode on the left (Figure 16), while on the right (Figure 17) we show the curve for the various non-dimerized diodes.

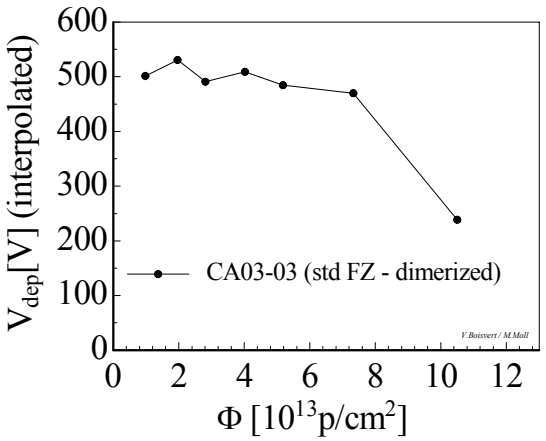

Figure 16: Irradiation with 24 GeV/c protons (CERN-scenario) of a dimerized std. FZ diode.

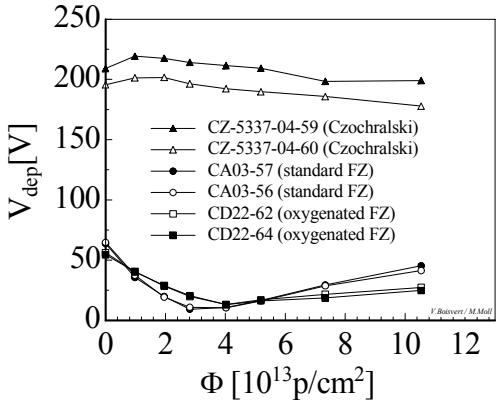

Figure 17.: Irradiation with 24 GeV/c protons (CERN-scenario) of the reference diodes.

So far these results are very different from the results that the Brunel group published [60, 61], although they had used an unknown dose from a ^{60}Co gamma source for the dimerization process. Preliminary interpretation of the results suggest that the dimerization process used in this experiment does not lead to a usable particle detector material. In fact the material is radically changed by the dimerization process and constitute a novel ground on which to perform macroscopic as well as microscopic characterization. It could be that the thermal donors (possibly chains of mono atomic oxygen atoms) that are created alongside the oxygen dimer, overwhelm the beneficial effects provided by the oxygen dimers.

4.4.5 IR and TSC measurements

We also report on very preliminary results from microscopic characterization. A Fast Fourier Infrared measurement of a Cz piece of silicon has been performed [62](see Figure 18). The spectrum shows clearly the presence of the oxygen dimer (concentration of $4x10^{16}$ cm^{-3} and the VO_2 defect (concentration of $2x10^{16}$ cm^{-3}). We also see the VO defect, indicating that the temperature during the dimerization was slightly less than 350°C. Studies by the Lund group [62] tend to indicate that the fraction of dimer produced is 4% of the initial oxygen concentration, independent of the oxygen concentration. Figure 19 shows a Thermally Stimulated Current measurement [63]. DLTS measurements were not possible since the diodes are too full of defects. The TSC spectrum shows that, similarly to the macroscopic measurements, the standard float zone diode gives the strongest TSC signal since it is less full of defects than the oxygenated float zone and the Cz diodes. These results are preliminary and we are currently analyzing them.

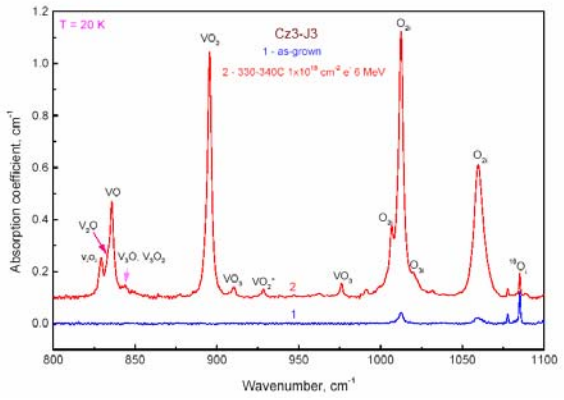

Figure 18.: FTIR spectrum at 20K of a Cz piece of bulk silicon showing the as grown signal and the dimerized signal [62].

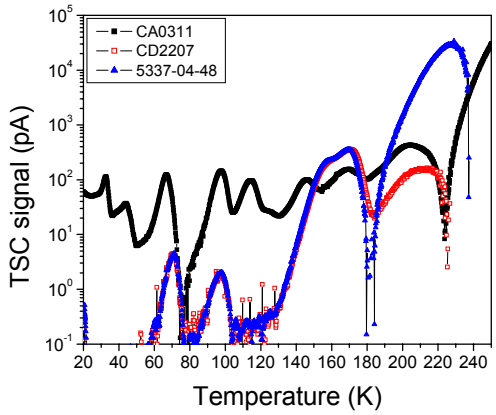

Figure 19.: TSC spectrum after forward injection at 20K (reverse bias of 100V) of three dimerized diodes: CA03-11 is a float zone, CD22-07 is an oxygenated float zone and 5337-04-48 is a Cz diode [63].

4.5 Defect engineering by pre-irradiation treatments

Pre-irradiation of silicon by fast neutrons followed by thermal annealing leads to the formation of sinks for primary radiation defects. These sinks are complexes of radiation induced defects with neutral impurities, such as C and O that are always present in silicon crystals. Such a method of

preliminary irradiation is expected to increase the radiation hardness of silicon. The best effect is achieved in each concrete case by optimizing the concentration of sinks [64, 65, 66].

The influence of various pre-radiation processes with subsequent annealing on the radiation hardness of float zone (FZ) silicon was tested by optical transmission measurements [67]. The preliminary irradiation was performed by reactor neutrons ($\Phi=10^{16}$ n cm^{-2}). After pre-radiation processing all samples, including the reference samples, were annealed for two hours at 800°C. Then all samples were re-irradiated with neutrons of the same fluence (10^{16} n cm^{-2}).

The optical analysis, based on infrared transmission spectra, is the most sensitive method to study defects produced by fast neutrons in FZ silicon. The so-called near-edge absorption monotonically decreases with wavelength. The selective absorption band with a maximum at 1.8 μm is related to the presence of divacancies. The additional near-edge absorption in Si which appears after irradiation with a fluence ~ 10^{16} n/cm^2 is caused by disordered regions that have a vacancy type nature. The investigation of absorption spectra in the spectral range 1.1÷2 microns on a large set of samples were carried out to study various combinations of pre-irradiation procedures. Typical transmission spectra in the spectral range 1.1÷2 microns are shown in Figure 20 for non-irradiated samples annealed at 800°C for 2 hours (curve c), for samples annealed at 800°C for 2 hours and then irradiated by fast neutrons $\Phi=10^{16}$ n/cm^2 (curve a) and for samples pre-irradiated by fast neutrons ($\Phi=10^{16}$ n/cm^2), then annealed and once more irradiated by the same fluence of fast neutrons (curve b). By comparing curve b (sample pre-irradiated) with curve a one can see a decrease in the additional absorption. The apparent distinction in intensity of the transmission spectra should be only due to the pre-irradiation treatment by fast neutrons. As follows from Figure 20, the intensity of the absorption of the reference samples is greater than in pre-irradiated samples. Thus, the given results evidently show that pre-irradiation treatment yields in a less intensive formation of radiation induced defects [68].

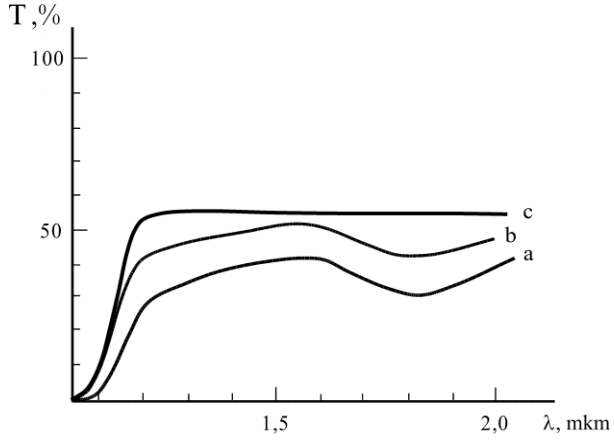

Figure 20.: Optical transmission spectra measured after different irradiation treatments (see text).

Neutron transmutation doping (NTD) of silicon is a particular process of pre-irradiation and is expected to improve the radiation tolerance of silicon [65]. The neutron transmutation doping was carried out in a thermal column of a Kiev reactor WWR-M type. Reference p-type Si samples had a specific resistivity of (2-10) kΩcm. After irradiation with thermal neutrons and annealing at 850°C for 2 hours we obtained p- type Si samples with a resistivity of (12-40) kΩcm and n- type Si samples with a resistivity of 3.07 kΩcm corresponding to a carrier concentration of $n=1.4\times10^{12}cm^{-3}$. Carrier removal studies on n- and p-type NTD silicon were performed by irradiation with ^{60}Co gamma rays and fast reactor neutrons with an effective energy of E_n~1 MeV. The resulting carrier removal rates of the n-type NTD sample are about a factor 10 smaller for gamma irradiation and a factor 2 for neutron irradiation compared to the reference samples [69,70]. This reduction could be due to sinks for defects introduced in the silicon bulk by neutron transmutation doping and the

particular annealing procedure. However, further investigations especially on diodes produced from NTD material have to be performed.

The next step will be the processing of test detectors on pre-irradiated and untreated high resistivity FZ and Cz silicon by ICT-IRST in Trento, and investigations of the radiation tolerance of these devices will be performed.

5 Pad Detector Characterization (PDC)

5.1 Introduction

The macroscopic effects of radiation-induced defects can be classified into three categories [37].

First, the defects introduce generation-recombination centers that in turn result to increased detector leakage current. However, operating the detectors at a moderately reduced temperature of about -10°C, the reverse current is largely reduced.

Second, the radiation-induced acceptor type defects compensate the initial positive space charge of n-type silicon created by the donor doping. Silicon particle detectors are pin-structures designed to operate in full depletion mode at a moderate reverse bias voltage. Therefore, radiation induced defects increase the voltage required for full depletion. In the worst case, the breakdown voltage of the pin-structure may be reached before the end of the experiment.

The third macroscopic effect is the deterioration of charge collection efficiency due to the trapping of charge carriers which eventually leads to the reduction in the signal height.

24 out of the 55 RD50 institutes are participating the Pad Detector Characterization (PDC) research line. Defect engineering has turned to be a successful approach to improve the radiation tolerance of silicon detectors. Therefore, the PDC and Defect Engineering (DE) research lines cannot be treated completely separately. On the practical working level, most of the PDC institutes are also participating DE research line.

5.2 PAD Detector Mask

The research activity of RD50 Pad Detector Characterization research line includes processing of pad detectors (test diodes), irradiation of test structures and characterization of irradiated devices with different measurement methods. In order to efficiently distribute test devices to the collaborators, RD50 has designed a common photolithography mask set. The common test structure design excludes the possible contribution of different device geometries to the macroscopic effects. A microscopic view of a RD50 pad detector is shown in Figure 21 .

The increase of the detectors leakage current and evolution of the full depletion voltage are measured usually with conventional probe stations equipped with proper SMU's (Source Meter Unit) and LCR's (capacitance measurement unit). Special requirement in radiation hardness studies is the need for often very high measurement voltages. As part of the CERN Silicon Facility a detector laboratory war recently constructed in Building 28. This laboratory is, as the bond lab, under the control of the EP-TA1-SD section, which is providing also service for the RD50 project. As a first installation a CV/IV bench test with a manual probe for measuring test structures was built and can now be partly used by RD50.

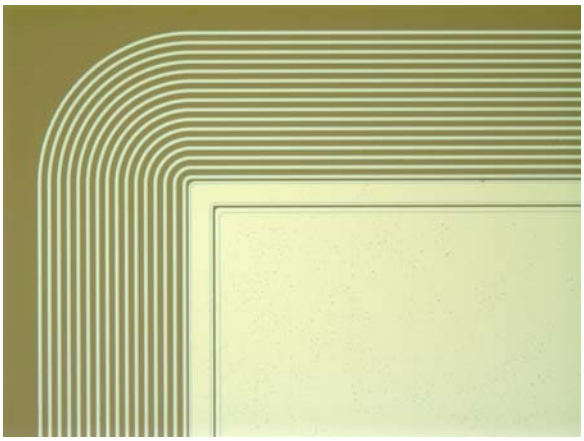

Figure 21.: Corner of RD50 pad detector. From left to right: multi-guardring structure (16μm), wide guard ring (100μm) and detector's active area. The distance between the active area implant and the first guard ring is 10μm.

In the middle of the pad detector (not seen in Figure 21), there is an opening in the metallization for the optical excitation. This is needed for the TCT (Transient Current Technique) measurements (see e.g.[71]). From the current transients, information of the detector's internal electric field can be obtained, thus the TCT is a suitable tool for characterization of type inversion (SCSI) and also for measurement of full depletion voltage. In the TCT measurement, the pin-diode is illuminated with a red laser that has an absorption depth of only a few micrometers in silicon. Thus, just one type of charge carriers will drift across the detector: electrons when the laser illuminates the p^+ side or holes when the laser illuminates the n^+ side. Before the SCSI, the silicon bulk is n-type and thus the junction is on the p^+ side, and electrons drift from the high field to the low field with a decreasing induced current with time. On the other hand, holes drift from the low field to the high field with an increasing induced current with time. After the SCSI, the bulk is n-type and the junction is near the n^+ side, and the shapes of the electron and hole currents are reversed compared to those before the SCSI. Thus, the type of the bulk can be deduced from the shape of the drift current, or the shape of the electric field, in the detector.

During the first year of RD50, the collaborating institutes have performed several irradiation campaigns. The motivation to irradiate devices with various sources arises from the fact that, the introduction of defects into the silicon crystal depends on the type of the incident radiation. The pad detectors, often defect engineered, have been irradiated in proton beams with various energies, with neutrons, electrons, gammas and Li ion beams. Electrical (macroscopic) properties of silicon detectors depend crucially on the (microscopic) defect formation processes in silicon material. The defects can be divided roughly into two categories: point defects (mainly vacancies and their complexes) and defect clusters. In a defect cluster the concentration of point defects exceeds 10^{18} cm^{-3}, i.e. the solid solubility of oxygen into the silicon. Generally, low energy (e.g. 10 MeV) protons cause points defects and high energy (e.g. >50 MeV) induces in addition to point defects, also clustered defect complexes into the silicon lattice. Additionally, the interaction of oxygen atoms with defects, or the beneficial effect of oxygenation, is affected by the complexion of defects, i.e. it is dependent on the energy of the incident proton irradiation.

According to the Non Ionizing Energy Loss (NIEL) hypothesis, the effects of radiation damage caused by any type of radiation and energy can be scaled. The scaling is typically expressed in 1 MeV neutron equivalent fluencies. However, the NIEL hypothesis does not hold in the case of silicon material with high oxygen concentration. According to one proposed explanation, the oxygen atoms do not effectively interact with the clustered defect complexes. One subject of the RD50 Pad Detector Characterization research line is to verify experimentally these models based on numerical calculations. To that end we need to irradiate silicon with high oxygen concentration (Cz-Si, DOFZ) and silicon with low oxygen concentration (Fz-Si) using different beams and beam energies.

5.3 STFZ, DOFZ and CZ diodes irradiated with 24 GeV/c protons

5.3.1 STFZ and DOFZ - CERN scenario and annealing studies after hadron damage

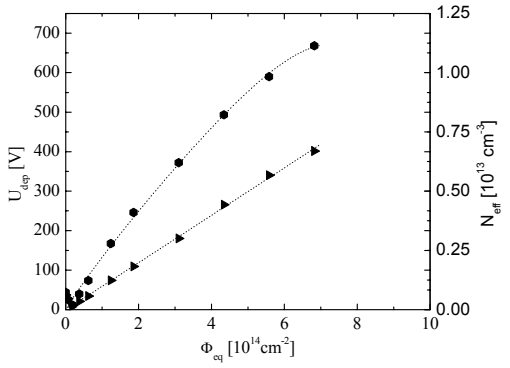

Figure 22a: CERN scenario experiment with 24GeV/c protons. Comparison of STFZ (top, $\beta = 2.2 \cdot 10^{-2}$/cm for $\Phi_{eq} < 2e14 cm^{-2}$) and DOFZ (bottom curve, $\beta = 9.5 \cdot 10^{-3}$ cm^{-1}).

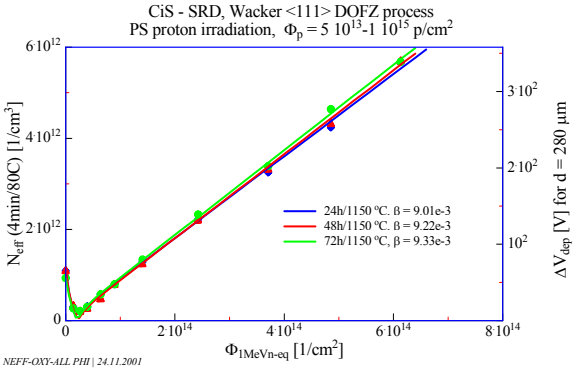

Figure 22b: CERN scenario experiments for DOFZ diodes. Practically no difference between oxygen enrichment with 24, 48 and 72h/1150C observed ($\beta = 9.5 \cdot 10^{-3}$ cm^{-1}).

Results shown already on the 1st RD50 workshop at CERN, October 2002 (see [49]), have meanwhile been complemented by additional measurements resp. confirmed [72]. Although in CERN scenario measurements (with 24 GeV/c proton irradiation) a large improvement in the beta-value was observed for DOFZ (diffusion oxygenated float zone) samples as compared to STFZ (standard float zone), see Figure 22a, there is practically no difference between a 24h/1150C and a 72h/1150C Oxygen diffusion, see Figure 22 b.

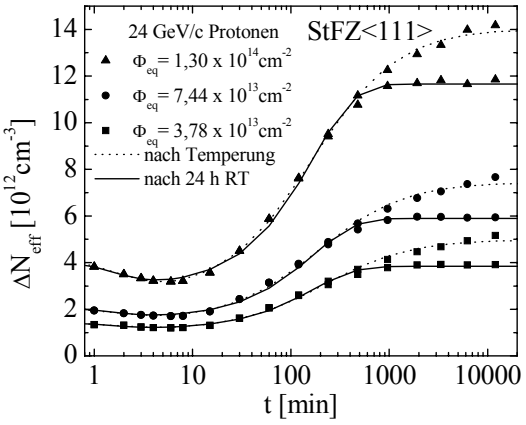

Figure 23.a: Annealing curves for STFZ samples after PS-proton irradiation

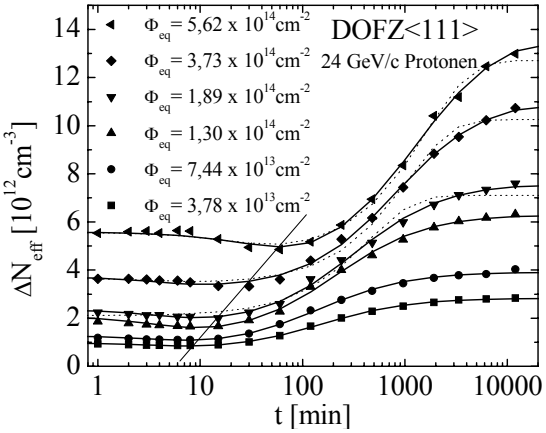

Figure 23b.: Annealing curves for DOFZ samples after PS-proton irradiation

Also the results of the long term annealing studies at 80°C after 24 GeV/c proton irradiation have been confirmed with a new batch of diodes, using 72h/1150C O-diffusion [72]. Figure 23 gives an

overview of all measured annealing curves after 24GeV/c proton irradiation. Especially for the STFZ material it proved essential to store the diodes after each annealing step for 24 h at RT.
While in this case immediately after each annealing step the curves could be best fitted with a 2nd order approach fits performed after each 24h RT storage revealed a 1st order exponential behavior. In the case of DOFZ an overall 2nd order seems to work as well. The Hamburg-model analysis of these curves [72] confirmed the earlier evaluation [49]. The stable damage N_C and reverse annealing amplitude N_Y are plotted in Figure 24. An updated set of parameters is available on request. As already commented in [49] it is now confirmed that while the reverse annealing time constant as measured for STFZ does not depend on the fluence (τ_Y = 200min ± 10%), in the case of DOFZ one gets a linear increase with fluence (rising to 1250 min at $\Phi_{eq} = 6*10^{14}/cm^2$, see Figure 25). This delay in reverse annealing is certainly a large beneficial effect, since it reduces the effect of reverse anneal at RT maintenance periods after higher irradiation fluences. It should be emphasized however that for a real 2nd order reverse annealing the time constant should instead be proportional to the inverse of the fluence! This discrepancy would need further investigation.

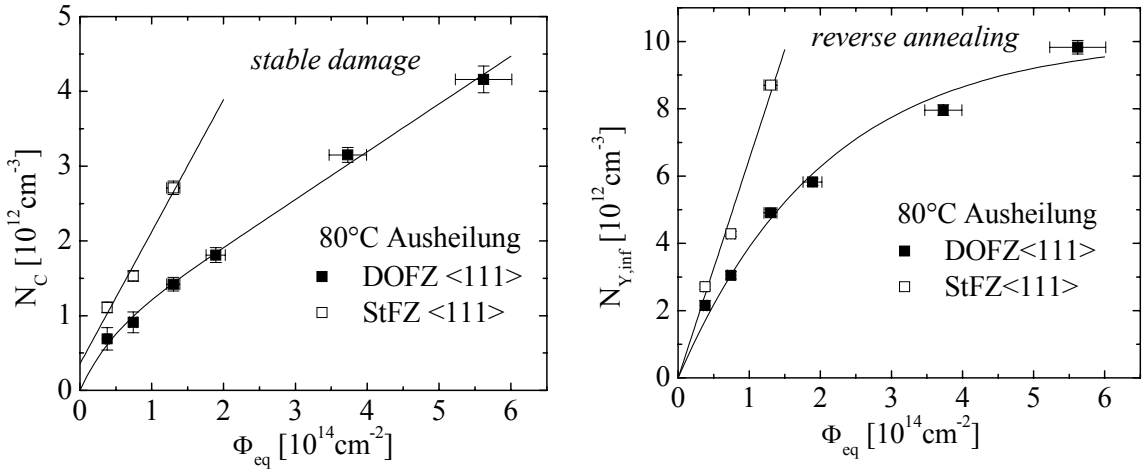

a) b)

Figure 24.: Hamburg model analysis parameters extracted from annealing after 24 GeV/c proton irradiation. a): stable damage parameter N_C, b): reverse annealing amplitude $N_{Y,inf}$

Annealing studies for N_{eff} after neutron irradiation as well as the development of the reverse current (both after proton and neutron irradiation) have also been performed again. The earlier results have widely been confirmed and will not be discussed here (see overview in [73]and literature cited there).

A general note of caution should be added. The Hamburg model parameters can only be regarded to give a parameterization, useful for projections to LHC or SLHC operational scenarios but do not claim that we have reached a complete understanding of the physics background. Also it should be emphasized that the parameters may vary according to the different used silicon material and manufacturing process. Such the results shown here are valid for diodes as processed by CiS on Wacker <111> n-type silicon, within narrow limits they are independent of the individual manufacturing batch!

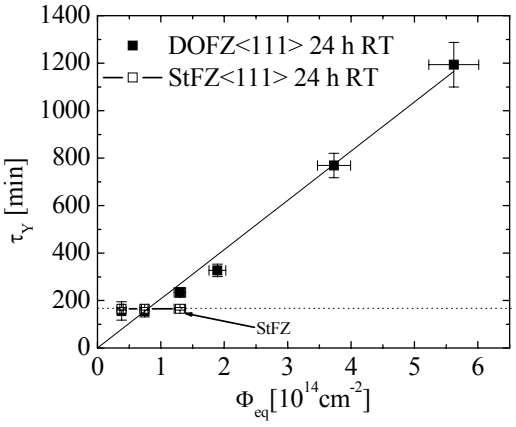

Figure 25.: Reverse annealing time constant for proton irradiated STFZ and DOFZ diodes, each measured after 24h RT relaxation (see text)

5.3.2 Cz-diodes, CERN scenario and annealing studies after hadron irradiation.

In contrast to FZ results, test diodes manufactured on Czochralski material (1300 Ωcm after TD kill process) do not show any type inversion during a CERN scenario experiment (result proven with TCT measurements [72, 74]), see Figure 42. The annealing curves (after proton irradiation) look rather strange, see Figure 26. It is interesting to note, that at the maximum of these curves at around 5 min at 80C the V_{dep} has always a larger value than that before irradiation! Hence in the Hamburg-model analysis of ΔN_{eff} the stable damage parameter N_C is negative! During prolonged annealing the material will then eventually also undergo type inversion, especially proven by additional TCT measurements. Disregarding the plateau of the annealing curves it is however possible to parameterize the fits in such a way that both the stable damage N_C and the reverse annealing amplitude value $N_{Y,inf}$ (from ΔN_{eff} reached at very large annealing times) can be displayed as function of the 1MeV neutron equivalent fluence Φ_{eq}, see Figure 27.

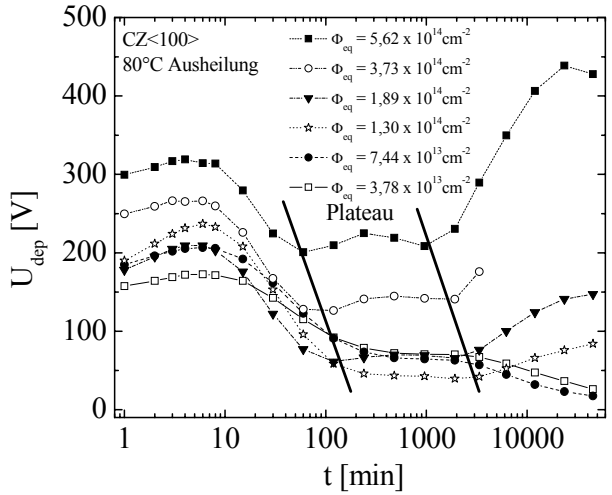

Figure 26.: Annealing curves (measured depletion voltage) at 80C of Cz-diodes after 24 GeV/c p-damage

Measurements of the reverse current as well as its annealing give practically identical results as those obtained from STFZ and DOFZ diodes. Also the effective trapping probabilities for electrons resp. holes are the same as obtained for STFZ and DOFZ diodes (see [72]).

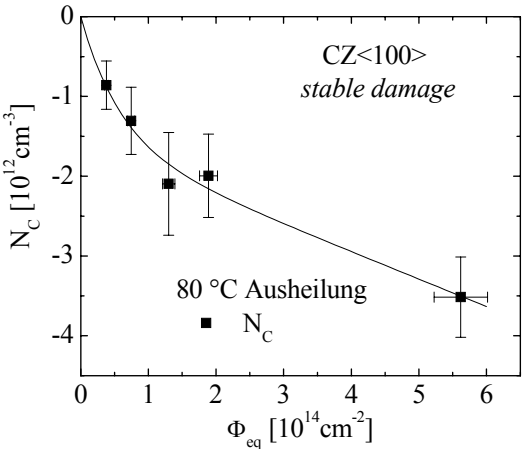

Figure 27.a: stable damage N_C for p-irradiated Cz

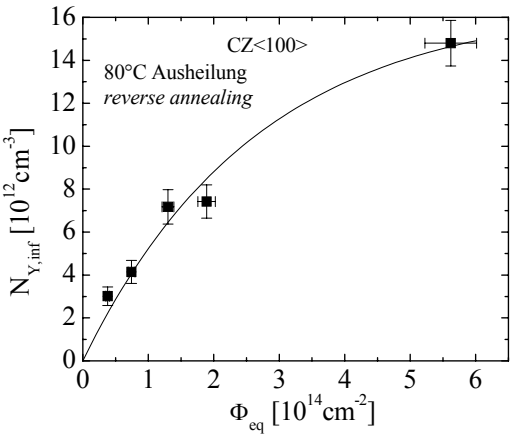

Figure 27b: reverse annealing amplitude $N_{Y,\infty}$ for p-irradiated Cz diodes

5.3.3 STFZ, DOFZ and Cz-diodes, trapping and charge collection after 24 GeV/c proton irradiation

Systematic TCT measurements have been performed by several groups within RD50 using 670nm red laser injection. Trapping of both electrons and holes have been measured in STFZ, DOFZ and CZ diodes. No material difference was found. However, comparing the results of different RD50 groups some discrepancies arise: While one RD50 group was observing almost the same inverse trapping times for holes and electrons [75, 78] other RD50 groups report on a stronger hole trapping than electron trapping [76, 77]. For completeness both results are shown in this section. One of the tasks of RD50 for 2004 will therefore be to clarify why these differences are observed although the same measurement technique is used.

Trapping probabilities ($1/\tau_{e,h}$) as reported by the Hamburg group are shown in Figure 28 [76]. As can be seen the electron and hole trapping is not much different. The inverse trapping time can be parameterized as: $1/\tau_{e,h} = \beta_{e,h} * \Phi_{eq}$ with $\beta_e = (4.68 \pm 0.15) 10^{-16} cm^2 ns^{-1}$ and $\beta_h = (5.72 \pm 0.50) 10^{-16} cm^2 ns^{-1}$.

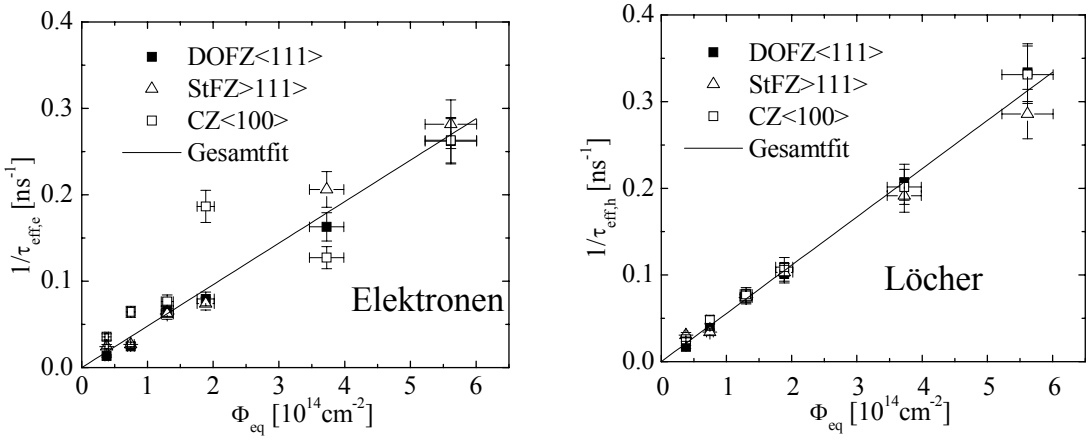

Figure 28.: Trapping probability $1/\tau_{e,h}$ for a): electrons and b): holes in STFZ, DOFZ and Cz-diodes as function of Φ_{eq} after 24 GeV/c proton irradiation

For STFZ and DOFZ diodes also the temperature dependence of the effective trapping probabilities had been measured between 210 and 292K. With respect to the LHC or likely also the SuperLHC operational temperature of –10C the increase in $1/\tau_{e,h}$ is rather marginal (less than 20%). Measurements on absolute values for charge collection were carried out with alpha particles. Results will be shown together with the discussion on epi-diodes (Section 5.10).
The results of the Dortmund group obtained on 5x5mm^2 DOFZ pad detectors with the TCT method are presented in Figure 29 and Figure 30. The inverse trapping times for holes and electrons after irradiation with 24 GeV/c protons are shown in Figure 29. As for the data presented above, a clear linear dependence of the inverse trapping times on the fluence is observed ($1/\tau_{e,h} = \beta_{e,h}*\Phi_{eq}$). The results of the according straight line fit are: $\beta_e = (5.13\pm0.16)10^{-16}$cm^{2}ns^{-1} and $\beta_h = (5.04\pm0.18)10^{-16}$ cm^{2}ns^{-1}.

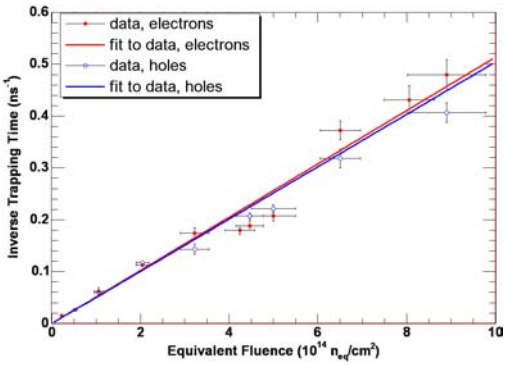

Figure 29.: Inverse trapping times for holes and electrons in proton irradiated samples.

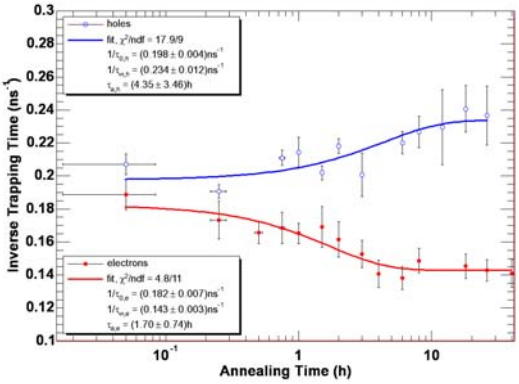

Figure 30.: Annealing of the inverse trapping time at 60°C.

The annealing of inverse trapping time has been studied with a sample irradiated to 4.5*10^{14} n$_{eq}$/cm² [75]. The annealing was accelerated by heating the sample to 60°C (Figure 30). In order to describe the data the function

$$\frac{1}{\tau}(t) = \frac{1}{\tau_0}\cdot\exp\left(-t/\tau_a\right) + \frac{1}{\tau_\infty}\cdot\left(1-\exp\left(-t/\tau_a\right)\right)$$

was fitted to them. The resulting parameters are $\tau_{a,e}$ =(1.70±0.74)h and $\tau_{a,h}$ =(4.35±3.5)h. The trapping probability for electrons decreased by ca. 20% while the trapping probability for holes increased by about the same amount. A result which is in agreement with the data presented in [76]. The time constant of the annealing are in the order of some hours, but they have a large error.

The results from the TCT measurements will be used in simulations of the charge collection efficiency for the ATLAS pixel detector. First preliminary results from a simple simulation of a pad detector of 250µm thick detector irradiated to 10^{15} n$_{eq}$/cm² show that the charge collection efficiency drops to 50% with a moderate overdepletion of 50V [78].

5.4 CZ, STFZ and DOFZ diodes, results from Co^{60}-Gamma irradiation

Very reliable results of damage induced effects both on N_{eff} and the leakage current have been obtained up to dose values of about 1 Grad. While for STFZ diodes a type inversion was seen at about 200 Mrad, the DOFZ diodes stayed n-type throughout the dose range with a small increase in the donor doping concentration. The results have been discussed in the Florence conference 2002

and will be shortly published in NIM A (see also [73]). Some comments are to be found in the DE (Defect Engineering) section of this report. A broader discussion is to be found in the DMC (Defect and Material Characterization) section. It should be emphasized here that the microscopic measurements on defect generation have led for the first time to a full understanding of the macroscopic diode properties. This is regarded as a major break through in the understanding of the damage mechanism and will hopefully pave the way for further design developments of radiation tolerant detectors.

5.5 STFZ and DOFZ diodes irradiated with 27 MeV p and 58 MeV Li ions.

The objective of our research is to develop feasible sensor solutions that would stand fluences of hadrons up to 10^{16}cm^{-2}, as planned for the LHC upgrade [79].The irradiation times needed to reach these high hadron fluences at nowadays proton irradiation facilities are typically very long, thus often preventing the systematic experimental studies. A possible way to decrease the irradiation times to more practical values could be to irradiate devices with energetic heavy ions, taking advantage of the large non-ionizing energy-loss (NIEL), which significantly increases with the atomic number of the impinging ions. The ion energies need to be sufficiently high to ensure that the particle range is larger than the detector thickness (usually 300 μm) to ensure a uniform energy loss within the detector.

Diodes manufactured on float zone silicon substrates standard (STFZ, [O]≈10^{16} cm^{-3}) or oxygenated by diffusion at high temperature (DOFZ, [O]>10^{17} cm^{-3}) have been irradiated with 58 MeV Lithium (Li) ions at the SIRAD irradiation facility [80]of the Tandem-XTU Van de Graaff accelerator at the INFN National Laboratory of Legnaro (Padova, Italy). SRIM simulations [81] have been performed in order to investigate the energy loss of such ions in silicon showing that the range of 58 MeV Li ions is 400 μm, i.e. substantially larger than the standard 280-300 μm thick diodes used in this study. This ensures that Li ions, which are n-type doping impurities, are not implanted in the silicon substrate. In addition the highly damaged region generated at depths close to the ion range, where the non-ionizing and ionizing energy loss are maximum, is outside the silicon substrate. The non-ionizing energy loss of 58 MeV Li ions is 2.003×10^{-4} MeV×cm^2/mg, i.e. 27.3 times higher that the corresponding value for 27 MeV protons (7.34×10^{-6} MeV×cm^2/mg); the NIEL scaling hypothesis suggests that a scale factor of ≈27 may be used to relate a fluence value obtained with 27 MeV protons to a fluence value obtained with 58 MeV lithium ions.

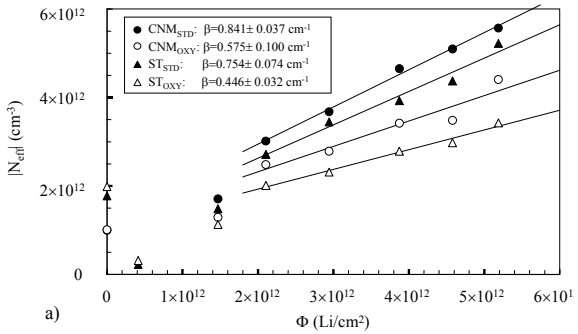

Figure 31.: Effective substrate doping concentration as a function of the 58 MeV Li fluence for standard (close symbols) and oxygenated (open symbols) CNM (circles) and ST (triangles) diodes.

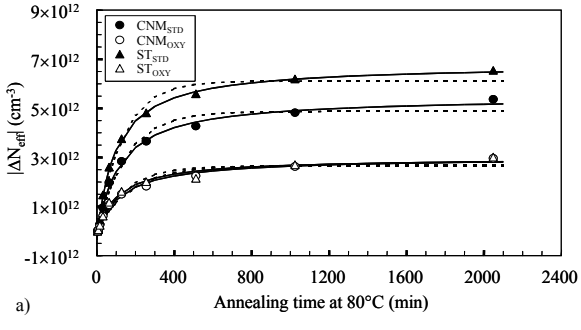

Figure 32.: Reverse annealing at 80°C of the effective substrate doping concentration for standard (close symbols) and oxygenated (open symbols) CNM (circles) and ST (triangles) 58 MeV lithium ions irradiated devices.

The evolution of the effective substrate doping concentration as a function of the Li irradiation fluence is shown in Figure 31. The behavior of diodes during the isothermal annealing at 80^0C up to 2000 minutes is shown in Figure 32.

It can be concluded from the presented results that the ion irradiation generates deep acceptor defects in the silicon substrate causing the space charge sign inversion (SCSI) effect, similarly to what is observed after hadron irradiation. Moreover the acceptor introduction rate (β) and the amplitude of the reverse annealing for the effective substrate doping concentration are lower for DOFZ devices, highlighting the positive effects of the substrate oxygenation also after Li ion irradiation and suggesting that from a microscopic point of view the bulk damage induced by Li ions is similar to protons (not to neutrons)

The reference data after 4 minutes of annealing at 80ºC for the leakage current density increase rate (α) and for the acceptor introduction rate (β) of the STFZ and DOFZ diodes from the two manufactures after irradiation by Li ions and 27 MeV protons are compared in Table 5 [56]. It is worth to note that both the α and β ratios present a low data dispersion, confirming the strong correlation between the damage induced by 58 MeV Li ions and 27 MeV protons and suggesting that the damage induced by Li ions and protons can be rescaled to a first approximation for radiation hardness tests in High Energy Physics applications by the following values: $\alpha_{58\ MeV\ Li}/\alpha_{27\ MeV\ protons}\approx 25$ (in agreement with the NIEL scaling hypothesis within 8.2%) and $\beta_{58\ MeV\ Li}/\beta_{27\ MeV\ protons}\approx 15$.

Diode label	$\alpha_{27\ MeV\ protons}$ (A/cm)	$\alpha_{58\ MeV\ Li\ ions}$(A/cm)	$\alpha_{58\ MeV\ Li}/\alpha_{27\ MeV\ protons}$
CNM_{STD}	$(8.48\pm0.06)\times10^{-17}$	$(204.9\pm3.9)\times10^{-17}$	24.2±0.6
CNM_{OXY}	$(8.35\pm0.04)\times10^{-17}$	$(205.3\pm4.5)\times10^{-17}$	24.6±0.7
ST_{STD}	$(8.26\pm0.06)\times10^{-17}$	$(204.0\pm3.9)\times10^{-17}$	24.7±0.6
ST_{OXY}	$(8.12\pm0.14)\times10^{-17}$	$(208.0\pm5.0)\times10^{-17}$	25.6±1.1
All data	$(8.21\pm0.05)\times10^{-17}$	$(205.6\pm2.0)\times10^{-17}$	25.0±0.4

Diode label	$\beta_{27\ MeV\ protons}$ (cm^{-1})	$\beta_{58\ MeV\ Li\ ions}$ (cm^{-1})	$\beta_{58\ MeV\ Li}/\beta_{27\ MeV\ protons}$
CNM_{STD}	0.0243±0.0019	0.3735±0.0306	15.4±2.5
CNM_{OXY}	0.0208±0.0024	0.3366±0.0359	16.2±3.6
ST_{STD}	0.0286±0.0030	0.3197±0.0126	11.2±1.6
ST_{OXY}	0.0170±0.0019	0.2599±0.0188	15.3±2.8

Table 5.: The α (up) and β (down) parameters for devices irradiated by 27 MeV protons and 58 MeV Li ions .

5.6 Gettered n-type detectors irradiated with 24 GeV/c protons

At the Ioffe PTI, St.Petersburg, Russia pad detectors were produced from standard Wacker n- and p-type silicon. The detectors were subjected to an unconventional gettering step during the processing in order to investigate the influence of gettering steps on the radiation hardness. The samples were irradiated with 24 GeV/c protons at CERN facilities in the fluence range $1.1\cdot10^{11}$-$3.6\cdot10^{15}$ cm^{-2}. C-V measurements revealed that the introduction rate of negative space charge β for the n-type detectors is 0.0035 cm^{-1}. That is significantly smaller than the values referred in literature for standard and oxygenated Si, namely 0.01 cm^{-1} and 0.0047 cm^{-1} for STFZ and DOFZ, respectively [43]. Therefore, the use of the applied gettering method might be a promising technology to reduce the introduction rate of the radiation induced negative space charge.

5.7 Cz-Si, STFZ and DOFZ irradiated with low energy protons.

Pad detectors made of Cz-Si, standard Fz-Si and and diffusion oxygenated Float Zone silicon were irradiated with 10 MeV and 20 MeV protons. The detectors were processed at the Microelectronics Center of Helsinki University of Technology [48] and were irradiated with 10 MeV and 20 MeV protons at Jyväskylä University Accelerator Laboratory, Finland [82]. The Cz-Si wafers were manufactured by Okmetic Ltd. The resistivity of the wafers was about 1100 Ωcm. The wafers have a homogenous oxygen concentration of about $4 \cdot 10^{17}$ cm^{-3}. This concentration is above the value that can be achieved by the diffusion oxygenation process, but less than the solid solubility of oxygen into the silicon. Thus, the bulk is essentially free of oxygen precipitations that in turn simplifies the detector fabrication process. The results of irradiations are shown in Figure 33 and Figure 34.

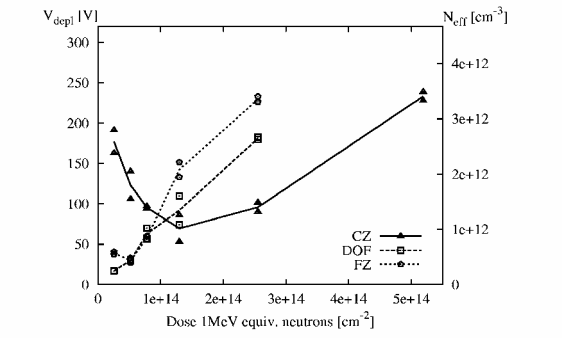

Figure 33.: Evolution of full depletion voltages (V_{fd}) and effective doping concentrations (N_{eff}) in Cz-Si, diffusion oxygenated (DOF) Fz-Si and standard Fz-Si irradiated with 10 MeV protons.

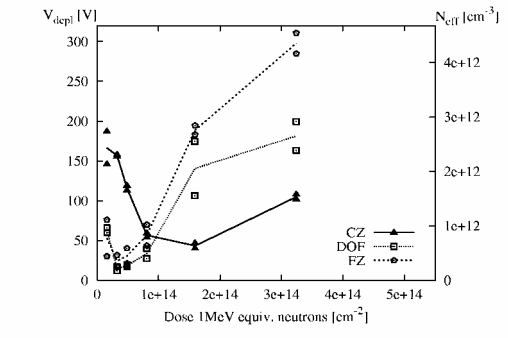

Figure 34.: Evolution of full depletion voltages (V_{fd}) and effective doping concentrations (N_{eff}) in Cz-Si, diffusion oxygenated (DOF) Fz-Si and standard Fz-Si irradiated with 20 MeV protons.

As seen in Figure 33 and Figure 34 , the depletion voltage of Cz-Si is less sensitive to the increased radiation dose than the depletion voltage of standard Fz-Si or DOF Fz-Si. Even after the maximum dose of $5*10^{14}$ protons cm^{-2}, the depletion voltage of the Cz-Si diodes is smaller than the initial depletion voltage before the irradiation 260V normalized to 300 μm thickness [83].

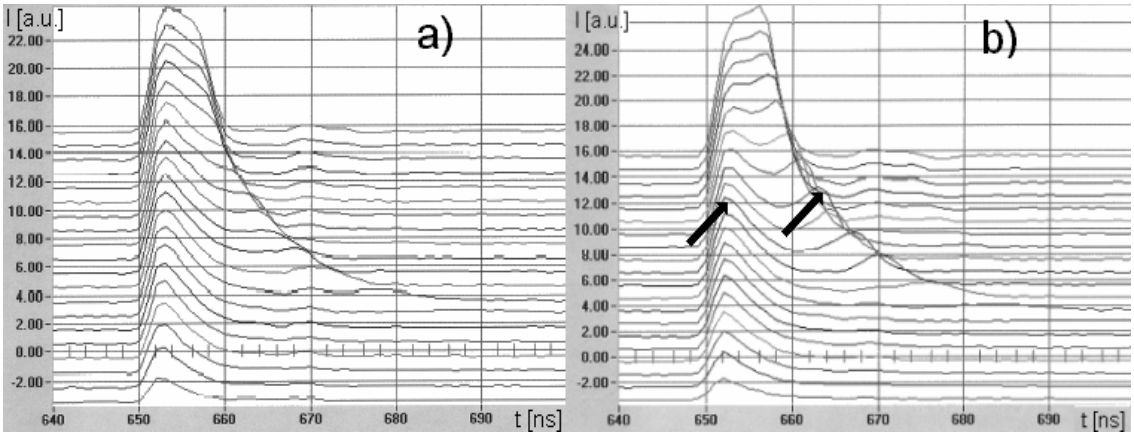

Figure 35. Oscilloscope pictures of the current transients of two Cz-Si diodes measured by TCT method. The samples are irradiated with a) 10 MeV protons, dose $1.3*10^{14}$ cm^{-2} and b) 20 MeV protons, dose $3.2*10^{14}$ cm^{-2}.

As seen in Figure 33 and Figure 34, in Fz-Si and DOF materials the SCSI takes place around the dose of $0.5*10^{14}$ cm^{-2}. On the other hand, in the Cz-Si samples the full depletion voltage seems to reach its minimum at the dose of approximately $1.5*10^{14}$ cm^{-2}. In order to study the SCSI in the Cz-Si samples, electric field profiles before and after the minimum of the full depletion voltage were measured using Transient Current Technique (TCT). Figure 35, shows the current transients of two differently irradiated Cz-Si diodes. The set of curves correspond to TCT measurements with different bias voltages, ranging from some volts to several hundreds of volts. The laser was illuminating the front p^+-side of the diodes.
In Figure 35 a) and b), the uppermost five curves are current transients in the case when the diodes are biased clearly over full depletion. In Figure 35 a), after irradiation with the dose of $1.3*10^{14}$ cm^{-2}, the current first raises fast and then decreases with respect of time, thus indicating electrons drifting from the front p^+ junction towards the back plane of the diode. Thus, the bulk is still n-type. In Figure 35 b), the shape of the transient is different: The fast rise in the current is absent and the current increases with respect of time. This indicates that the electric field increases towards the back plane of the diode where the inverted bulk forms a pn^+ junction. Furthermore, there is a clear double peak in the current transients of Figure 35 b), especially around the depletion voltage. The double peaks are clear signs of the SCSI. A comprehensive analysis of the origin of the double peak/double junction effect is presented in Ref. [84]. The results of TCT measurements performed on six different diodes are summarized in Table 6.

Table 6. TCT analysis of six irradiated Cz-Si samples. Samples were annealed at 80^0C for 20 minutes before the measurements.

Proton energy (MeV)	1 MeV/n eq. Dose (cm^{-2})	Full depletion voltage (V)	SCSI	SC sign	Double peak in the TCT signal
10	$1,3*10^{14}$	215	No	+	Weak
10	$2,6*10^{14}$	134	Yes	-	Clear
10	$5,2*10^{14}$	260	Yes	-	Clear
20	$0.8*10^{14}$	225	No	+	No
20	$1,6*10^{14}$	213	No	+	Weak
20	$3,2*10^{14}$	188	Yes	-	Clear

As seen in Table 6, the SCSI takes place in the Cz-Si material between the doses of $1.3*10^{14}$ cm^{-2} and $2.6*10^{14}$ cm^{-2} in the case of the lower proton energy (10 MeV) and between the doses of $1.6*10^{14}$ cm^{-2} and $3.2*10^{14}$ cm^{-2} in the case of the higher proton energy (20 MeV). For example, in the inner part of CMS Tracker this corresponds about 10 years of LHC operation [85].

5.8 Proton irradiation results of Fz-Si with different resistivities

Eight STFZ diodes were used in this study. The devices were manufactured by CSEM. The diodes were made of two different STFZ substrates: four of them with the <100> crystal orientation and with low resistivity (≈2.5 kΩcm), and another four with the <111> orientation and with high resistivity (≈6 KΩ cm). All diodes have the same geometry: they are 300 μm thick and their active area is a square of $0.24*0.24$ cm^2, surrounded by a single guard ring.
One low and one high resistivity silicon diode was irradiated simultaneously. Diodes were subjected to four different fluences at the Research Centre in Karlsruhe (Germany). The Karslruhe facility provides a 34 MeV proton beam, produced by an isochronous cyclotron with a beam spot of 8-10 mm of radius. During the irradiation, the structures were placed in a cooling box with dry

air ventilation and were kept unbiased. The temperature was kept at -10 ^{0}C. The highest fluence used in this study was about 1*10^{14} p/cm^2. In this content, the fluences are expressed as 1 MeV neutron equivalent, evaluated by means of the leakage current.
For comparison, we have also irradiated diodes from the same processing batches with 24 GeV/c protons at CERN-PS in the same range of fluences [86].
All the CV measurements were performed on diodes with guard ring set to 0V, at a frequency of 10kHz. The full-depletion voltage V_{dep} was determined from the kink in the $1/C^2$-V plot.

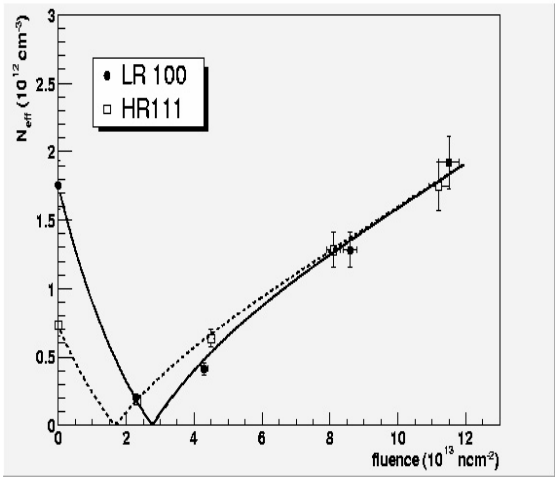

Figure 36.: Measurement after beneficial annealing (see text).

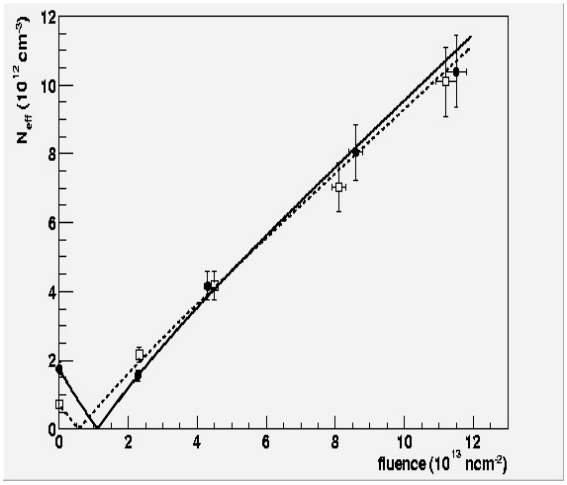

Figure 37.: Measurement after complete reverse annealing (see text).

The measured values of $|N_{eff}| \propto V_{dep}$ as a function of fluence for the two different kind of detectors are compared in Figure 36 and Figure 37. The values were measured after the beneficial annealing (t_1 ~ 7 days @ room temperature) and after the complete reverse annealing (t_2 ~ 10^8 min @ room temperature), respectively. In order to determine the inversion fluences and the slope of the curves after the inversion, we have fitted the experimental points with the expected behavior of $|N_{eff}|$ evaluated according to the parameterization commonly used within the Rose collaboration[♣] [87]:

$$N_{eff}{}^{\Phi} = N_{eff}{}^{0} - N_{C0}(1 - e^{-C\Phi}) - \beta\Phi \ .$$

The values of β extracted by fitting the experimental points measured after exposure to 24 GeV/c and 34 MeV protons give almost the same values for the low and the high resistivity material and can thus be represented by one value:

- 24 GeV/c protons (t1 ~ 7 days @ RT) : 0.014 cm^{-1}
- 34 MeV protons (t1 ~ 7 days @ RT) : 0.016 cm^{-1}
- 24 GeV/c protons (t2 ~ 10^{8}min @ RT) : 0.088 cm^{-1}
- 34 MeV protons (t2 ~ 10^{8}min @ RT) : 0.095 cm^{-1}

For the measurements performed at the minimum of the annealing curve (t_1) the experimental values of Beta parameter ($\beta(t_1) \sim g_C$) for 34 MeV protons are a little bit higher than the ones for 24

[♣] Note that within the Rose community and the Hamburg model N_{C0} is extracted from a plot of N_C (extracted from individual annealing curves) vs. fluence, while here the parameter N_{C0} is extracted from a plot of N_{eff} vs. fluence for a certain annealing stage. In this sense the equation is identical, but the parameters have to be interpreted differently.

GeV/c protons; this shows that the individual damage parameters related to the stable acceptors introduction rate g_C scale differently with the particle energy.
For all diodes the β values measured after the reverse annealing (t_2) are higher than the ones observed at t_1, since in this case the observed slope depends also on the reverse annealing introduction rate g_Y ($\beta(t_2) \sim g_C + g_Y$). For both low and high energy irradiation, and independently on annealing time, the big initial difference in N_{eff} and, hence, V_{dep} typical of LR and HR structures decreases with the radiation fluence, and above type inversion the relative curves tend to merge. This result can be explained by the hypothesis of complete donor removal for both low and high-energy proton irradiation [87]. A completely different behaviour was observed after neutron irradiation [88,89]: at any fluence the measured depletion voltage depends substantially on the initial resistivity.

5.9 High-Energy Electron Irradiation of Different Silicon Materials

Irradiations up to a fluence of $1.4*10^{15}$ e/cm^2 have been performed with the 900 MeV electron beam of the LINAC injector at the synchrotron light facility Elettra in Trieste (Italy). Tested devices are $p^+/n^-/n^+$ diodes fabricated on different silicon substrates, namely standard and diffusion-oxygenated float-zone (which in the following we will address as FZ and DOFZ respectively), Czochralski (CZ) and epitaxial (EPI) silicon. A more detailed report can be found in [55].
A set of standard and oxygenated float-zone devices has been manufactured by CiS (Erfurt, Germany) on Wacker (111) substrates of typical resistivity of 3-4 kΩ*cm. Oxygen diffusion for DOFZ devices has been performed in an N_2 environment for 72 hours at 1150^0 C. A second set of FZ diodes has been fabricated by ITC-IRST (Trento, Italy) on wafers from Topsil, with a resistivity of 10-20 kΩ*cm. Some of the substrates had been previously converted to DOFZ by a 12 hour oxidation at 1150^0 C followed by a 36 hour diffusion in N_2 at the same temperature, resulting in an oxygen concentration of $1\text{-}3*10^{17}$ cm^{-3} across the substrate. Czochralski and epitaxial devices have also been processed by CiS. CZ diodes are manufactured on (100) wafers of resistivity 1.2 kΩ*cm from Sumitomo; EPI diodes are processed on a 50 μm thick epitaxial layer (of resistivity 50 Ω*cm) grown by ITME (Warszawa, Poland) on a 300 μm thick low-resistivity (0.01 Ω*cm) Czochralski (111) substrate. The active area of all CiS diodes is of 0.5*0.5 cm^2, while devices fabricated by ITC-IRST have an area of 0.35*0.35 cm^2. All diodes are provided with a 100 μm wide guard-ring (which is connected to ground during the measurements), surrounded by several additional floating guard-rings. The substrate thickness for all devices is of about 300 μm.

Devices have been kept unbiased during irradiation, at a temperature of 25^0C. Between irradiation and the first measurements the samples have been kept at room temperature. After the first series of measurements devices have been stored at about -7^0C. The C-V measurements have been performed at 10 kHz frequency, and the depletion voltage V_{dep}has been estimated from the saturation of the C^{-2}-V or of the logC-logV curves. The temperature in the laboratory during the measurements varied between 22 and 24^0 C. All measured currents have been normalized to 20^0C.

Figure 38 and Figure 39 show the values of N_{eff} as a function of the electron fluence for the FZ and DOFZ devices manufactured respectively by IRST and CiS. A negative sign has been assigned to those values of N_{eff} that we consider likely to correspond to an inverted (p-type) substrate, based on the criterion of obtaining a smooth curve.
Type inversion appears around $1.5*10^{14}$ e/cm^2 for the IRST devices (fabricated on higher resistivity material), and at about $3*10^{14}$ e/cm^2 for the CiS devices. After type inversion, the slope of N_{eff} versus fluence is about $-1.5*10^{-3}$ cm^{-1} for IRST FZ devices, $-1.9*10^{-3}$ cm^{-1} for CiS FZ diodes, $-0.9*10^{-3}$ cm^{-1} for IRST DOFZ structures and $-0.7*10^{-3}$ cm^{-1} for CiS DOFZ devices. A lower slope

appears to be associated with DOFZ substrates. Differences between diodes fabricated by IRST and by CiS could be due to different starting materials and oxygen diffusion treatments.

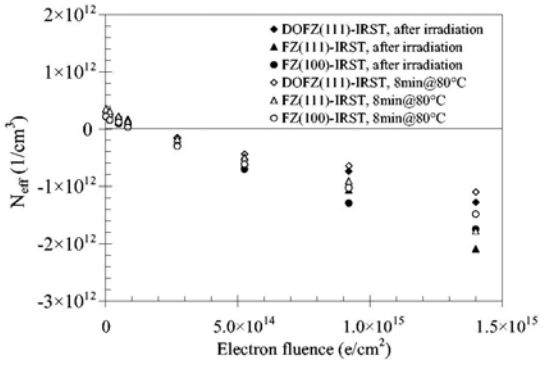

Figure 38. Effective dopant concentration for FZ and DOFZ devices from IRST measured soon after irradiation (closed symbols) and after 8 minutes of thermal annealing at 80^0 C (open symbols).

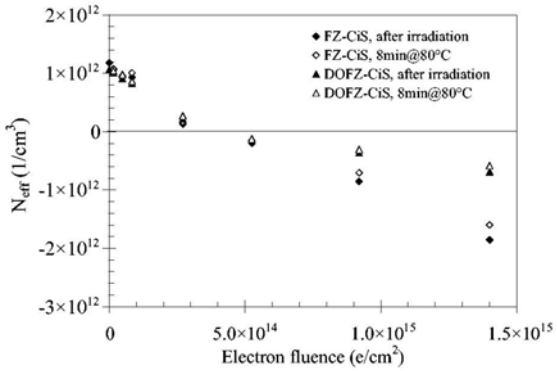

Figure 39. Effective dopant concentration for FZ and DOFZ devices from CiS measured soon after irradiation (closed symbols) and after 8 minutes of thermal annealing at 80C (open symbols).

The electron irradiation results of CZ diodes are presented in Figure 40. Due to the fact that the samples used for the various irradiations had non negligibly differing values of initial resistivity, the following “equalization" procedure has been applied, in order to obtain a meaningful dependence on fluence: for each device, the variation in N_{eff} due to irradiation $N_{eff,\ after}$-$N_{eff,\ before}$ has been added to the average value of the initial effective dopant concentration, taking all devices into account.

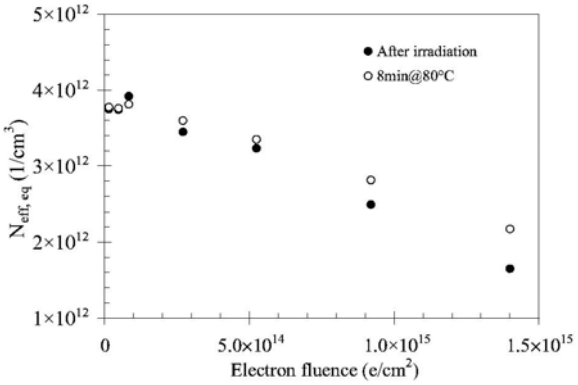

Figure 40.: Effective dopant concentration for CZ devices measured soon after irradiation (closed symbols) and after 8 minutes of annealing at 80^0 C (open symbols). The values reported have been equalized according to the procedure described in the text

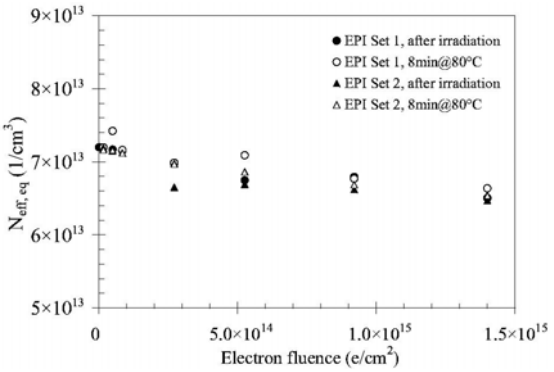

Figure 41.: Effective dopant concentration for two different sets of EPI devices measured soon after irradiation (closed symbols) and after 8 minutes of annealing at 80^0 C (open symbols). The values reported have been equalized according to the procedure described in the text.

After the first steps of irradiation, the curve in Figure 40 appears to be approximately linear, with a slope of about $-1.5*10^{-3}$ cm^{-1}. Nevertheless, it does not appear to be possible, within this limited range of fluences, to separate the relative contributions to the observed rate of change of N_{eff} coming from (a) the initial part of an exponential decay of the donor concentration or (b) a linear introduction of acceptors. Previous irradiations of the same type of devices with charged hadrons

(24 GeV/c protons and 190 MeV/c pions) have shown no type inversion even at fluences up to $1*10^{15}$ cm^{-2} [49]. In our case, a simple linear extrapolation of the observed fluence dependence would suggest that type inversion will occur at a fluence of about $3*10^{15}$ e/cm^2. Such values of fluence are feasible with our experimental setup and we plan to reach them in future irradiations, in order to distinguish between the previously mentioned contributions to the slope of N_{eff} and to find out whether the observed linear trend continues up to type inversion or rather a different behavior appears.
Figure 41 shows the corresponding plot for the EPI devices. Again, the above-described ``equalization'' procedure has been applied in order to account for differing initial dopant concentrations. For these devices, the relative changes in N_{eff} are quite small and comparable with the uncertainty in the evaluation of the depletion voltage. Although a decrease of the effective dopant concentration with increasing fluence is apparent from the plot, substrate type inversion is not even approached at the fluences considered, in agreement with what already observed after irradiation with 24 GeV/c protons [90, 91].
The observed fluence dependence of the volume density of the reverse leakage current does not depend on the substrate material, as already observed after hadron irradiation [92]. The damage constant α, referred to the actual electron fluence and coming from the leakage current measured after 8 minutes at 80^0 C, is equal to $1.35*10^{-18}$ A/cm. The hardness factor k of 900 MeV electrons with respect to 1 MeV neutrons can be estimated from the ratio of the damage constant α thus measured to that reported in the literature for 1 MeV neutrons (after the same annealing cycle), namely $4.0*10^{-17}$ A/cm [92]. This yields a value $k=3.4*10^{-2}$. It is interesting to note that the ratio of the NIEL (Non-Ionizing Energy Loss) values for high energy electrons and for 1 MeV neutrons is about $8.1*10^{-2}$ (we have used the results of NIEL calculation relative to 200 MeV electrons [93], the highest available energy in the literature). This indicates that, at equal NIEL values, high-energy electrons are about 2.4 times less effective than 1 MeV neutrons in degrading the carrier generation lifetime of the material, providing further evidence that the NIEL scaling hypothesis is not adequate when comparing electrons with hadrons, even in the GeV electron energy range.
Thermal annealing effects have also been studied: several cumulative annealing steps at 80^0 C have been performed for FZ/DOFZ and epitaxial diodes irradiated at two highest fluences, up to a total time of about 100 hours. For the first ones (inverted) an initial beneficial annealing can be observed, leading to a minimum of N_{eff} after about 8 minutes, followed by an increase (reverse annealing). Epitaxial devices (non-inverted) show an increase in the N_{eff} that amounts to approximately 2-3% after about 100 hours at 80^0 C. Meaningful differences in the annealing behavior between the various devices and the two irradiation fluences are not apparent.
Finally, the charge-collection efficiency (CCE) has been measured with the Transient Current Technique on all samples made by CiS, annealed for 8 minutes at 80^0 C. The decrease of CCE at the two highest fluences is of 1-3%, more pronounced for FZ and DOFZ devices.

5.10 Thin EPI Diodes

CERN scenario and annealing studies after hadron irradiation

A first comparison between the epi-diodes and those fabricated from STFZ, DOFZ and Cz-material was obtained via CERN scenario measurements, revealing the superiority of their radiation tolerance, see Figure 42 ([18]). In the full range of measured fluences (meanwhile extended up to Φ_{eq} = 5.5e15/cm²) there is no type inversion! Starting from an initial depletion voltage of 120 Volts, even after 2.5e15/cm² V_{dep} changed only to 160 Volt, whereas for all other diodes values well above 1000 V would have been needed.

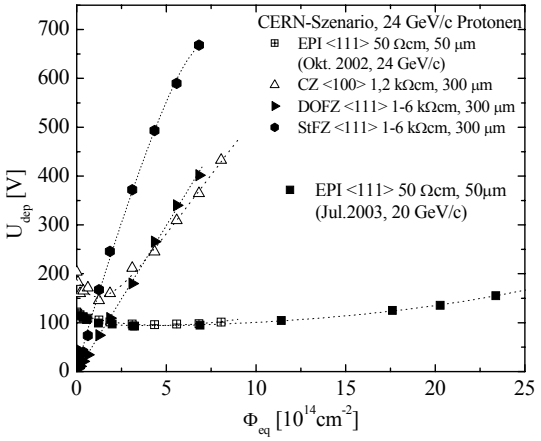

Figure 42.: CERN-scenario results at 24 GeV/c p-irrad iation for epi-diodes in comparison with STFZ, DOFZ, and Cz-diodes.

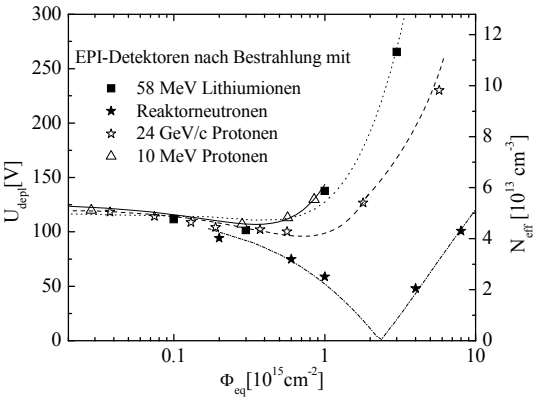

Figure 43.: N_{eff} after 8 min@80C annealing as function of fluence measured in epi-diodes with different particle irradiation.

Figure 43 shows the development of N_{eff} resp. V_{dep} after 8min@80C annealing of the epi-diodes after irradiation with neutrons, low and high energy protons as well as Li-ions covering a range of Φeq up to $1 \cdot 10^{16}$/cm² [72]. There is a distinct difference between neutron irradiation and that with charged particles. While in the case of neutrons type inversion occurs at about $2 \cdot 10^{15}$/cm², no type inversion is seen for all charged particle irradiations. The strong increase of N_{eff} for fluences higher than 2e15/cm² is believed to be due to increasing point defect generation (bistable donors, see DMC report, also discussed in [18]). Annealing experiments have therefore been performed in order to see, in how much this initial donor generation would either anneal out or get compensated by acceptor like defect generation.

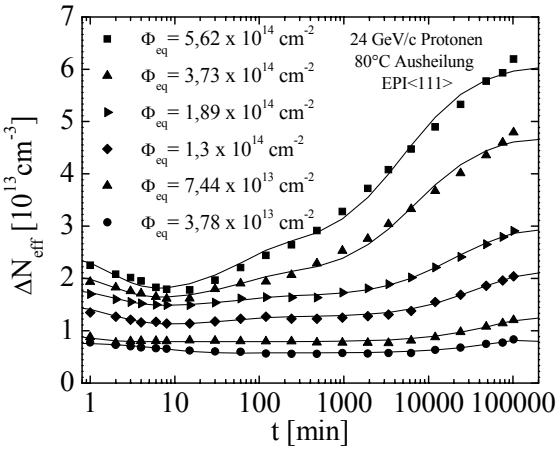

Figure 44 a) annealing curves (ΔN_{eff}) measured at 80C for epi-diodes after 24GeV/c proton irradiation.

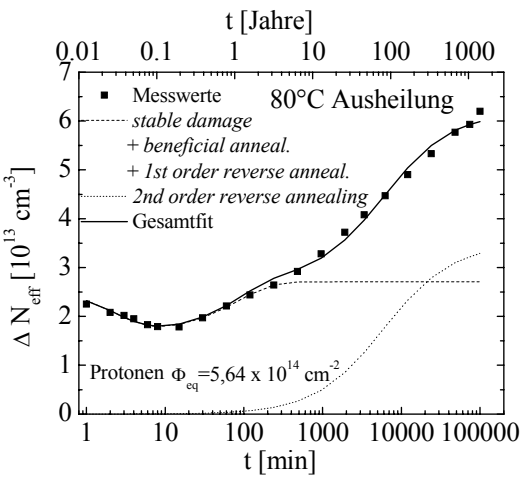

Figure 44b): fit to annealing curve with both 1st (short) and 2nd order (long) component.

Remember that in FZ diodes the reverse annealing effect is believed to be caused by acceptor generation, leading to type inversion already at an early stage. An example of annealing curves as measured for epi-diodes is given in Figure 44. There is no doubt that the shorter time component in

the reverse annealing (Figure 44 b) is of 1st order while the long annealing times are governed by a real 2nd order process ($\tau_Y \propto 1/\Phi_{eq}$, see Figure 45_b [72]; in contrast to DOFZ, see Figure 25. The total reverse annealing amplitude (sum of short and long term component) shows a linear dependence on the fluence with a generation rate $g_y \approx 8*10^{-2}$ cm^{-1} (see Figure 45_a).

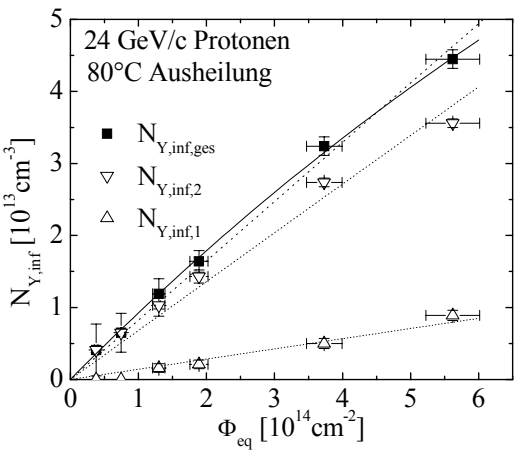

Figure 45 a): Reverse annealing amplitudes for epi diodes after 24 GeV/c proton irradiation with short ($N_{Y,inf\ 1}$) and long ($N_{Y,inf\ 2}$) components as well as total sum. A change in N_{eff} of $5*10^{13}$ /cm³ is equivalent to a change of the depl. Voltage of 95 Volt only!

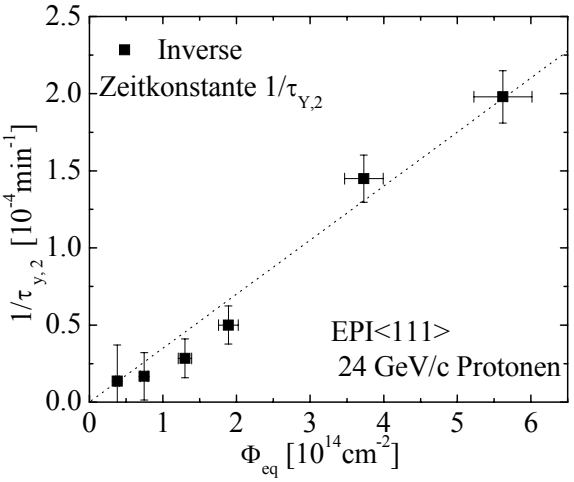

Figure 45_b): Reverse annealing time constant for the long component as function of fluence. $1/\tau_Y$ is shown to be proportional to $/\Phi_{eq}$ as expected for real 2nd order annealing

Preliminary results (including annealing at 60°C) suggest that the reverse annealing is governed by the same activation energy as found for FZ material. Hence by using this we can project the 80°C time scale to that expected for RT annealing. This is done in the top scale in Figure 44b. This would mean that for LHC operation up to 10 years one may not at all need cooling of such detectors at all, since the combined damage generation and annealing will never exceed even type inversion! If this would be confirmed by annealing measurements now undertaken also at 40°C, this would be of tremendous advantage. Instead of cooling as necessary also during the beam off periods for DOFZ devices, for epi detectors the RT storage during beam off every year would be highly beneficial!
Comparing the results of Figure 43 with those of Figure 45 we see that for very large fluences the initial dominance of the donor generation (roughly 10^{14}/cm³) could be compensated by the acceptor generation during reverse annealing. Choosing a proper maintenance scenario close to room temperature, only moderate changes of N_{eff} during the entire SLHC operation can be maintained. This is the most important feature of epi-Si diodes, even exceeding the expectation from the much larger initial dopant concentration.
As to comparison of the donor generation in epi-diodes as seen here in macroscopic measurements with defect characterization studies see the DMC section of this report.

Charge carrier trapping and charge collection efficiency

For epi-diodes no TCT measurements are possible since the charge collection times are much below 1 nsec and therefore time resolved studies of the current pulse fail. However absolute charge

collection efficiencies have been measured using alpha-particle charge injection. The results are shown in Figure 46 and Figure 47 [72].

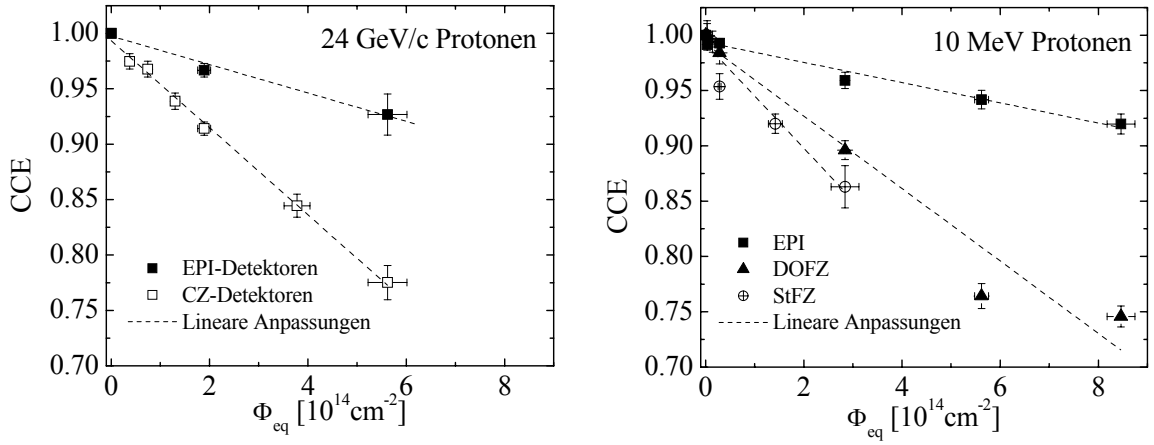

Figure 46.: Charge collection efficiency measured in epi diodes in comparison with results STFZ, DOFZ and Cz-diodes. Left: 24GeV/c-proton irradiation, right: 10 MeV proton irradiation.

Regardless of the proton energy the studies show that for the epi-diodes the charge collection efficiency drops only to about 90% at $8*10^{14}$/cm² while the cce-drops for all other diodes to 70% at the same fluence. The cce studies for epi-diodes are extended to $\Phi_{eq} \approx 10^{16}$/cm² (Figure 47). Also at this almost SuperLHC fluence the epi diodes still show a charge collecetion efficiency of 75% after proton irradiation and a slightly worse value after neutron damage.

In Figure 47 b) experimental results are shown in comparison with a simulation for which the electron and hole trapping probabilities as displayed in Figure 28 have been used (see also [18]). These values had however to be extrapolated over more than one order of magnitude for Φ_{eq}. The good agreement between experimental values and simulations lead to the conclusion that the effective trapping times in epi-diodes are indeed comparable with the ones in FZ-Si material.

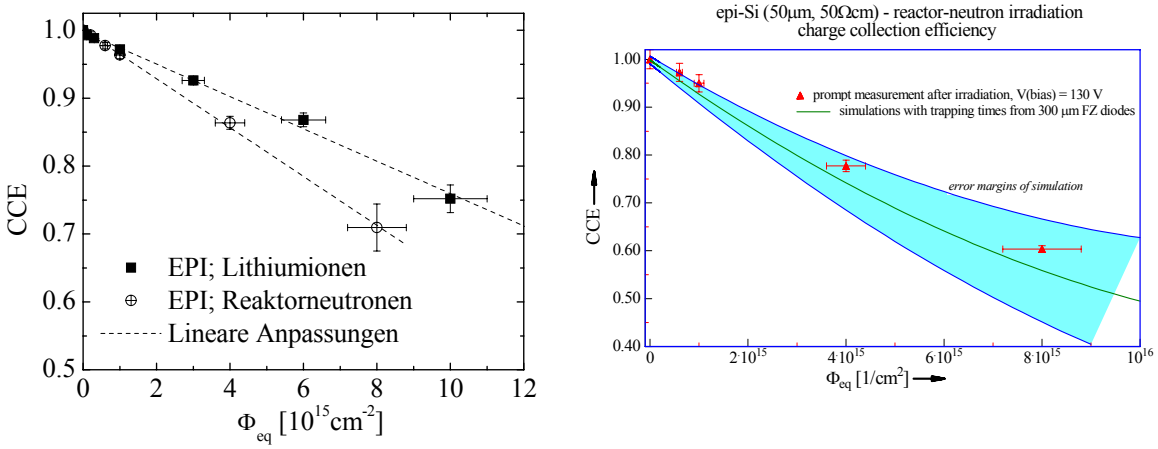

Figure 47.: Absolute charge collection efficiencies, measured in epi diodes up to $\Phi_{eq} = 10^{16}$/cm².

a): damage by 56 MeV-Li-ions and reactor neutrons. b): Comparison between measured values for neutron irradiation and simulations (see text).

Summary for epi-diodes

In summary epi-Si detectors exhibit properties similar to the normal FZ-detectors (especially as the bulk generated current and the effective trapping times are concerned). The use of a much smaller diode thickness leads to an appreciably higher charge collection efficiency at moderate voltages even after very large hadron fluences. Estimates based on our experimental findings show that for $\Phi_{eq} = 10^{16}/cm^2$ and an average electric field of 25 kV/cm (V_{dep} = 125V) the charge collection efficiency for mip's in a segmented (pixel) detector would still be 40%, roughly corresponding to a most probable signal of 1400 e. Such signals should allow efficient operation by using state of the art electronics. The small thickness allows also the use of a high doping concentration (about 100 times the value used for FZ detectors). This is of course extremely advantageous, since the damage induced change in the doping concentration does not play such a big role as in FZ-detectors. However in addition to these geometry related positive effects (to be expected also in equivalently thin FZ devices) it had been shown that the stable damage is (in contrast to FZ diodes) dominated by shallow donor generation. A possible explanation, still to be checked, is proposed in [18]. During annealing this damage induced donor concentration is successively compensated by acceptor creation (component similar as in FZ). This rather unexpected effect of the interplay between a strong donor generation and the annealing related acceptor creation leads to the possibility of designing a maintenance scenario with storage close to RT (FZ have to be cooled all the time!) by which the depletion voltage could be hold at a very moderate level for the whole SuperLHC operational period. Once the annealing measurements at all temperatures under investigation (80, 60 and 40ºC) will have been finished a reliable projection for SLHC application will be possible.

6 New Structures

6.1 3D detectors

6.1.1 Conventional and '3D' detectors

In a standard detector geometry, electrodes are placed on opposite sides of the semiconductor, in a parallel plate capacitor geometry. Charge generated as a result of incident radiation drifts normal to the plane of the semiconductor wafer to the oppositely biased electrodes. To maximize the amount of charge generated by the incoming radiation requires large electrode separation. To lessen sensitivity to radiation damage requires minimum electrode separation, so charge can be swept out of the detector before radiation induced traps can have any effect.

In the parallel plate geometry, both requirements cannot be met simultaneously. However, in the '3D' configuration, the generated charge drifts in the plane of the wafer. This time the electrode separation is independent of the material thickness, so charge generation is decoupled from sensitivity to radiation damage. Thus, the 3D geometry may be designed to both maximize signal response to incident radiation and minimize sensitivity to defects arising from radiation damage.

6.1.2 Fabricating 3D detectors

Three different routes to fabricating the 3D geometries have been developed. Depending on particular material system and requirements, one or other of these methods is to be preferred. The electrodes may be made by a plasma etching technique (micro-machining), a femtosecond laser drilling technique, or a photo-electrochemical (PEC) etching technique (Figure 48).

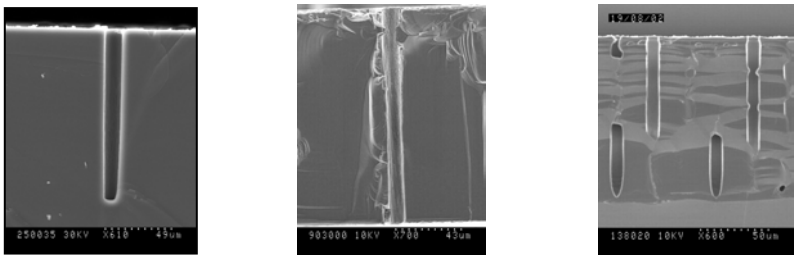

Figure 48.: Cross-section SEMs of 3D pores made by the three methods: (a) plasma etching, (b) laser ablation, (c) PEC etching.

The plasma etching technique is the most compatible with micro-fabrication processes. However, for 3D detector manufacture it works only for silicon and is limited to an aspect (depth-to-width) ratio for the holes currently of about 20:1. PEC will in principle produce holes of arbitrary aspect ratio, but the geometries usable are more limited due to the nature of the process. The laser drilling technique is the most cumbersome, as each electrode is made in sequence. However, it will work for any material system. For silicon, plasma etching and PEC produce electrodes in parallel, so both those methods are best suited for volume production of 3D detectors. Plasma etching and laser machining are independent of crystal orientation. PEC only works for specific crystal orientations; the standard commercially available silicon wafers has the preferred orientation. Once these vias have been made, the electrodes may be formed and deposition of metal tracks on the top surface completes the device.

6.1.3 3D detector characterization

3D detectors have been produced at Glasgow by plasma etching with 200μm thick silicon and 85μm pore spacing. Both I-V and C-V measurements were made on fabricated silicon 3D detectors [94]. Several silicon 3D detectors were irradiated at the 300 MeV/c pion beam at the Paul Scherrer Institute (PSI), Villigen. The pion beam had a flux corresponding to $10^{14}\ \pi/\mathrm{cm}^2$/day. The devices were irradiated to fluences of 10^{12}, 10^{13}, and $5\times10^{14}\,\pi/\mathrm{cm}^2$. The measurements show an improvement in both the leakage current and biasing requirements with increased fluence, although the exact reason for this is not understood. The I-V curves at pion fluences of $10^{12}\,\pi/\mathrm{cm}^2$ or less have (not quite ideal) diode characteristics (see Figure 49). At higher fluences the I-V curves are much more symmetric, indicative of the formation of back-to-back diodes or the breakdown of Schottky barrier diode behavior into ohmic behavior.

The C-V measurements whilst indicating the presence of defects in the low frequency response, show that full depletion is reached at progressively smaller voltages with higher fluence. The full depletion for these structures goes from above 30 V for the unirradiated samples down to about 20 V at $10^{14}\,\pi/\mathrm{cm}^2$ (see Figure 50).

Pulse height spectra of these devices were measured before and after irradiation. The charge collection efficiencies were measured for 5.48 MeV α particles from a $^{241}\mathrm{Am}$ source. The device was enclosed in a vacuum chamber with a background pressure of ~23 mBar and the $^{241}\mathrm{Am}$ source placed about 1 cm from the detector; the energy scale on the multi-channel analyser was calibrated using a spectroscopic source and a reference silicon detector.

The measured charge collection efficiency drops from ~60% to ~45%, presumably due to the presence of defects causing charge loss. This is a slightly bigger drop than has been measured for optimized silicon diodes (in such devices the charge collection efficiency drops by a factor 0.80-

0.85 after equivalent radiation fluences). The difference is ascribed to non-optimized fabrication procedures. Charge collection efficiency measurements with β-particle ^{90}Sr source will be performed next year on non-irradiated and irradiated devices.

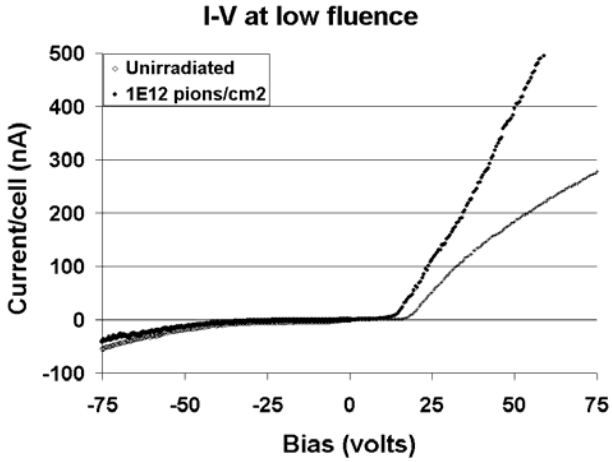

Figure 49.:I-V characteristics of 3D detectors before and after irradiation with 10^{12} π/cm^2.

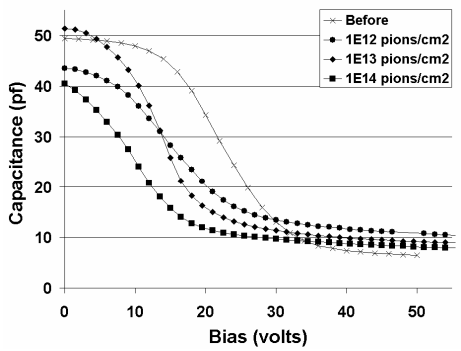

Figure 50.:C-V characteristics of 3D detectors before and after pion irradiation up to 10^{14}π/cm^2.

6.1.4 3D detector designs for LHC experiments

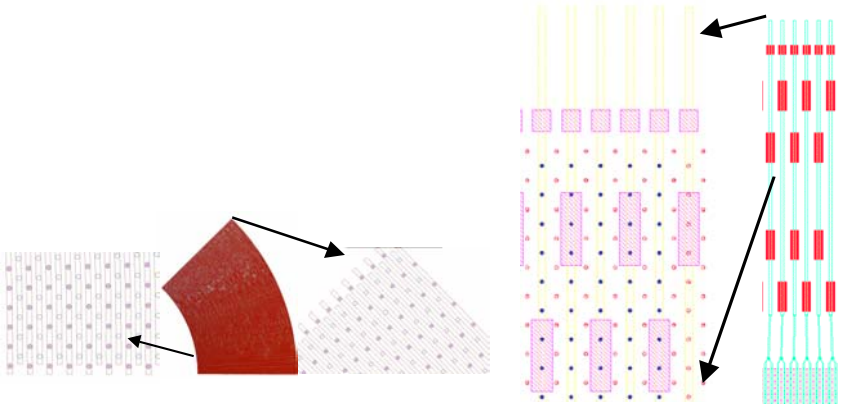

Figure 51: 3D detector design for (left) LHCb Velo and (right) Atlas.

A 3D detector in the LHCb Velo format has been designed. Use of 3D technology offers a number of technical advantages over more conventional approaches. The first is the improved radiation tolerance. Coupled with improved (oxygen incorporating) silicon substrates which are known to offer better radiation resistance, one can hope to achieve a design that offers excellent radiation tolerance. Additionally, a 3D design may be used to make the silicon sensitive right to the edge of the material, replacing the current 1mm of guard ring. From Gaudi/Brunel simulations made of current Velo guard ring designs, the reduction in dead space would offer ~10 % improvement in impact parameter resolution. A proposed 3D electrode design for Velo is shown in Figure 51.

Two Atlas designs have also been made with the 3D electrode configuration. One uses a hexagonal layout for the electrodes, but has a relatively complex biasing arrangement. The second uses a rectangular layout for the electrodes. Completed structures remain to be tested due to production difficulties. However, good signals have been obtained with 3D cells bonded to deep submicron readout electronics.

6.2 Thin detectors

The active thickness of the device after heavy fluence irradiation is limited by the carrier effective drift lengths, estimated for electrons and holes respectively ~150μm and ~50μm after 1MeV neutron irradiation at 10^{15}cm^{-2} [95]. The RD50 collaboration has proposed to investigate the use of thin Si detectors to get constant and low V_{dep}, limited leakage currents and high inversion fluences. The latter effect is achieved by means of low resistivity bulk material (typically 50-100Ωcm), as the high initial shallow doping will shift type inversion to the very high fluence range. Two technical approaches have been investigated: thinning of Si and use of epitaxial Si wafers (for this latter see section 5.10).

Processing of thin detectors

Processing and electrical characterization of Si thinned detectors have been performed by the group of IRST Trento [95]. The fabrication process of devices on thin silicon membranes has been based on a preexistent process developed for PIN diodes. In particular, in order to produce the membrane, a wet etching of silicon using a TMAH solution has been included in the standard process sequence. Devices have been fabricated starting from 100-mm-diameter, floating zone (FZ), 300-μm-thick, <100>-oriented, phosphorus-doped silicon wafers. This procedure has never been used before for the production of Si particle detectors, thus a comparison with thick conventional Si particle detectors was mandatory. For this reason, the process was first undergone with high resistivity material (6 kΩcm).

With reference to the schematic flowchart of Figure 52, the fabrication process can be outlined as follows: A) Isolation oxide (wet oxidation, 800 nm); p+-region: definition, boron implant and diffusion. n+ region (cut lines): definition, phosphorus implant and diffusion. B) TEOS and silicon nitride deposition; Back side definition: oxide and nitride etching. C) Membranes definition: TMAH etching, back side doping: P-deposition and annealing. D) Contact opening; Metal deposition (1.6 μm), and definition. Sintering.

The fabrication process requires 5 mask steps: 4 on the front and one to define the membranes. In summary, the key features of the described technological approach are as follows.

- A thick oxide (isolation oxide) is grown at the beginning of the process;
- The etching of silicon is performed in a TMAH solution, (the etch rate is ~40μm/h);
- The n+ region on the back side of the wafer is obtained with a deposition from solid source;
- The boron implant is performed through a screen oxide.

We have etched two set of wafers for different times in order to obtain two different silicon membrane thickness respectively of about 50μm and 100μm (see Table 7).

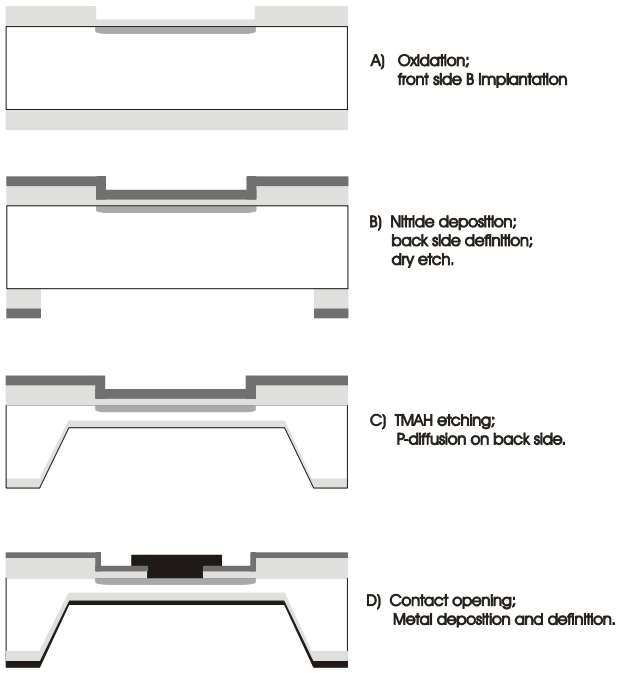

Figure 52 Schematic cross section of a diode in different phases of the fabrication process.

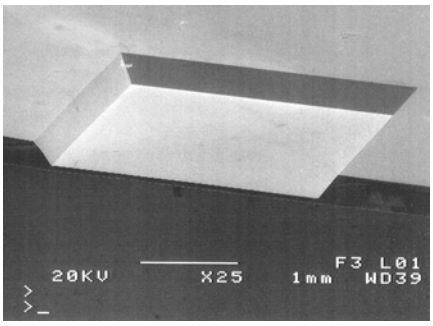

Figure 53 SEM micrograph showing a cross section of a silicon membrane obtained on the back-side of a TMAH etched silicon wafer.

Figure 53 shows a SEM micrograph of a locally thinned region. Furthermore, we processed in the same batch two wafers as reference samples (using the same process but without the TMAH etching) in order to study the influence of the thinning process step on the electrical characteristics of the devices.

Table 7 Final thickness of silicon membranes obtained after TMAH etching

Wafer #	3	4	5	6	7
Membrane thickness [μm]	105±3	99±2	99±7	57±8	57±4

Devices description

We adopted a wafer layout already available, defined by a mask set designed for the production of PIN diodes with different active areas (see Figure 54). We only added a new mask dedicated to the definition of the back-side areas to be thinned. Furthermore, the layout includes standard test structures (diodes, MOS capacitors, gated diodes) for monitoring the main parameters characterizing the fabrication technology.

Figure 54: Layout of thinned diodes available on the processed wafers. a) Circular diode having an area of 2.27 mm^2 and double guard ring; b) Square diodes of various area: 0.75, 1.9, 3.5, 11.35 mm^2.

Electrical characterisation

6.2.1 Test Structures

On all the processed wafers (TMAH etched and reference) test structures on 300µm thick substrate have been measured and the main parameters characterizing the fabrication technology have been determined. The results, grouped by reference and TMAH etched wafers, are summarized in Table 8. The Full Depletion voltage (V_{dep}), the doping concentration level (N_d) , the leakage current density (J) and the carrier generation lifetime (τ_g) are extracted from test diodes; the oxide thickness (T_{ox}), the fixed oxide charge density (Q_{ox}) and the flat band voltage (V_{fb}) are obtained from MOS capacitors with the isolation oxide as dielectric, and the surface generation velocity (s_0) is evaluated on gate controlled diodes. The values evidence that the etching step in TMAH solution does not induce any detrimental effect on the electrical behavior of the devices.

	V_{dep} [V]	N_d [10^{11}cm^{-3}]	J [nA/cm^2]	τ_g [ms]	T_{ox} [nm]	V_{fb} [V]	Q_{ox} [10^{10}cm^{-2}]	s_0 [cm/s]
No TMAH	17.6	2.6	2.7	18	438	0.77	1.4	2.5
With TMAH	13.5	2.0	2.2	22	437	0.77	1.37	3.0

Table 8. Parameters extracted from the electrical characterization of the test structures.

Thinned diodes

TMAH etched wafers have been electrically characterized by C-V and I-V measurements on devices realized both on the thinned membranes and on the full thickness bulk. The C-V measurements have been performed on the circular diodes shown in Figure 54a. The $1/C^2$-versus-V graphs, calculated from the experimental C-V curves, are reported in the Figure 55 and Figure 56 for wafers having membranes of 99µm and 57µm respectively. The full depletion voltages

determined from these plots are reported in Table 9. Values of about 1V have been obtained for the thickness of 99µm, while the 57µm thick membranes are fully depleted below 1 V. For the devices with a 300 µm thick substrate the depletion voltage is about 12 V.

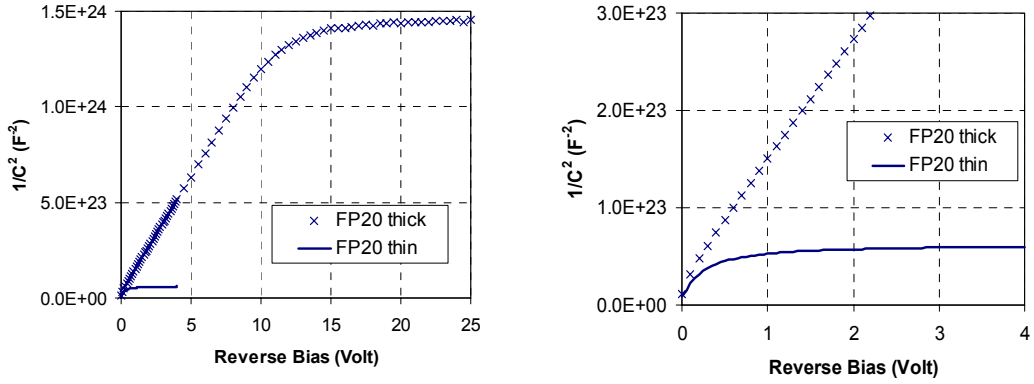

Figure 55: $1/C^2$ measurements: FP20 diodes (thickness:99µm)

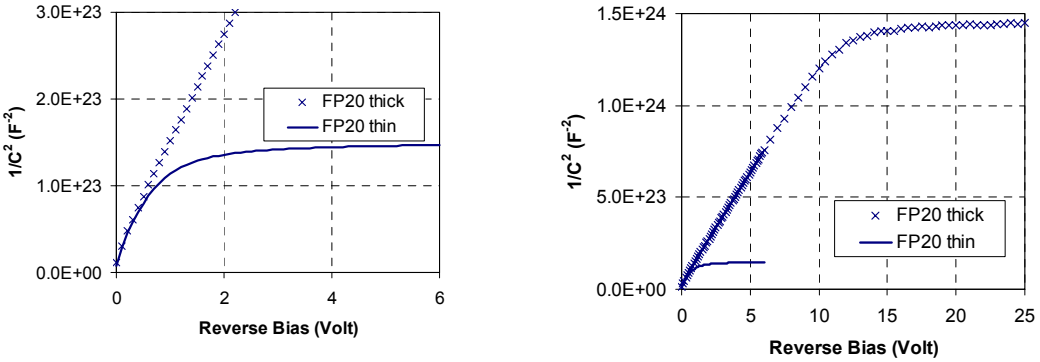

Figure 56 $1/C^2$ measurements: FP20 diodes (thickness:57µm)

I-V characteristics measured on square diodes having an area of 3.25mm^2 are reported in Figure 57 and Figure 58 for two wafers with different membrane thickness. The thinned diodes show very low leakage current densities with respect to the values obtained for the devices on the full bulk thickness. The result cannot be explained only by the difference in the generation volume underneath the junctions.

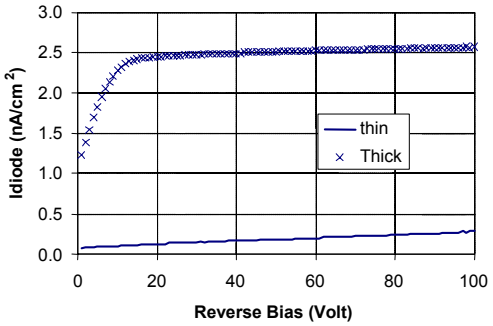

Figure 57.: IV characteristics: square PIN diodes (thickness:99 µm)

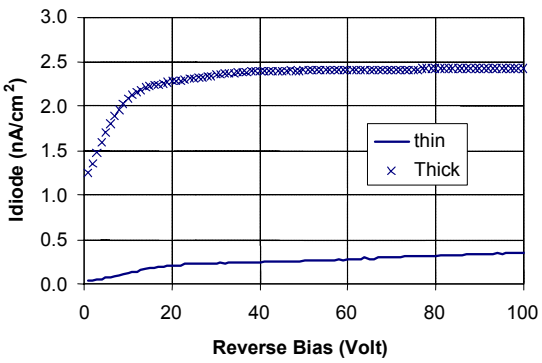

Figure 58.: IV characteristics: square PIN diodes (thickness:57 µm)

In fact, Table 9 shows that also the leakage current density per unit volume is lower for the thinned samples. A possible explanation can be an improved gettering action when the thickness of the substrate is reduced.

Table 9 Volume leakage current density and full depletion voltage

Membrane thickness [μm]	Leakage current [nA/cm3]	Full depletion voltage [V]
300	80	12
99	30	~1
57	55	<1

This study proved that TMAH-etching is a suitable technique for producing PIN diodes on thinned substrates. Irradiation with protons and radiation damage measurements of the existing structures has been planned. In near future, the same procedure will be applied to low resistivity (50Ωcm) Cz and FZ Si to perform a quantitative comparison with epitaxial Si detectors (see section 5.10).

6.3 3 Semi-3D detectors

This research activity is carried out by the US-RD50 groups [96]. In semi-3D detectors both p+ and n+ strips are implanted on an n-type substrate while the backside has a uniform n+ implant. In this novel structure, all n+ strips are connected to a positive bias while each p+ strip is connected to an electronics channel for signal readout. Before space charge sign inversion (SCSI), the depletion develops both vertically from p+ strips to the back n+ plane and laterally from p+ strips to the neighboring n+ strips. Therefore, the full depletion voltage will be about 20% higher than a conventional single-sided p+/n/n+ strip detector. After the sensors are inverted the depletion develops both from the n+ strips in the front side, and the n+ plane towards the p+ readout electrodes and we expect a reduction in full depletion voltage of about a factor of 3 to 4. The advantages of these novel p+-n+/n/n+ Semi-3D detectors are:
1) Planar technology which is easier to process than 3D sensors
2) Single-sided processing
3) Large reduction in detector full depletion voltage after SCSI. The mask set design and production have been completed, with the ordering of the whole set of masks for the processing of p^+-n^+/n/ n^+ Semi-3D Si detector prototype. The processing of the first prototype p^+-n^+/n/ n^+ Semi-3D Si detector batch has been started at BNL and the fabrication has been 60% completed. We expect in another month the fabrication of the first prototype batch will be finished, and the electrical tests can immediately start following the completion of the processing. We also plan the laser and beam tests of the Semi-3D Si detectors before and after neutron and or proton radiation.

In the meantime, Syracuse and Purdue groups have been doing detailed simulations of Semi-3D Si detector processing, electric properties and CCE properties before and after irradiation. Preliminary results are shown below. Figure 59 shows the 2D profile of the electric potential for a p^+-n^+/n/ n^+ Semi-3D Si detector before irradiation (no SCSI). The electric field lines, which point out the directions of hole movement (electrons move in the opposite directions), are marked by black arrows.

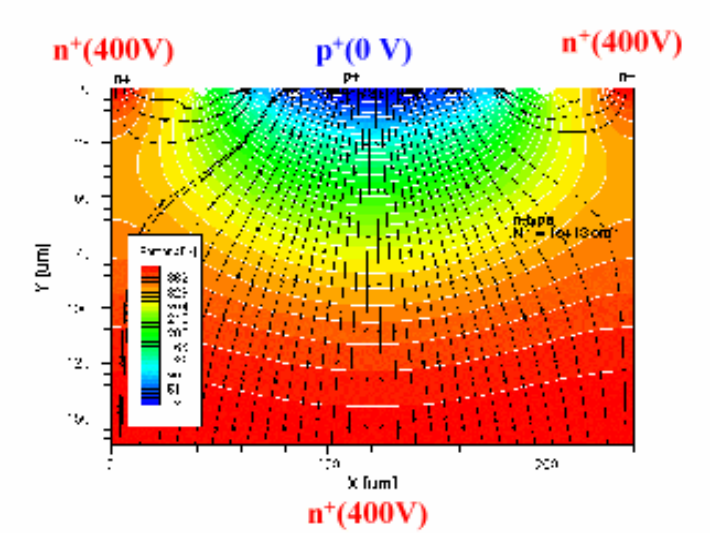

Figure 59 Simulation of a p^+-n^+/n/ n^+ Semi-3D Si detector before radiation (no SCSI). The colored profile is electric potential, and the black lines with arrows are electric field lines.

It is clear that the filed lines convert into the p^+ electrode (strip) that is the collection strip for holes. Electrons will go to the back n^+ plane and the front n^+ strips. The depletion extends vertically from the p^+ electrode (strip) to the back n^+ plane and laterally to the neighboring n^+ strips.

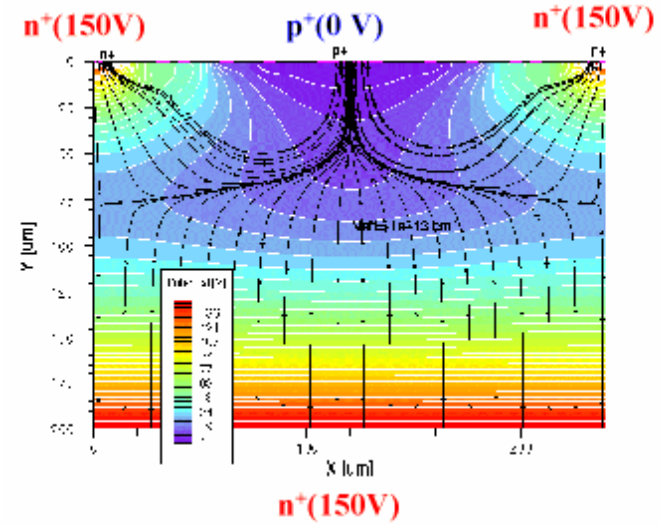

Figure 60.: Simulation of a p^+-n^+/n/ n^+ Semi-3D Si detector after radiation (SCSI). The colored profile is electric potential, and the black lines with arrows are electric field lines.

After irradiation to about $5x10^{14}$ n/cm^2, the detector is SCSI, and the space charge is negative and in high concentration ($1x10^{13}$ cm^{-3}). Since now the n^+ plane and the front n^+ strips are the electrodes with junctions (high E-field), the depletion extends vertically from the n^+ plane and the front n^+ strips toward the center of the detector and to the p^+ electrode (strip), and laterally from the front neighboring n^+ strips to the p^+ electrode (strip). Since the depletion now starts from both sides of the detector, the full depletion voltage is greatly reduced, by a factor of about 3, as compared to the standard structure. The electric field lines all first convert to the center of the detector, before finally converging to the collecting p^+ electrode (strip). Further simulations of CCE of the Semi-3D Si detector are under way.

7 New Materials

7.1 Introduction

The Collaboration proposes to investigate new, potentially radiation hard semiconductor materials, as possible candidates for the production of tracking detectors at very high luminosity colliders. A working group focussed on the development of SiC detectors has been set-up. A study of other new semiconductor materials has also started, in particular focussed on III-V compounds, which are characterised by large bandgap, and as SiC, have physical properties between Si and diamond (see Table 10). During this first year of RD50 Collaboration, the research activity has been focussed on SiC and GaN.

Property	Diamond	Si	4H- SiC	GaN
E_g [eV]	5.5	1.12	3.3	3.39
μ_e [cm^2/Vs]	1800	1450	800	1000
μ_h [cm^2/Vs]	1200	450	115	30
e-h pair creation [eV]	13	3.6	8.4	8.9
Displacement [eV]	43	13-20	25	≥15
Density [g/cm^3]	3.515	2.329	3.22	6.15
E Breakdown [V/cm]	10^7	$3x10^5$	$2.2x10^6$	$4x10^6$
saturation velocity [cm/s]	$2.2x10^7$	10^7	$2x10^7$	$2.5x10^7$
Dielectric constant	5.7	11.9	9.7	9.6

Table 10.: Properties of SiC and GaN as compared to diamond and Si.

7.2 Silicon Carbide

The activity on SiC is subdivided in the study of detectors based on: semi-insulating bulk SiC (thickness ~100μm) and epitaxial SiC layers (thickness 7-50μm)

7.2.1 Bulk Semi-Insulating SiC radiation detectors

7.2.1.1 - Detectors characteristics before irradiation

SiC detectors have been produced from bulk semi-insulating single crystal 4H-SiC, 550μm thick, obtained from Cree Research (USA). A vanadium compensation process is used by CREE to give very high material resistivities, $\rho > 10^{11}\ \Omega$ cm. The material is then thinned by lapping and polishing to ~100μm. The SiC detectors were made in a standard parallel plate configuration by depositing a nickel ohmic contact on the back surface and a titanium Schottky contact 0.5 mm in diameter on the front surface. To minimise surface leakage effects, a titanium guard ring was used to surround the top contact, coupled with silicon nitride passivation of remaining free SiC surfaces. The pulse height spectrum of SiC detectors have been measured with 5.48 MeV α–particles with reverse bias voltages in the range 50-600 V. At the maximum reverse voltage the charge collection efficiency was found to be only about 60%. This suggests the presence of defect levels that trap and recombine the charge before it can be collected. A study of the defects in native samples has been therefore carried out.

The effect of defects was probed initially by biasing the detector, then removing the bias voltage and recording the resulting current decay. The measured curves are well described by a model considering three defect levels involved, with time constants respectively 4.2s, 15.3s, and 125.3s.
The energy levels of the involved defects were inferred using thermally stimulated current measurements. Four energy levels were found in the sample corresponding to activation energies of 0.32eV, 0.39eV, 0.63eV and 0.92eV below the conduction band edge [97]. The 0.92 eV center is related to the vanadium compensation and the 0.63 eV level is related to the Z-center. Two of the measured levels are quite close in energy (0.32eV and 0.39 eV) and may result in similar emission times. This may therefore explain the three characteristic time constants observed in the current decay measurements.

7.2.1.2 - Detectors characteristics after irradiation and simulation of results

Several SiC detectors were irradiated at the 300 MeV/c π beam at the Paul Scherrer Institute (PSI), Villigen with fluences of 10^{12}, 10^{13}, and $5x10^{14}$ π/cm^2.
The I-V curves from detectors irradiated to different fluences are essentially unchanged for reverse bias voltages up to about 300 V. Beyond this voltage the characteristics initially deteriorate at low fluence, but then recover at high fluence. At $5x10^{14}$ π /cm^2 the reverse leakage current was back at the levels found for the unirradiated detectors right up to reverse bias voltages of 600 V.
Pulse height spectra were measured for SiC detectors irradiated to 10^{12} π /cm^2 and 10^{13} π /cm^2. The measurements were taken to the largest reverse bias voltage possible before breakdown at a given fluence. There is a slight deterioration of the charge collection efficiency due to irradiation, down from 60% to ~50% compared to the unirradiated detectors.
Detailed simulations of the SiC detectors have been carried out using the simulation package Medici, which solves the drift-diffusion equations for both charge types, coupled with the Poisson equation in the presence of trapping effects.
Three trap levels were incorporated into the SiC simulations: the Z-centre at energy $E_1 = E_c - 0.66$ eV (cross-section 10^{-14}cm^2), the vanadium center at energy $E_2 = E_c - 0.98$ eV (cross-section 10^{-15}cm^2), and a mid-gap level found to be important in irradiated samples at energy $E_3 = E_c - 1.6$eV (cross-section 10^{-13}cm^2).
Preliminary studies using a level at $E_c - 0.4$ eV showed that this had little impact on the charge transport, so it was omitted in the final simulations. The vanadium center was assumed not to change as a function of the fluence. The Z-center and mid-gap levels were assumed to be introduced at rates of 35 cm^{-1} and 5 cm^{-1} per unit fluence, respectively, consistent with current data for fast hadrons.
Simulations show that, if the vanadium concentration is of the order of $5x10^{17}$cm^{-3}, as in the investigated samples, the charge collection efficiency is about 60% in agreement with the experimental results [98].
The analysis suggests that vanadium compensated materials should be avoided in the production of SiC detectors. Recently non-vanadium containing semi-insulating SiC has become available from some manufacturers. In near future bulk detectors made from the improved substrates will be studied by the collaboration.

7.2.2 Epitaxial SiC detectors

High crystalline quality with corresponding low defect densities can be obtained by growing epitaxial layers on SiC bulk substrates. The main achievements regarding the epitaxial SiC detectors during the first year of RD50 collaboration are given below.

7.2.2.1 Growth of epitaxial 4H-SiC

Six 2" n-type 4H-SiC epilayers (different thickness and doping) were grown by IKZ-Berlin to be investigated within the RD50 collaboration. These epilayers were characterized first with contactless methods by means of minority carrier lifetime and thickness mapping: measurements show the high quality of the epitaxial layers. On two of the epilayers simple Ni Schottky contacts were deposited for checking the homogeneity of the doping (by C-V measurements) and of defects existing in as-grown material (by DLTS measurements – mapping). The results on one epilayer are shown in Figure 61 and Figure 62.

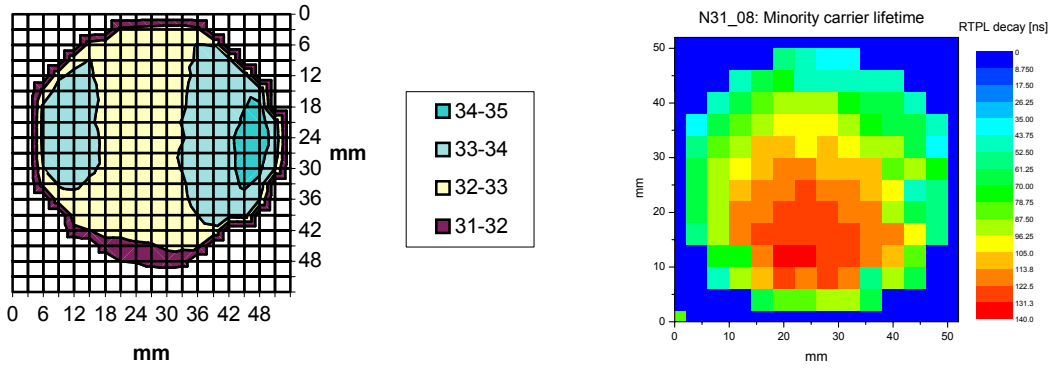

Figure 61.:Epilayer N31_08 - Measurements of the thickness and minority carrier lifetime

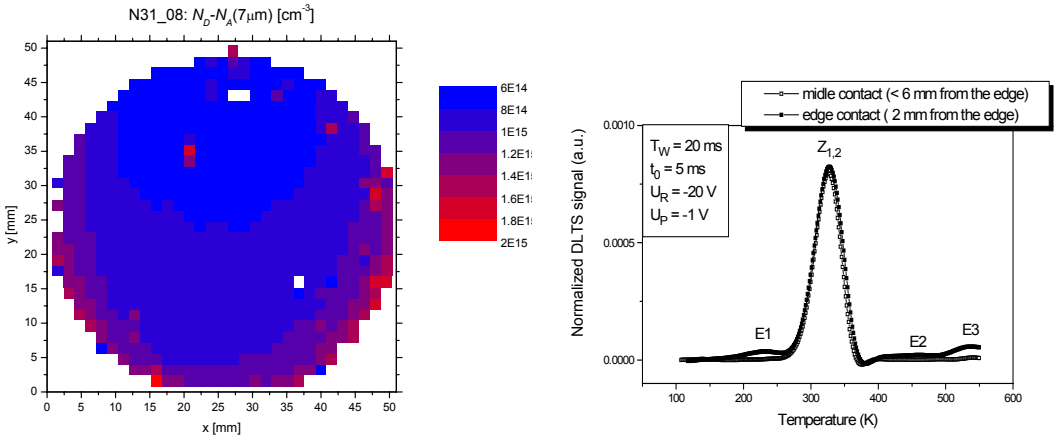

Figure 62.:. Epilayer N31_08: a) doping mapping b) defects in as-grown material.

7.2.3 Masks Design and fabrication

It was designed and fabricated one mask for processing Schottky contacts on the epilayers grown by IKZ (see Figure 63).

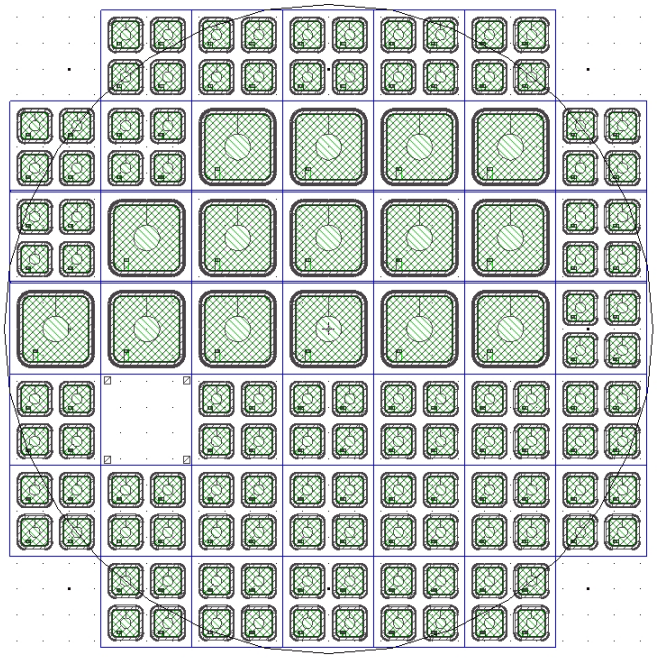

Figure 63.: Mask for RD50 SiC test structures

7.2.4 Fabrication of single pad detectors

A number of different test structures have been already fabricated/studied this year:

A: Detectors based on Au, Ni_2Si, Ti or Ni Schottky contacts (see Figure 64) with a thickness up to 40μm and doping down to $5 \cdot 10^{13}$ cm^{-3}.

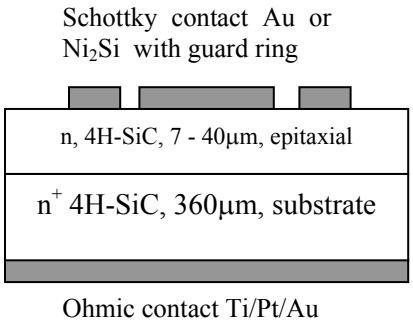

Figure 64.: Detector structure based on Schottky contacts

B: Transistor detector structures based on low doped epitaxial films of p-type 4H- and 6H-SiC, with N_{eff} of ~$0.7\text{-}5 \cdot 10^{15}$ cm^{-3} and thickness up to ~30 μm. The contact to the base region of the triode structure was performed as Schottky barrier.

C: Detector structures with semitransparent windows on the Schottky contact and with guard rings, made using the mask shown in Figure 63, on one of the IKZ epilayers.

Detectors characterization before and after irradiation

A. Schottky diodes

Detector characteristics before irradiation

Leakage current of the order of 1-10pA/cm^2 have been measured with applied electric fields of the order of 1-10V/μm [99]. C-V characteristics measured at room temperature are shown in Figure 65 for two Schottky diodes with Au contact of different active area evaporated on a 20μm-thick epilayer. The effective doping concentration N_{eff} and epitaxial layer thickness, evaluated by C-V analysis, resulted: N_{effA}~5.7x10^{14}cm^{-3}, d_A=20.3μm, N_{effB}~6.1x10^{14}cm^{-3}, d_B=20.8μm. No change has been observed in the C-V characteristics in the frequency range 1KHz-1MHz [100].

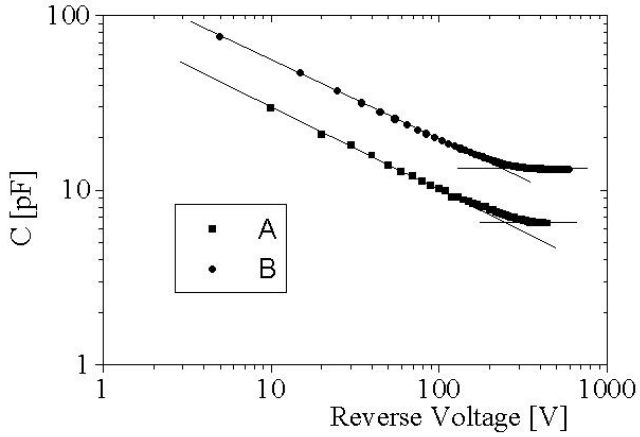

Figure 65 C-V characteristics two Au Schottky barrier 4H-SiC detectors measured at room temperature with a 100KHz test signal frequency.

Charge collection properties have been tested by 5.5 MeV α-particles from ^{241}Am source and with β particles from a 0.1 mCi ^{90}Sr source. The measurements with the β-source have been performed with an Amptek A255 charge integrating preamplifier (noise ENC~280e+10e/pF, shaping time 2μs). The trigger signal is given by a miniature scintillator connected with a photomultiplier.

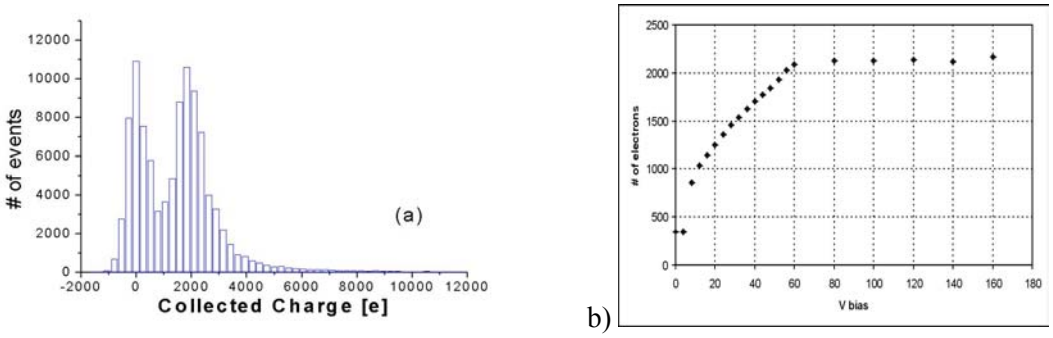

a) b)

Figure 66.: Unirradiated detector with 38.2μm epilayer: a) Charge collection for β-particles from ^{90}Sr at full depletion voltage b) Charge collection of the Schottky 4H-SiC diode as a function of reverse voltage under β particles from ^{90}Sr source at room temperature.

A 100% charge collection efficiency (CCE) has been observed with α– and β-particles using 4H-SiC epilayers with different thickness and doping concentrations [99-101]. The signal is stable and reproducible: no priming or polarization effects are observed. The charge collection

spectrum for β-particles from ^{90}Sr at full depletion voltage is shown in Figure 66a for a 40μm-thick detector with N_{eff} down to $5x10^{13}cm^{-3}$: the pedestal (noise) is clearly separated by the signal (Landau distribution) [100,101]. The collected charge is plotted as a function of the reverse bias. Figure 66b: a full detection efficiency corresponding to ~2100 e-h pairs generated by the β-particles is obtained at full depletion voltage of 60V (reverse voltage required to fully deplete the epitaxial layer).

After irradiation

The devices described in the previous section are now under irradiation with 24 GeV protons up to $10^{16}cm^{-2}$ at CERN: CCE, C-V and I-V characteristics will be measured after irradiation. Similar detectors, but with lower thickness and higher doping densities (N_{eff} = $2.5x10^{15}cm^{-3}$, W~20μm) have been irradiated with electrons (8.2 MeV) and γ-rays (^{60}Co source) at fluences and doses ranging from 0 to 9.48×10^{14} e/cm^2 and 40 MRad, respectively. The charge collection efficiency (CCE) has been studied by means of 4.14 MeV α-particles impinging on the Schottky contact. The results are described in refs. [102, 103]: here we summarise the most meaningful evidences. No increase in the leakage current was observed after irradiation up to the highest fluence/dose. A decrease of N_{eff} to $6.9x10^{14}cm^{-3}$ was measured after irradiation with the highest electron fluence. A 100% charge collection efficiency has been measured for reverse voltages higher than the one needed to have a depletion region equal to the α-particle projected range, even after irradiation with the highest fluence/dose. By comparing measured CCE values with the outcomes of drift-diffusion simulations, values are inferred for the hole lifetime, τ_p, within the neutral region of the charge carrier generation layer. τ_p was found to decrease with increasing radiation levels, ranging from 300 ns in non-irradiated detectors to 3ns in the most irradiated ones [102].
A different batch of samples, with N_{eff} = $3\text{-}5x10^{15}cm^{-3}$ and thickness ~7μm have been irradiated by 6.5MeV protons. Samples characteristics are listed in Table 11: Schottky contact type, proton fluence, effective doping concentration and its change with respect to the fluence. Donor removal rates seems to be similar to those of Si starting with the 3rd fluence. The I-V characteristics are given in Figure 67. It was evidenced that new defect-associated energy levels are produced by irradiation, some of them in concentration as high as $5x10^{14}$ cm^{-3} (see section 3.5)
. Even though this value is of the same order of magnitude as the epilayer doping density, the Richardson's plot shows that the charge carrier transport is nearly unaffected by irradiation. This is likely due the relatively shallow level position in the gap of the irradiation induced defects [104].

Schottky Contact	Fluence [cm^{-2}]	N_{eff} [cm^{-3}]	ΔN_{eff}/Fluence [cm^{-1}]
Ti + 400°C	Unirradiated	$4.43\cdot10^{15}$	-
Ti + 400°C	$1.0\cdot10^{11}$	$4.39\cdot10^{15}$	400
Ti + 400°C	$1.0\cdot10^{12}$	$4.30\cdot10^{15}$	130
Ti + 400°C	$3.2\cdot10^{13}$	$3.33\cdot10^{15}$	38
Ni	$3.2\cdot10^{13}$	$3.40\cdot10^{15}$	31
Ni	$6.4\cdot10^{13}$	$2.88\cdot10^{15}$	24

Table 11.: Change in the effective doping concentration after irradiation with 6.5MeV protons up to fluences of $6.4\cdot10^{13}cm^{-2}$ in 4H-SiC epitaxial Schottky diodes (epilayer thickness: 7μm) [104].

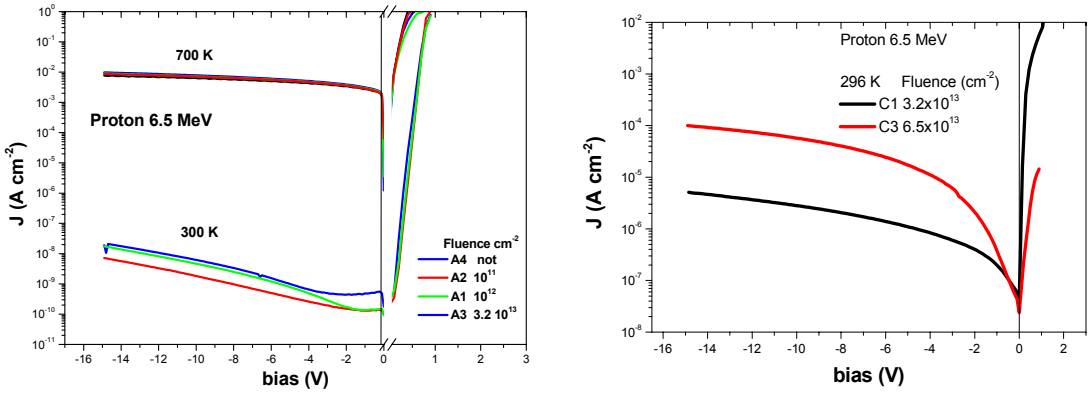

Figure 67.: I-V characteristics for diodes with: a) Ti contacts; b) Ni contacts [6.7].

7.2.4.1 B. Detectors based on triode structures

The main idea for the development of triode structures is to get amplification of the charge generated in the detector bulk and to obtain a gain of the detector signal. In this preliminary study two types of epitaxial p-type layers have been grown on n^+ SiC wafers: 6H-SiC (processed in the Ioffe Institute) with N_{eff} ~$7.5 \cdot 10^{14}$ cm^{-3} and W~10 μm and 4H-SiC (processed in Linkoping University, Sweden), with $N_{eff} = (3\text{-}5) \cdot 10^{15}$ cm^{-3} , W ~30 μm. The contact to the base region of the triode structure was performed as a Schottky barrier. Thus, the triode detector had the following structure: emitter: n^+ SiC wafer, base: p^+ epi-layer, collector: Schottky barrier. The structures were investigated before and after irradiation by 8MeV protons up to $10^{14} cm^{-2}$ by means of C-V characteristics and charge collection efficiency using an α-particle source with the energy of 5.48 MeV.

Irradiation of the 6H-SiC triode resulted in a significant change of C-V characteristics: full depletion voltage $V_{dep} \approx 2.5$ V and effective doping concentration of $N_{eff} \approx (1.8\text{-}2.6) \cdot 10^{13}$ cm^{-3} were measured after irradiation. Previous studies on 6H-SiC diodes [105] already shown compensation after irradiation with fluences beyond 10^{13} cm^{-2}, due to the creation of radiation induced deep levels in the SiC detector bulk. Charge collection efficiency was measured by reducing the energy of the α-particles to 3.5 MeV such that the range is 10μm (equal to the epi-layer thickness). A 100% CCE was measured before and after irradiation for $V_{rev} \geq V_{dep}$; maximum value of gain was 18, obtained at a reverse voltage V_{rev} = 125 V (Figure 68).

In 4H-SiC epi-layers both the effective doping concentration and their thickness were higher than in 6H-SiC. Therefore it could not be achieved the full depletion of the non-irradiated 4H-SiC to obtain the signal gain specific for triode structures. The charge collection efficiency as a function of the square root of the reverse bias after irradiation is shown in Figure 69. These measurements were performed using α-particles with the energy of 5.5 MeV. The gain effect was not obtained in these structures even with a reverse voltage close to 1 kV. Estimations showed that for these 4H-SiC structures the depth of the high field region in the epitaxial layer of irradiated samples is close to 15 μm that is only a half of the total layer thickness (30 μm). In this region the structures act as standard diodes. The maximum value of the CCE after irradiation is ~80%, achieved at 700V, the energy resolution is ~2%.

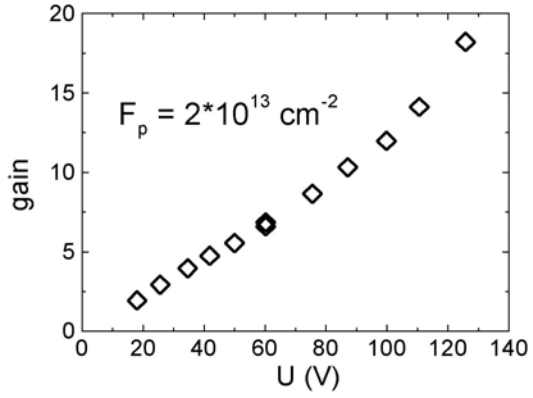

Figure 68: Gain as a function of reverse voltage measured with a 6H-SiC triode structure after irradiation with 2x10^{13} cm^{-2} 8 MeV protons.

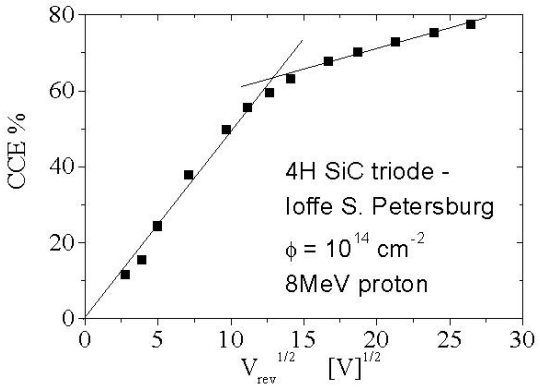

Figure 69: Charge Collection Efficiency, measured with α-particles as a function of the square root of the reverse voltage for a 4H-SiC triode structure after irradiation with 10^{14} cm^{-2} 8 MeV protons.

7.3 Gallium Nitride

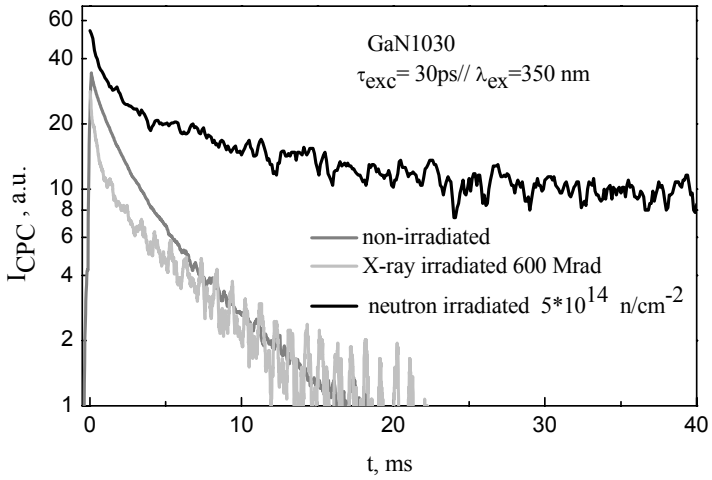

Figure 70.:Decay of non-equilibrium conductivity in non irradiated , X-ray irradiated up to 600MeV and neutron irradiated SI-GaN

A preliminary research on GaN has been carried out using epitaxial layers grown by MOCVD technology with a different trimethylgallium (TMG) flow rate that allowed to grow the semi-insulating GaN (SI-GaN) layers [106, 107]. These samples were fabricated from semiinsulating epitaxial GaN, grown at the University of Tokushima in Japan. The epitaxial material was grown on a sapphire substrate, and consisted of a 2.5 μm thick SI-GaN upper layer upper grown on a n-type

GaN buffer layer. Pad detector test structures were fabricated using 1.5 mm diameter evaporated gold Schottky contacts. Samples have been irradiated by X-rays (10 keV up to 600 Mrad) and neutrons (>100 keV up to the fluence of $5 \cdot 10^{14} cm^{-2}$). The charge collection properties have been studied with α – particles from ^{241}Am by Glasgow and Surrey: the CCE was found to be approximately 92% before irradiation, 77% and after neutron irradiation. Negligible effects on charge collection efficiency have been observed after X-ray irradiation. A scanning beam (2 MeV α–particle accelerator) was used to probe the charge collection uniformity at Surrey: good uniformity was found with no field enhancement at edges. It was also observed that irradiation changed the non-equilibrium conductivity decay (Figure 70) evidencing the presence of radiation induced defect structures.

These preliminary results showed that GaN is a promising radiation hard material. Further investigations on GaN are now planned with thicker samples. High resistivity GaN with thickness up to ~500 μm manufactured by the Lumilog (Vallauris, France, http://www.lumilog.com) will soon be available to the RD50 collaboration.

8 Full Detector Systems (FDS)

The FDS research line of RD50 aims to test the properties of segmented detectors after heavy irradiation. These tests are particularly important because they allow to choose the optimal geometry (diode structure, detector thickness, cell size…) for the targeted radiation fluence and to validate the use of non-standard silicon substrates for the production of large area segmented devices. During this first year our tests concentrated on the most relevant parameter for detector applications, namely the charge collection efficiency as a function of the applied voltage after irradiation (CCE(V)). The knowledge of the CCE(V), combined with the geometrical characteristic of the detector and the performances of the read-out electronics allow to evaluate the signal over noise (S/N) performances of the system as a function of the irradiation and therefore to anticipate the limit of operation of the devices in the experiments. Simulation of electric field profile and charge collection efficiency up to a fluence of fast hadron of $10^{16} cm^{-2}$ have been also carried out.

Main interest of this project is also to perform tests on radiation hard segmented devices in LHC-like experimental conditions, through the close collaboration between RD50 and the groups involved in the production of silicon vertex trackers of future LHC experiments: to this purpose a number of research activities have been activated in this year.

8.1 Oxygenated p-type substrates

The CCE(V) of irradiated silicon detectors depend on the trap density and on the collection time (t_c), therefore on the drift velocity of the charge carriers. The amount of the trapped charge is inversely proportional to t_c. The charge carrier velocity v depends on the local electric field, E(x), like $v = \mu_{e,h} E(x)$ until saturation velocity. As a consequence a lower trapping is expected for carriers moving in high electric field (smaller t_c). Silicon detectors are usually manufactured by implanting high doped p-type strips on high resistivity n-type substrates. An ohmic contact (high doped n-type) is implanted on the back-plane (p-in-n diode structure). After inversion the junction, and the high electric field, migrates on the back-plane contact. In this situation, after type inversion, a better charge collection is obtained by segmenting the n-type implant (n-in-n). Figure 71 shows the advantage in term of CCE(V) obtained by n-in-n detectors compared to p-in-n [108].

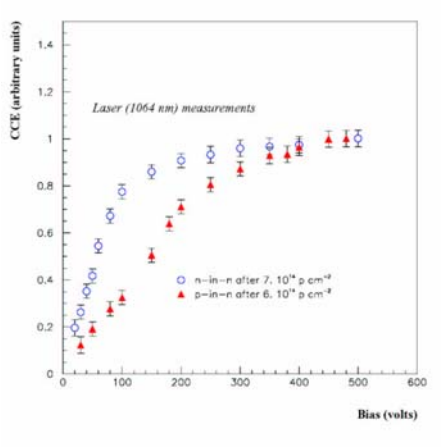

Figure 71.: Comparison between charge collection efficiency of a n-side readout detector after $7 \cdot 10^{14} p/cm^2$ and a p-side detector after $6 \cdot 10^{14} p/cm^2$.

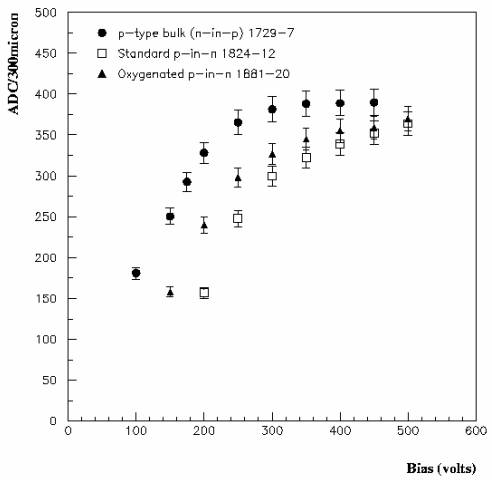

Figure 72: Comparison of charge collection vs bias voltage between n-in-p and p-in-n proton irradiated microstrip detectors after irradiation with 24 GeV/c protons [109].

The n-side read out can be implemented on n-type or p-type substrates. The use of p-type substrates has the advantages of avoiding type inversion and providing the cheapest processing cost, due to the possibility of one side processing, compared to the double side processing required by n-type silicon substrates. In previous works, a substantial improvement of charge collection at low bias voltages was observed after irradiation when compared to the p-side read-out [109] (Figure 72).

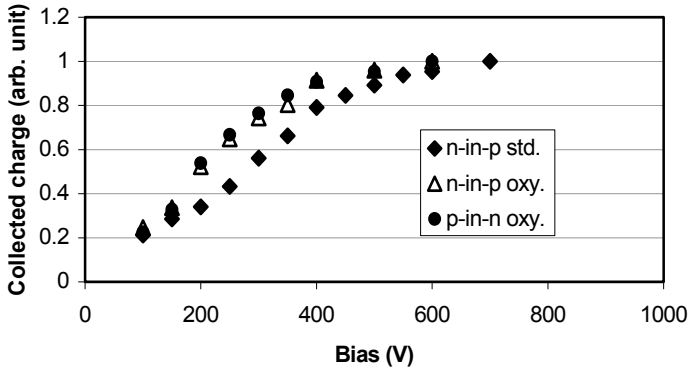

Figure 73.: Charge collection of oxygenated and standard n-in-p detectors in diode configuration after $1.1 \times 10^{15} cm^{-2}$ (24GeV proton) The collected charge is normalized to the maximum charge collected at 700 volts.

We investigated the charge collection properties of microstrip n-in-p detectors made with oxygenated p-type Si substrates, comparing their performances with p-in-n standard and oxygenated Si detectors [110]. P-type wafers have been oxygen enriched by CNM Barcelona. Miniature micro-strip detectors have been produced for the first time with these oxygenated p-type substrates. Two sets of oxygenated and standard detectors have been irradiated to 2.7 and 11.5×10^{14} p cm^{-2} with 24GeV protons at the CERN-PS, at room temperature and unbiased. After irradiation they were kept at low temperature. Their charge collection properties have been measured in diode configuration, with all the strips connected together and read out with a fast

current amplifier (< 1ns rise time). This technique is used to measure the maximum collected charge and the full depletion voltage, to provide a comparison of different substrates in "diode" configuration. The signal is though due to both electron and holes charge carriers and the advantage of n-side read out in segmented devices (mainly electron signal) is not evidenced. This is shown in Figure 73, where the charge collection efficiency, normalized to the value collected at 700 V, is plotted for oxygenated and standard detectors after the highest radiation fluence for p-in-n and n-in-p geometry. The relative charge collection at low biases is improved in the oxygen enriched detectors whatever geometry was used.

Figure 74 shows the charge collection efficiency, normalized to the value before irradiation, of the oxygen enriched detectors for two irradiation fluences. Figure 75 shows the dependence of the full depletion voltage (V_{fd}) on the proton fluence. These detectors show good charge collection properties also after heavy irradiation (~70% of the charge is collected after 1.1×10^{15} p·cm^{-2}). The oxygenated p-type detectors show a slightly higher charge collection at low bias voltages, after heavy irradiation, compared to standard p-type substrates, due to a reduced value of V_{fd}. They both show a reduced dependence of V_{fd} on the radiation fluence (Figure 75). This may be due to the low resistivity starting silicon or to a reduced change in the effective space charge in this type of material. Further studies with initial higher resistivity p-type silicon are needed to demonstrate this option for lower cost high radiation tolerant detectors.

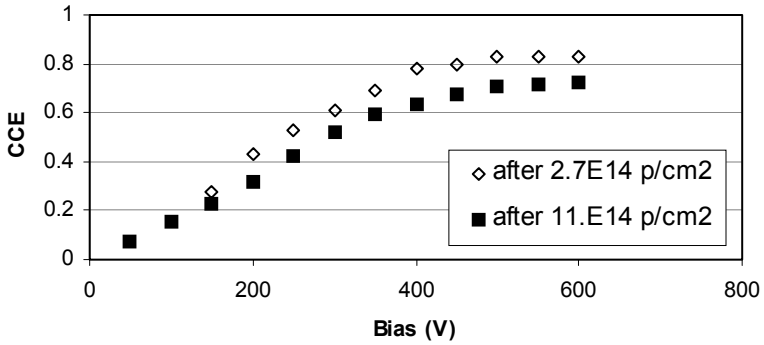

Figure 74.: Charge collection efficiency, normalized to the preirradiation value, of oxygen enriched p-type substrate silicon detectors after 2.7 and $11.0\cdot10^{14}$ p cm^{-2}.

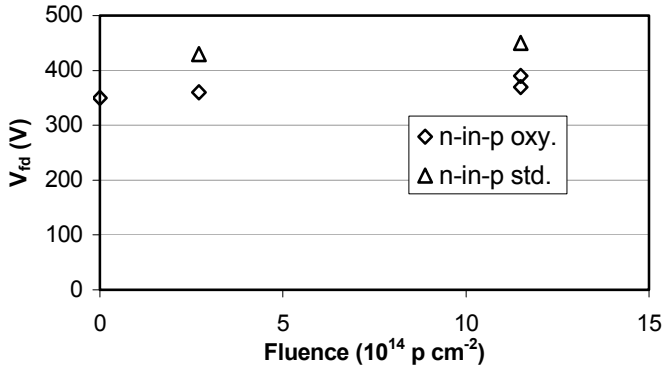

Figure 75.: V_{fd} (from fit to the CCE characteristics) as a function of the proton fluence.

8.2 Electrical characterization of Magnetic Czochralski Si microstrip detectors

Recent developments in the crystal growth technology of Czochralski silicon have enabled the production of wafers with sufficiently high resistivity and with well-controlled, high concentration of oxygen [45]. The Helsinki Institute of Physics has processed large area strip detectors on wafers grown with the magnetic Czochralski (MCZ) method [48, 51]. This MCZ material offers potential advantages for high energy physics applications, like the extended controllable range of oxygen dissolving from the silica crucible during the crystal growth and the ability of produce very large area wafers (300 mm diameter). It is worth to mention that large area wafers can be cost effective when large size detector are required in the experiments.

The MCZ detectors have been studied before and after irradiation with 10 MeV protons and compared with standard FZ devices. Current-voltage (IV) and capacitance-voltage (CV) measurements were done to the irradiated strip detectors at University of Karlsruhe, Germany, using a probe station equipped with vacuum cold chuck. The measurement temperature was -10^0C $\pm 1^0$C. Frequency of the capacitance measurements was 10 kHz. During the measurements the outermost guard ring of the multi-guard ring structure of the strip detectors was grounded.
The results of the CV measurements are shown in Figure 76.

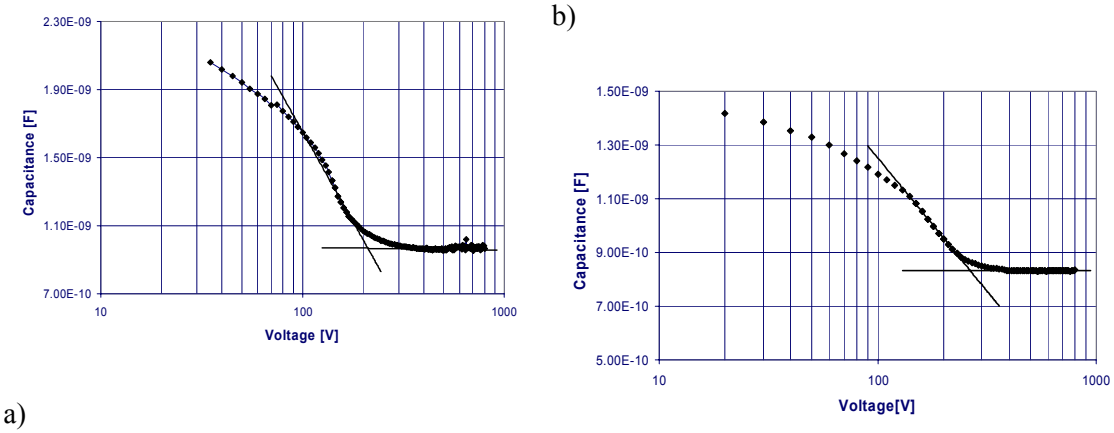

Figure 76.: Capacitance vs voltage curves of strip detectors after (a) 1.6×10^{14} 1 MeV neutron eq. cm^{-2} and (b) 8.5×10^{13} 1 MeV neutron eq. cm^{-2}. These curves are used to extract the full depletion voltage.

The measurement before irradiation gives a V_{fd} of 260V for a 300 μm thick substrate, corresponding to an initial resistivity of about 1200 Ωcm. At full depletion the leakage currents of the MCZ detectors are somewhat higher than in Fz-Si detectors. This is explained by higher concentrations of crystal defects in MCZ silicon. It has to be stressed that the current before irradiation is not a critical parameter for detectors to be used in high radiation environments. When irradiated with 10 MeV protons the leakage current of the MCZ devices does not increase linearly as a function of irradiation fluence, as is the case with standard Fz-Si devices, showing a comparatively reduced damage. Further tests are needed to better evaluate the qualities of the MCZ material when irradiated with high energy charged particles (e.g. 24GeV/c protons), but the results obtained with large area segmented devices are promising.

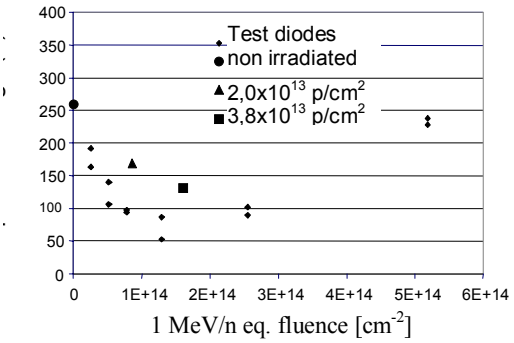

Figure 77.: Changes of full depletion voltage of microstrip detectors and diodes made on the same MCZ substrate with proton dose (1 MeV neutrons/cm^2 equivalent). The depletion voltage is scaled to the value required for the depletion of a 300µm thick detector.

8.3 Electric field profile in segmented detectors as a function of the fluence

The knowledge of the electric field profile in irradiated devices is important to correctly predict the current pulse shape and calculate trapping effects, with the main aim to simulate the CCE(V) as a function of fluence. In past works a double peak in transient current has been observed when shallow ionisation (alpha particles from ^{241}Am or red light impinging at the electrode) takes place on the n^+ in n implant of detectors irradiated above the type inversion fluence, due to the presence of high electric field regions on both sides of the detector (double junction) [111,112,113].The group of St.Petersburg studied this effect and the evolution of the electric field profile as a function of the irradiated fluence.

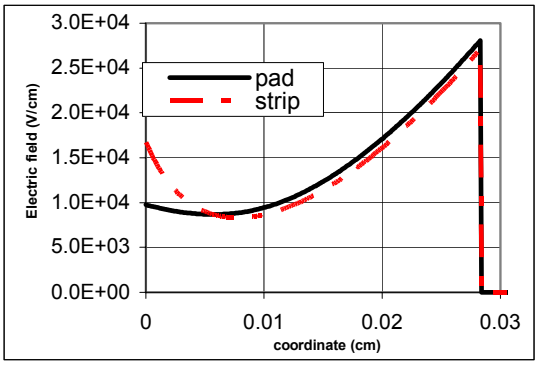

Figure 78.: Comparison of the electric field profile in single pad and microstrip detectors irradiated up to $2\cdot10^{14}$ cm^{-2} 1MeV neutronequivalent (V_{rev} = 400V, T = 290K). The coordinates x = 0 and x = d correspond to the p^+ and the back n^+ contacts, respectively.

Electric field in single pad detectors is calculated as described in [114], for microstrip detectors the model has been adapted by focusing the field lines to the segmented electrodes. A polynomial parameterization was used, with parameters defining the strip detector topology (e.g. strip width 18µm, pitch 80µm, thickness 285µm). The effect of trapping was added to the model considering two deep levels with trap parameters: E_d-E_v = 0.48eV, E_c-E_a = 0.525eV, σ =10^{-15}cm^2 and corresponding introduction rates: g_d =6cm^{-1} g_a =3.7cm^{-1}. Figure 78 and Figure 79 evidence the change in E(x) introduced by the segmentation of the electrodes. Figure 80 shows the creation of two high field regions on both sides of the detectors at high irradiation fluences.

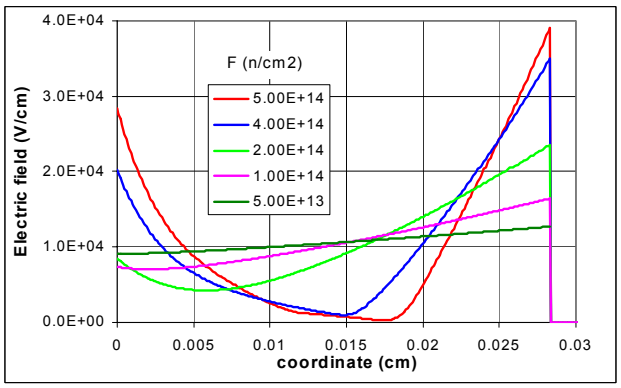

Figure 79.: Electric field profile in detectors irradiated at different neutron fluences at the operational temperature of 290 K and a bias voltage of 300 V.

8.4 Pixel Detectors

At high particle fluences (up to 10^{16} cm^{-2}) trapping times is comparable with charge collection times so losses due to drifting charge trapping become significant. Simulation has been carried out to quantify the impact of trapping on the sensor charge collection properties and to evaluate if thin pixel detectors can successfully operate at such fluence levels. The current induced at the electrodes by a point charge q drifting in the electric field of a reversely biased silicon detector is:

$$I_{e,h}(t) = q \exp(-\frac{t}{\tau_{eff,e,h}}) E_W(r_{e,h}(t)) \mu_{e,h} E(r_{e,h}(t))$$

The exponential term is due to trapping, with $\frac{1}{\tau_{eff,e,h}} = \beta_{e,h}\phi_{eq}$ and $\beta_e = 5.7 \cdot 10^{-16}$ cm^2/ns $\beta_h = 7.7 \cdot 10^{-16}$ cm^2/ns and E_W is the weighting field. Uniform charge generation along the track and uniform effective doping concentration in the bulk have been assumed. Simulated (W = 50μm, N_{eff}=0.0071cm^{-1} ·ϕ_{eq}) induced currents for DOFZ Si pixels operated at full depletion are plotted in Figure 80: the charge collection time is found about 0.15ns at 10^{16}cm^{-2}. Figure 81 shows the calculated collected charge as a function of the fluence for n^+-n and p^+-n 70x70μm^2 pixels: the results shows that at the highest fluence of 10^{16}cm^{-2} at best only 1000-2000 e are collected, with small differences between different pixel thicknesses [115].

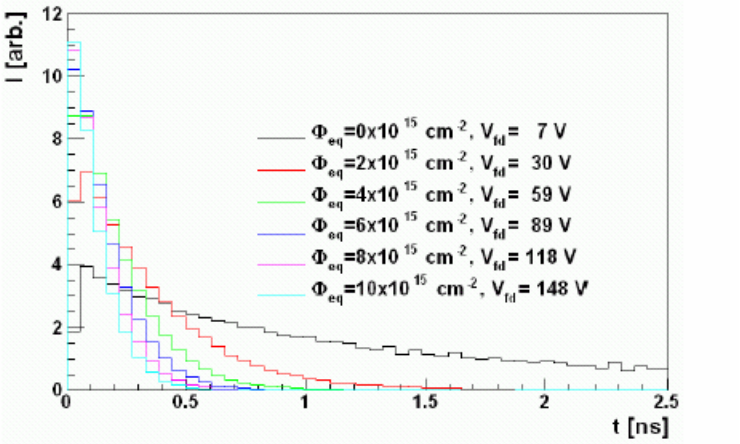

Figure 80.: Simulated induced current decay in Si DOFZ pixel detectors for different irradiation fluences (1MeV equivalent) up to 10^{16}cm^{-2}.

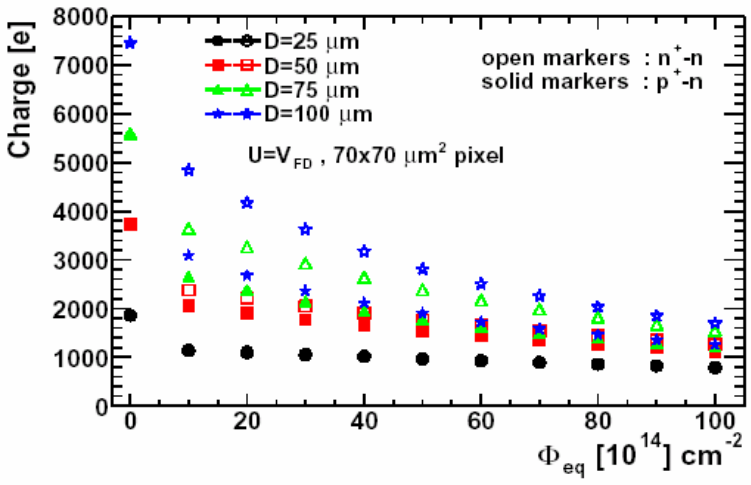

Figure 81.: Collected charge at full depletion in Si DOFZ 70x70μm^2 n^+ n and p^+ n pixel detectors vs. fluence (1MeV equivalent) for different material thickness.

8.5 RD50 Common Mask for segmented Si detectors

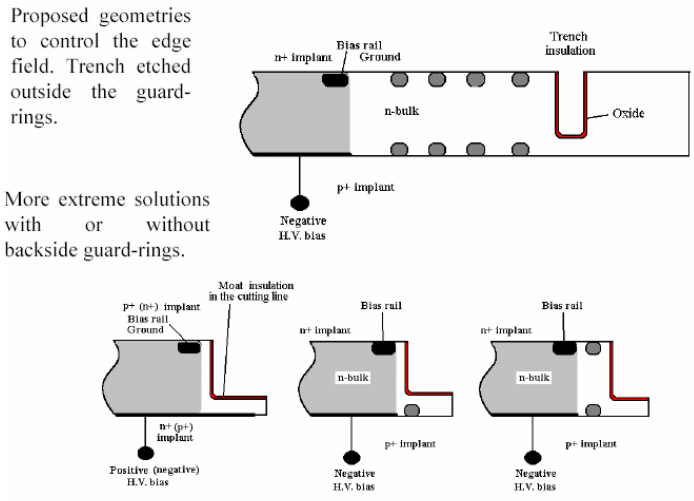

Figure 82.: Proposed geometries to control the edge field.

The design of a set of masks for the production of segmented and single pad Si detectors has been completed and presently under process. The mask set will be used to process detectors by different manufacturers with the two-fold intent to provide common tests structures to the RD50 collaboration and to compare similar devices produced by different manufacturers. In fact, it was previously observed that processing plays a significant role in the radiation hardness of Si detectors, especially in the case of standard FZ Si. This comparison will be carried out in the next year. The mask set has been designed to provide miniature microstrip detectors with about 100 strips suitable for bonding to available 40MHz analogue electronics. A reduced distance between the edge to the active area, with trench etched outside the guard rings, has been implemented (see Figure 82). This last feature aims to study the breakdown properties of the detectors when a minimum distance d of the active volume from the cut edge of the detector is required by the experiment (e.g. TOTEM, LHCb VELO). The optimization of d and of the maximum applied bias,

below breakdown can be studied with the various microstrip detector designs implemented in this mask.

8.6 Research activities in collaboration with LHC experiments

- ATLAS and CMS pixel groups

A simulation [116] has been performed using parameterizations of N_{eff} and lifetimes as a function of the fluence and annealing procedure, taking into account the ATLAS pixel detectors geometry. Simulation has been carried out for different thickness, operating conditions (bias, temperature) and electronics parameters (threshold, noise). Figure 83 shows the simulated efficiency vs. fluence with 3000e threshold of Si DOFZ ATLAS pixels for different thickness [117], plot evidences that present n+/n DOFZ silicon sensors are adequate up to $2x10^{15}$ $n_{eq}cm^{-2}$. At the highest fluence of irradiation $10^{16}cm^{-2}$, the average collected charge is about 1800 electrons resulting into a detection efficiency around 10%, independent of the thickness.

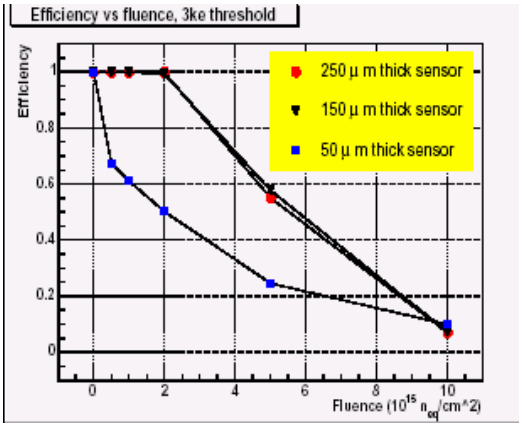

Figure 83 Simulated efficiency vs. fluence with 3000e threshold of Si DOFZ ATLAS pixels for different thickness.

A report on the status and recent tests of silicon sensors for the CMS pixel detector has been presented at the 3rd RD50 Workshop on Nov. 5, 2003 [118]. It has been decided to start the process of a few RD50 Si high resistivity Magnetic CZ with the CMS pixel technology. The CZ Si pixels detectors will be processed soon and characterized during the next year.

- Cz-Si microstrip detectors for LHCb VeLo

A collaboration started this year between LHCb VeLo and RD50 with the aim to test with the 120 GeV/c muon and pions beam the first microstrip detector produced with Magnetic Cz Silicon and equipped with LHC speed electronics. Initial results appear promising, data analysis is in progress [119].

9 Workplan and Milestones for 2004

1. Defect / Material Characterisation

Workplan/Milestones

1. Multivacancy-oxygen centers in irradiated silicon. The activities regarding assignment of the so-called X- and I-centers will be intensified. The outcome is very crucial in to order to understand and properly model the defect evolution during irradiation (this has strong implications on both the defect engineering and the device modelling).

2. Characterization of irradiation-induced defect clusters in silicon. Correlation between PL- and DLTS-results on defect clusters will be made using "identical" samples (that is, the samples are prepared simultaneously and under exactly identical conditions).

3. Characterization of irradiated silicon carbide samples. Detailed point defect characterization of n-type 4H-SiC "detector structures" irradiated with 24 GeV protons should be undertaken.

4. Characterization of hydrogenated silicon detectors (see also DE line)

5. Characterization of dimerized silicon and silicon detectors (see also DE line)

2. Defect Engineering

Workplan

1. Processing and systematic studies on specific process steps for controlled introduction or annealing of thermal donors and introduction of hydrogen will be performed on:
   - Oxygen enriched FZ-silicon
   - High resistivity n- and p-type MCZ-silicon (Okmetic/Finland)
   - Epitaxial silicon layers (material: ITME)

   Hydrogenation in hydrogen plasma will be performed by Minsk and Florence. The needed material and defect characterizations will be performed in close cooperation with the DMC-project.

2. For an optimization of the epi-layer thickness the processing of 25 µm and 75 µm thick epi-layers at CiS is foreseen for the beginning of 2004. A production of epi-layers on oxygen lean low resistivity FZ-substrates is envisaged.

3. Defect engineering by oxygen-dimer enriched silicon: This work will be performed in close collaboration with the DMC-project line. The workplan for 2004 includes:
   a. Characterization of the microscopic defects present in the first batch of dimer-enriched samples that have been produced in 2003 using TCT, TSC and IR.

b. IR and CV/IV analysis of the dimer enriched samples irradiated with 24 GeV/c protons in November 2003
c. Improvement of the simulation program using the results of the microscopic characterizations mentioned above
d. Based on the above mentioned analyses and simulations: Performance of an experiment to produce dimers in silicon with improved parameters compared to the first experiment in 2003 (temperature, particle type and fluence of the irradiation).

4. Defect engineering by pre-irradiation:
The processing of test detectors on pre-irradiated and untreated high resistivity FZ and Cz silicon by ICT-IRST in Trento is proposed for the beginning of 2004. Material and device characterization will be performed in close collaboration with the DMC-project. First irradiation experiments with high energy protons and investigation of the radiation tolerance of these devices are foreseen for the next PS irradiation run in 2004.

Milestones

1. Processing and characterization of detectors on defect engineered FZ-, n- and p-type MCz- , epitaxial silicon with different thicknesses and pre-irradiated FZ- and MCz-silicon.

2. Study of radiation hardness of all defect engineered FZ-, Cz- and epitaxial silicon and pre-irradiated silicon up to fluences of 10^{16} cm^{-2} (1 MeV neutron equivalent) with charged hadrons and neutrons.

3. Verification of hydrogenation of different silicon in a hydrogen plasma and investigation of hydrogen related defects after irradiation with low energy electrons and/or gammas.

4. Optimization of the oxygen dimerization process and thermal treatments for the development of detector grade material with a sufficient high dimer concentration.

3. New Materials

Workplan/Milestones

1. Study before and after irradiation up to fast hadron fluences of $10^{16}cm^{-2}$ of detectors made with epitaxial 4H-SiC of IKZ, Berlin and CREE. Tests will be performed with common RD50 Schottky barriers and $p^{+}n$ junctions.

2. Possible acquisition of thicker SiC epilayers and assessment of their charge collection efficiency.

3. Study of the charge collection properties and perform preliminary radiation hardness studies on detectors made with semi-insulating SiC without vanadium as a compensating doping.

4. Study of the charge collection properties and perform preliminary radiation hardness studies on thick high resistivity GaN Schottky barrier detectors

4. Pad Detector Characterization

Workplan/Milestones

1. Processing and electrical characterization (I-V, C-V, CCE with α- and β-particles) of the test structures produced with the common RD50 mask, with all defect engineered FZ-, Cz- and epitaxial silicon. To be carried out in collaboration with Defect Engineering project

2. Development of a common irradiation program of the new RD50 test structures with different particles (proton, neutron, high energy electrons, ions) and energies with fluences up to 10^{16}cm^{-2}.

3. Electrical characterisation (I-V, C-V, CCE with α- and β-particles) after irradiation and assessment of radiation hardness of the defect engineered detectors. To be carried out in collaboration with Defect Engineering project.

5. New Structures

Workplan/Milestones

1. 3D detectors. Aim to improve fabrication method, going to junction doping technique. CNM Barcelona and IRST Trento will work with Glasgow in this. Last year's Glasgow production was hit by machine down-time and lack of finding another suitable machine elsewhere. An aim for 2004 continues to be the manufacture of suitable 3D detector designs for LHCb/Velo, with the improved fabrication techniques. Testing of individual devices will be also done with MIPS in collaboration with Florence.

2. Semi 3D detectors. Semi-3D device fabrication will be completed. Testing will verify operation against simulations. Irradiations and characterization will be done during the summer.

3. Thin Detectors. Testing of initial thin detector structures will be completed. Further thin detectors in the CMS tracker format will be completed and tested. An irradiation program will be undertaken to verify improved radiation tolerance. A comparison between the performances of epitaxial Si detectors and thinned low resistivity and high resistivity Si detectors before and after irradiation will be carried out.

6. Full Detector Systems

Workplan/Milestones

1. Continuing the studies of the charge trapping parameters (quantification of the characteristic trapping times for electrons and holes) in order to establish a reliable parametric model valid for very high fluences an annealing times. Cross check of the values obtained with different techniques.

2. Selecting the manufacturers for the RD50-FDS detectors made with the different substrate materials shown in Table 12. Manufacturing and distributing the detectors among the various groups. Irradiation of the detectors at CERN (24 GeV/c protons) and at Ljubljana (reactor neutrons) up to particle fluences of $3x10^{15}$ cm^{-2}.

3. Cross check of the results between segmented and pad detectors made with different materials and from different manufacturers to extract the influence of the parameters involved in changing the detector properties (influence of the bulk material, different manufacturing processing, diode segmentation …).

4. Evaluation of the breakdown characteristics as a function of the different distances of the active volume from the cut edge and of the fluence (in view of possible applications in experiments where the active volume is as close as possible to the edge, e.g. TOTEM).

5. Determination of the *survival scenario* of microstrip detectors when coupled to the available LHC speed electronics (study of the signal to noise ratio for devices with different thickness and capacitive load as a function of fluence).

6. Feedback to the simulation activities to improve the incorporation, in the software package, of the radiation effects (the electric field properties in the inter-diode region are influenced by radiation induced interface state). Use of the simulation tools for updating the design of the segmented devices.

Table 12.: Materials to be processed in the first RD50 FDS production run

producer	type	resistivity	orientation
Wacker	n type	7k.cm	<111>
Wacker	p-type	10k.cm	<111>
Cz-HR	n-type	1.2 k.cm	<100>
Cz-HR	p-type	2 k.cm	<100>
Wacker	n type	4k.cm	<111>
Wacker	p-type	10k.cm	<111>
Cz-HR	n-type	1.2 k.cm	<100>
Cz-HR	p-type	2 k.cm	<100>
Wacker	n type	4k.cm	<111>
Wacker	p-type	10k.cm	<111>
Cz-HR	n-type	1.2 k.cm	<100>
Cz-HR	p-type	2 k.cm	<100>

10 Resources

All participating institutes organize their own resources required for the research activities in their home laboratories. Integration in a CERN approved R&D project allows them to apply for national funding in terms of financial and manpower resources. The collaboration comprises several institutes, which have access to irradiation sources (reactors and accelerators), as well as clean room and sensor processing facilities. A very wide range of highly specialized equipment for characterization of sensors and materials is also available (see [1]) .

- Common Fund

RD50 has a Common Fund to which each institute contributes every year a certain amount. The Common Fund is used for project related investments, like processing of common test structures or purchasing of special material and equipment. Furthermore it is used to cover the organization of collaboration workshops, common irradiation runs, or other specific activities of common interest.

- Lab space at CERN

The RD50 collaboration was temporarily using existing infrastructure and equipment at CERN in 2003 and requests to continue to do so in 2004. As a member of the collaboration, the section EP-TA1/SD can provide access to available lab space in building 14 (characterization of irradiated detectors), in building 28 (lab space for general work) and in the Silicon Facility (hall 186, clean space). RD50 relies on an appropriate support of these facilities by CERN.

- Technical support at CERN

The collaboration intends to use the existing test beams (PS / SPS) and the irradiation facility in the CERN PS complex (24 GeV/c protons and neutrons) in 2004. The latter is under the responsibility of the section EP-TA1/SD, which can provide the required support (sample preparation / irradiation / dosimetry). EP-TA1/SD is also able to provide support in wire bonding and sensor mounting. The expected work volume for 2004 is however estimated to be very limited. A low level of support from EP-MIC, EP-ED and EP-ESS may be profitable.

11 References

[1] R&D Proposal - DEVELOPMENT OF RADIATION HARD SEMICONDUCTORDEVICES FOR VERY HIGH LUMINOSITY COLLIDERS, LHCC 2002-003 / P6, 15.2.2002.

[2] Electronic versions of the talks are available on the RD50 www-page under http://cern.ch/rd50/doc/

[3] Zheng Li on behalf of the RD50 Collaboration.

[4] Michael Moll on behalf of the CERN RD50 collaboration, "Development of radiation hard sensors for very high luminosity colliders - CERN - RD50 project – "Nucl. Instr. & Meth. in Phys. Res. A 511 (2003) 97-105.

[5] Mara Bruzzi on behalf of the CERN RD50 Collaboration, "Material Engineering for the Development of Ultra-Radiation Hard Semiconductor Detectors", Frontier Detectors for Frontier Physics, Elba, May 2003

[6] Panja Luukka on behalf of the CERN RD50 Collaboration "Status of Defect Engineering Activity of the RD50 Collaboration" to be published in NIMA.

[7] Gianluigi Casse on behalf of the CERN RD50 Collaboration

[8] Mara Bruzzi on behalf of the CERN RD50 Collaboration.

[9] The samples were provided by M.Moll (CERN) and are originating from the CERN/RD48 research program.

[10] J. Stahl, E. Fretwurst, G. Lindstroem and I. Pintilie "Deep defect levels in standard and oxygen enriched silicon detectors before and after Co-60-γ-irradiation", NIMA 512,111-116 (2003).

[11] I. Pintilie, E. Fretwurst, G. Lindstroem and J. Stahl, Appl. Phys. Lett. 81, 165 (2002).

[12] I. Pintilie, E. Fretwurst, G. Lindstroem and J. Stahl, Appl. Phys. Lett. 82, 2169 (2003).

[13] I. Pintilie, E. Fretwurst, G. Lindstroem and J. Stahl, "Results on defects induced by Co-60 gamma irradiation in oxygenated and standard silicon", NIM A 514 (2003) 18-24.

[14] E. Fretwurst, G. Lindström, J. Stahl, I. Pintilie, Z. Li, J. Kierstead, E. Verbitskaya and R. Röder, "Bulk damage effects in standard and oxygen-enriched silicon detectors induced by ^{60}Co-gamma radiation" NIM A 514 (2003) 1-8.

[15] I. Pintilie, E. Fretwurst, G. Kramberger, G. Lindstroem, Z. Li and J. Stahl, „Second order generation of point defects in highly irradiated float zone silicon-annealing studies", 22nd International Conference on defects in Semiconductors ICDS 22, Aarhus, July 2003, to be published in Physica B

[16] J. Stahl, E. Fretwurst, G. Lindstroem and I. Pintilie, "Radiation hardness of silicon-a challenge for defect engineering", 22nd International Conference on defects in Semiconductors ICDS 22, Aarhus, July 2003, to be publish in Physica B

[17] G. Lindstroem, E. Fretwurst, G. Kramberger and I. Pintilie, „Towards Super Radiation Tolerant Semiconductor Detectors for Future Elementary Particle Research", 4th International ROCAM Conference, September 2003, Constanta, to be publish in J. Optoel. and Advance Materials

[18] G. Kramberger et al., "Super radiation tolerance of thin epitaxial silicon detectors", Nucl. Instr. And Meth. A - in press.

[19] E.V. Monakhov, B.S. Avset, A. Hallén and B.G. Svensson, Phys. Rev. B65, 233207

[20] E.V. Monakhov, G. Alfieri, B.S. Avset, A. Hallén and B.G. Svensson, J. Phys. Condens. Matter 15, S2771 (2003).

[21] V.P. Markevich, A.R. Peaker, S.B. Lastovskii, L.I. Murin and J.L. Lindstrøm, J. Phys. Condens. Matter 15, S2779 (2003).

[22] G. Alfieri, E.V. Monakhov, B.S. Avset and B.G. Svensson, Phys. Rev. B, accepted (2003).

[23] M. Pesola, J. von Boehm, T. Mattila and R.M. Nieminen, Phys. Rev. B60, 11449 (1999).

[24] R. Jones, private communication and RD50 workshop, Oct.2002
[25] M. Bruzzi, D. Menichelli, S. Miglio, M. Scaringella, E. Fretwurst and I. Pintilie, to be published.
[26] T.R. Waite, J. Chem. Phys. 28, 103 (1958)
[27] S. Lazanu and I. Lazanu, submitted to Physica Scripta (2003).
[28] S.Lazanu and I.Lazanu, "Theoretical treatment of long-term damage in silicon at the LHC accelerator and beyond" presented on the 3rd RD50 Workshop, 3-5 November 2003, CERN
[29] R. Harding, S. Hayama and G. Davies, to be published.
[30] A.Castaldini, A.Cavallini, M.Rossi, S.Ferrero, F.Giorgis, L.Scaltrito and F.Pirri, to be published.
[31] J.P. Doyle et al., J. Appl. Phys. 84, 1354 (1998).
[32] D. Åberg, A. Hallén and B.G. Svensson, Physica B 273-274, 672 (1999).
[33] T. Talibor et al., Inst. Phys. Conf. Ser. No. 142, 517 (1996).
[34] C. Hemmingson, N.T. Son, A. Ellison, J. Zhang and E. Janzén, Phys. Rev. B58, R10119 (1998).
[35] Th. Eberlein, R. Jones et al., Phys. Rev. Lett., accepted (2003).
[36] D. Åberg, A. Hallén, P. Pellegrino and B.G. Svensson, Appl. Phys. Lett. 78, 2908 (2001).
[37] G. Lindström et al. (The RD48 Collaboration), Nucl. Instr. and Meth. A 466 (2001) 308.
[38] B. Dezillie et al., IEEE Trans. Nucl. Sci. Vol. 47, No.6 (2000) 1892
[39] B.C. MacEvoy, A. Santocchia, G. Hall, Physica B 273-274 (1999) 1045
[40] M. Huhtinen, Nucl. Instr. and Meth. A 491 (2002) 194
[41] E. Fretwurst et al., Damage results from Co-60 gamma irradiation in Si-diodes from different materials, 4th ROSE workshop on radiation hardening of silicon, CERN/LEB 98-11 (1998) p 221
[42] B. C. MacEvoy and G. Hall, Mater. Sci. in Semicon. Process. 3 (2000) 243
[43] Z. Li, B. Dezillie, M. Bruzzi, W. Chen, V. Eremin, E. Verbitskaya, and P. Weilhammer, HTLT Oxygenated Silicon Detectors: Radiation Hardness and Long Term Stability, Nucl. Instr. Meth. A 461 (2001) pp.126-132
[44] Z. Li, E. Verbitskaya, E. Fretwurst, J. Kierstead, V. Eremin, I. Ilyashenko, R. Röder and C. Wilburn. "Paradoxes of steady-state and pulse operational mode characteristics of silicon detectors irradiated by ultra-high doses of γ-rays", NIMA 514 (2003) 25-37.
[45] V. Savolainen et al., J. Crystal. Growth 243, 2 (2002) 243
[46] J.L. Lindström, T. Hallberg, Phys. Rev. Lett. 72 (1994) 2729
[47] L.I. Murin, T. Hallberg, V.P. Markevich, J.L. Lindström, Phys. Rev. Lett. 80 (1998) 93
[48] J. Härkönen et al, Processing microstrip detectors on Czochralski grown high resistivity silicon substrates, Nucl. Instr. and Meth. A., article in print.
[49] G. Lindström et al., Recent Damage Results from the HH-CiS Collaboration, 1-st RD50 - workshop on radiation hard semiconductor devices for very high luminosity colliders, CERN, 2-4 October 2002; http://www.cern.ch/rd50
[50] A. Bartsch et al., Surf. Sci.203-204 (2003) 396
[51] J. Härkönen et al., Particle detectors made of high resistivity Czochralski grown silicon, paper presented at NSM-2003
[52] M. Moll, Radiation damage in silicon particle detectors – microscopic defects and macroscopic properties-, PhD-thesis, DESY-THESIS-1999-040, December 1999.
[53] M.Moll, E.Fretwurst, G.Lindström. Investigation on the improved radiation hardness of silicon detectors with high oxygen concentration, NIMA 439 (2000) 282.
[54] ITME, Institute of Electronic Materials Technology, Warszawa, Poland
[55] S.Dittongo, L.Bosisio, M.Ciacchi, D.Contarato, G.D'Auria, E.Fretwurst, G.Lindstrom, results presented at the 7th European Conference on Radiation and Its Effects on Components and Systems (Noordwijk, The Netherlands, September 15-19, 2003) and at the 6th International

Conference on Large Scale Applications and Radiation Hardness of Semiconductor Detectors (Firenze, Italy, September 29-October 1, 2003) .

[56] D. Bisello, A. Candelori, D. Contarato, E. Fretwurst, A. Kaminski, G. Lindstrom, A. Litovchenko, R. Rando, A. Schramm, and J. Wyss, "Lithium ion irradiation effects on diodes manufactured on epitaxial silicon," presented at the Nuclear Science Symposium (NSS), Portland, USA, 19-25 October 2003.

[57] J.L. Lindström et al., Physica B 308-310 (2001) 284

[58] Y.L. Lee et al., Phys. Rev. B 65 (2002) 085205

[59] J.L. Lindström, et.al., Materials Science Forum Vols 258-263(1997) pp. 367-372

[60] C. Da Via, S.J. Watts, NIM B 186(2002) 111-115

[61] S.J. Watts, C. Da Via, A. Karpenko, NIM A 485(2002) 153-158

[62] Measurements performed by the Lund group. Provided by Lennart Lindstroem (Lund University, Sweden) and Leonid Murin (Institute of Solid State and Semiconductor Physics, Minsk, Belarus).

[63] Measurements performed by the Hamburg group. Provided by Ioana Pintilie (Hamburg University and National Institute of Material Physics, Bucharest-Magurele) and Eckhart Fretwurst (Hamburg University)

[64] A. Litovchenko, F. Lemeilleur, P. Litovchenko, A. Dolgolenko, L. Barabash, V Khivrich, V. Lastovezky, A. Ruzin, M. Glaser. The possibility to raise the radiation hardness of silicon//ROSE Meeting on Radiation Hardening of Silicon Detectors, CERN, 14-15 June, 1999.

[65] A. Litovchenko, F. Lemeilleur, P. Litovchenko, A. Dolgolenko, L. Barabash, V Khivrich, V. Lastovezky, A. Ruzin. The radiation hardness of high resistivity of neutron transmutation doping silicon//4th ROSE Workshop on Radiation Hardening of Silicon Detectors, CERN, 2-4 December 1998.

[66] A.P Litovchenko, P.G. Litovchenko, V.I. Varnina, A.A. Groza, G.G. Shmatko, L.S. Marchenko, A.K. Semenuk. The radiation defects Influence on oxygen thermally treated silicon// Ukrainian Journal of Physics, 2001, vol. 46, №2.

[67] A.P. Litovchenko, A.A. Groza, E.F. Venger, V.I. Varnina, R.Yu. Holiney, P.G. Litovchenko, L.A. Matveeva, M.I. Starchik, V.I. Sugakov, G.G. Shmatko. Influence of neutron irradiation on electrooptical and structural properties of silicon//Semiconductor Physics, Quantum Electronics and Optoelectronics, 2001. V. 4, N 3. P. 152-155.

[68] O.P. Litovchenko, W. Wahl, A.A. Groza, A.P. Dolgolenko, A.Ya. Karpenko, V.I. Khivrych, V.F. Lastovetsky, V.I. Sugakov, P.G. Litovchenko, V.K. Dubovy. Influence of preliminary irradiation on radiation hardness of silicon and indium antimonide// Semiconductor Physics, Quantum Electronics & Optoelectronics. 2001. V. 4, N 3. P. 152-155.

[69] P.G. Litovchenko, A.A. Groza, A.Ya. Karpenko, V.I. Khivrich, A.P. Dolgolenko, V.F. Lastovetsky, L.I. Barabash, D. Bisello, A. Candelori, A.P. Litovchenko, A. Kaminsky, W. Wahl, J. Wyss. Radiation hardening of silicon for detectors by preliminary irradiation, Proceedings of the 9th “European Symposium on Semiconductor Detectors”-New Developments on Radiation Detectors, Schloss Elmau, June 23 - 27, 2002, Germany

[70] P.G. Litovchenko, D. Bisello, A. Candelori, A.P. Litovchenko, A.A. Groza, A.P. Dolgolenko, V.I. Khivrich, L.I. Barabash, V.F. Lastovetsky, L.A. Polivtsev, W. Wahl, J. Wyss. Radiation hardening of silicon for detectors by preliminary irradiation// Solid State Phenomena, vol.95-96, 2004, pp. 399-404

[71] V. Eremin, N. Strokan, E. Verbitskaya and Z. Li, Development of transient current and charge techniques for the measurement of effective net concentration of ionized charges (Neff) in the space charge region of p-n junction detectors, Nucl. Instr. and Meth A, vol. 372, pp. 388-398, 1996.

[72] A. Schramm, diploma thesis, University of Hamburg, November 2003
[73] G. Lindström, Radiation damage in silicon detectors, NIM A 512 (2003) 30-43
[74] F. Hönniger, diploma thesis, University of Hamburg, October 2003
[75] O. Krasel, C. Goessling, R. Klingenberg, S. Rajek, R. Wunstorf, "Measurement of trapping time constants in proton-irradiated silicon pad-detectors", paper presented at the IEEE Nuclear Science Symposium 2003, Portland/USA, submitted to Transactions on Nuclear Science.
[76] G. Lindstroem, E. Fretwurst, D. Contarato, F. Hoenniger, G. Kramberger, M.Moll, E. Nossarzewska, I. Pintilie, R. Roeder, A. Schramm, J. Stahl, "Results on epi-diodes with superior radiation tolerance" presented on the 3rd RD50 Workshop.
[77] G. Kramberger, V. Cindro, I. Mandic, M. Mikuz, M. Zavrtanik, "Effective trapping time of electrons, and holes in different silicon materials irradiated with neutrons, protons and pions", Nucl. Instr. and Meth. Phys. Res. A481 (2002), p. 297-305
[78] Olaf Krasel, Claus Gößling, Reiner Klingenberg, Silke Rajek, Renate Wunstorf, "Measurement of Trapping Time Constants in Proton-Irradiated Silicon Pad Detectors", presented on the 3rd RD50 Workshop
[79] F. Gianotti et al. hep-ph/0204087: April 2002.
[80] J. Wyss, D. Bisello and D. Pantano, SIRAD: an irradiation facility at the LNL Tandem accelerator for radiation damage studies on semiconductor detectors and electronic devices and systems, Nucl. Instr. Methods, vol. A 462, pp. 426-434, 2001.
[81] A. Candelori, D. Bisello, G. F. Dalla Betta, P. Giubilato, A. Kaminski, A. Litovchenko, M. Lozano, J. R. Petrie, R. Rando, M. Ullán and J. Wyss, Lithium ion irradiation of standard and oxygenated silicon diodes, submitted to IEEE Trans. Nucl. Sci.
[82] A. Virtanen, J. Hyvönen, K. Ranttila, I. Rekikoski and J. Tuppurainen, Heavy ion and proton test site at JYFL-accelerator laboratory, Nucl. Instr. and Meth. A, vol. 426, pp. 68-71, 1999.
[83] E. Tuominen et al., Radiation hardness of Cz-Si studied by 10 and 20 MeV protons, IEEE Trans. Nucl. Sci., in press.
[84] V. Eremin, E. Verbitskaya, and Z. Li, The origin of double peak electric field distribution in heavily irradiated silicon detectors, Nucl. Instr. and Meth. A, vol. 476, pp. 556-564, 2002.
[85] Technical proposal, CERN/LHCC 94-38, 1994.
[86] D.Creanza, D.Giordano, M.dePalma, L.Fiore, S.My, V.Radicci, G.Selvaggi, P.Tempesta, A comparison on radiation tolerance of microstrip detectors built on <100> and <111> silicon substrates after proton irradiation, Nucl. Instr. and Meth. A 485 (2002) 109-115.
[87] G.Lindstroem et al., NIMA 466 (2001) 308.
[88] M.Moll, E.Fretwurst, G.Lindstroem, Investigation of the improved radiation hardness of silicon detectors with high oxygen concentration, NIMA439(2000)282.
[89] G.Calefato, D.Creanza, M.dePalma, L.Fiore, S.My, V.Radicci, G.Selvaggi, P.Tempesta, M.M.Angarano, G.M.Bilei, M.Biasini, M.Giorgi, O.Militaru, L.Servoli, A Comparison on Radiation Tolerance of <100> and <111> Silicon Substrates of Microstrip Detectors, Nucl. Instr. and Meth. A 476 (2002) 744-750.
[90] E.Fretwurst, results presented at the 2nd RD50 Workshop on Radiation hard semiconductor devices for very high luminosity colliders (CERN, May 18-20, 2003).
[91] G.Kramberger, D.Contarato, E.Fretwurst, F.Honniger, G.Lindstrom, I.Pintilie et al., ``Superior radiation tolerance of thin epitaxial silicon detectors," accepted for publication in Nucl. Instr. Methods A.
[92] M.Moll, E.Fretwurst, and G.Lindstrom, ``Leakage current of hadron irradiated silicon detectors - material dependence", Nucl. Instr. Methods, vol. A426, pp. 87-93, 1999.

[93] G.P.Summers, E.A.Burke, P.Shapiro, S.R.Messenger, and R.J.Walters, ``Damage correlations in semiconductors exposed to gamma, electron and proton radiations", IEEE Trans. Nucl. Sci., vol. 40, pp. 1372-1378, 1993.
[94] P. Roy, G. Pellegrini, R. Bates, L. Haddad, V. O'Shea, K.M. Smith, V. Wright, M. Rahman, Silicon 3D detectors irradiated with pions and protons 3rd RD50 Workshop October 19-25, 2003.
[95] S. Ronchin, M. Boscardin, G. F. Dalla Betta, P. Gregori, V. Guarnieri, C. Piemonte, N. Zorzi, Thin detectors fabrication at ITC-Irst , 3rd RD50 Workshop October 19-25, 2003.
[96] Z. Li on behalf of the US RD50: BNL, FNAL, Purdue, Rutgers, Syracuse, CMU, JHU, OSU and UCSC, Activities of the US Chapter of CERN RD50 On the Development of Semi-3D Si Detectors, 2nd RD50 - Workshop CERN, 18-20 May, 2003
[97] W. Cunningham, J. Melone, M. Horn, V. Kažukauskas, P. Roy, F. Doherty, M. Glaser, J. Vaitkus, M. Rahman, Nuclear instruments & methods in physics research. Section A - Accelerators, spectrometers, detectors and associated equipment 2003, vol. 509, p. 127-131.
[98] R. Bates, M. Rahman, W. Cunningham, T. Nelson and T. Quinn, "Simulation of SiC radiation sensors", 2nd RD50 workshop, may 2003.
[99] F. Nava, M. Bruzzi, G. Bertuccio, Performance of Silicon Carbide Radiation Detectors, IEEE 2003 NSS MIC RTSD, Portland, Oregon, USA, October 19-25, 2004.
[100] M. Bruzzi, F. Hartjes, S. Lagomarsino, F. Nava, S.Sciortino, P. Vanni, Recent results on particle detection with epitaxial SiC Schottky diodes, presented at the IEEE 2002 NSS-MIC Conference, Norfolk, Virginia, November 2002
[101] F. Nava, P. Vanni, M. Bruzzi, S. Lagomarsino, S. Sciortino, G. Wagner and C. Lanzieri, "Minimum ionising and alpha particles detectors based on epitaxial semiconductor Silicon Carbide", submitted to IEEE Trans. Nucl. Science.
[102] S. Miglio, M. Bruzzi, S. Lagomarsino, S. Sciortino, R. Schifano, A. Vinattieri, F. Nava, "Electrical and optical characterization of 4H-SiC detectors", presented at: ICSCRM - 10th International Conference on Silicon Carbide and Related Materials, Lyon, October 5 - 10, 2003.
[103] F. Nava, E. Vittone, P. Vanni, P. G. Fuochi and C. Lanzieri "Radiation Tolerance of epitaxial Silicon Carbide detectors for electrons and γ-rays", in press on Nucl. Instrum. Meth. A.
[104] A.Castaldini, A.Cavallini, M.Rossi, "Proton irradiation induced defects in 4H-SiC" presented at ICSCRM 2003, Lyon, France.
[105] A. Ivanov et al, Appl. Surf. Sci. 184 (2001) 431.
[106] J. Vaitkus, E. Gaubas, V. Kažukauskas, Y. Lacroix, S. Sakai,K. Smith, J. Storasta, and T. Wang. "Space charge effects and carrier capture transient behaviour in semi-insulating GaAs and GaN". To be published in SIMC-XII-2002 IEEE EDS Conference Proceedings, 2003.
[107] J.V.Vaitkus, E.Gaubas, S.Sakai, Y. Lacroix, T.Wang, K.M. Smith, M.Rahman, W.Cunningham, (ISSN=1012-0394) Polycrystalline Semiconductors VII. Volume 93-93 (2003) pp.301-306
[108] G. Casse et al., Nucl. Inst. and Meth. A511/1-2 (Sep. 2003) 112-117.
[109] G. Casse et al., IEEE Trans. Nucl. Sci., vol. 47, n. 3 (527-532), June 2000.
[110] G. Casse, First results with oxygenated n-in-p detectors after irradiation, 2nd RD50 Workshop on Radiation hard semiconductor devices for very high luminosity colliders (CERN, May 18-20, 2003).
[111] L.J. Beattie et al. ATLAS INDET-No 194, 10/12/1997.
[112] G. Casse ., Nucl. Inst. and Meth. A426 (1999) 140-146.
[113] V. Eremin, Z. Li, I. Iliashenko, Nucl. Instr. and Meth. A 360, (1995) 458.
[114] V. Eremin, E. Verbitskaya, Z. Li, Nucl. Instr. and Meth., A476 (2002) 556.

[115] D. Contarato et al. Simulation of Irradiated Silicon Pixel Detectors for Future High Energy Physics Experiments, 2nd RD50 Workshop, CERN, May 2003.
[116] T. Lari, ATLAS-INDET-2003-015 - CERN, 06 Aug 2003
[117] T. Lari, Simulation of irradiated silicon detectors performances, 3rd RD50 Workshop, CERN, 3-5 Nov. 2003.
[118] V. Chiochia et al., Tests of CMS sensors for CMS pixel detectors, 3rd RD50 Workshop, CERN, 3-5 Nov. 2003.
[119] J. Kennedy et al., Test Beam analysis of Czchralski Silicon Strip detector, 3rd RD50 Workshop, CERN, 3-5 Nov. 2003.